INTERACTION OF A FINITE TRAIN OF SHORT OPTICAL PULSES WITH A LADDER SYSTEM

by

HYOUNGUK JANG

B.S., Sungkyunkwon University, Korea, 2002

AN ABSTRACT OF A DISSERTATION

submitted in partial fulfillment of the
requirements for the degree

DOCTOR OF PHILOSOPHY

Department of Physics
College of Arts and Sciences

KANSAS STATE UNIVERSITY
Manhattan, Kansas
2010

Abstract

In recent years, advance in ultrafast lasers and related optical technology has enhanced the ability to control the interaction between light and matter. In this dissertation, we try to improve our understanding of the interaction of atomic and molecular ladder systems with short optical pulses. A train of pulses produced by shaping the spectral phase of a single pulse from an ultrafast laser allows us to control the step-wise excitation in rubidium (Rb) atoms. As a diagnostic method, we use magneto-optical trap recoil ion momentum spectroscopy (MOTRIMS) to prepare cold target atoms and to observe atomic ions as a result of the interaction.

We have explored the interactions of a finite number of optical short pulses in a train with a three-level Rb atom ladder system. Each pulse in the train is separated by a constant time interval with a fixed pulse-to-pulse phase change. In these experiments, two dimensional (2D) landscape maps show the interaction by measuring population in the uppermost state of the ladder system as a function of pulse-to-pulse time interval and phase shift. The observed structures in the 2D landscape are due to constructive or destructive interference in the interaction. Furthermore, different numbers of pulses in the train are applied to the atomic Rb three level ladder system in order to measure the effect on the interaction. The sharpness of the interference structure is enhanced by increasing the number of pulses. This phenomenon is analogous to increasing the sharpness in an optical multi-slit experiment by increasing the number of slits.

INTERACTION OF A FINITE TRAIN OF SHORT OPTICAL PULSES WITH A LADDER SYSTEM

by

HYOUNGUK JANG

B.S., Sungkyunkwon University, Korea, 2002

A DISSERTATION

submitted in partial fulfillment of the
requirements for the degree

DOCTOR OF PHILOSOPHY

Department of Physics
College of Arts and Sciences

KANSAS STATE UNIVERSITY
Manhattan, Kansas
2010

Approved by:

Major Professor
B. D. DePaola

Copyright

Abstract

In recent years, advance in ultrafast lasers and related optical technology has enhanced the ability to control the interaction between light and matter. In this dissertation, we try to improve our understanding of the interaction of atomic and molecular ladder systems with short optical pulses. A train of pulses produced by shaping the spectral phase of a single pulse from an ultrafast laser allows us to control the step-wise excitation in rubidium (Rb) atoms. As a diagnostic method, we use magneto-optical trap recoil ion momentum spectroscopy (MOTRIMS) to prepare cold target atoms and to observe atomic ions as a result of the interaction.

We have explored the interactions of a finite number of optical short pulses in a train with a three-level Rb atom ladder system. Each pulse in the train is separated by a constant time interval with a fixed pulse-to-pulse phase change. In these experiments, two dimensional (2D) landscape maps show the interaction by measuring population in the uppermost state of the ladder system as a function of pulse-to-pulse time interval and phase shift. The observed structures in the 2D landscape are due to constructive or destructive interference in the interaction. Furthermore, different numbers of pulses in the train are applied to the atomic Rb three level ladder system in order to measure the effect on the interaction. The sharpness of the interference structure is enhanced by increasing the number of pulses. This phenomenon is analogous to increasing the sharpness in an optical multi-slit experiment by increasing the number of slits.

Table of Contents

List of Figures

List of Tables

Acknowledgments

I have to start by thanking my family, friends, and the faculty at Kansas State. I could only have done my work in the graduate school with their support and care. I am grateful to my advisor, Professor Brett DePaola. I still remember my first meeting with him in his laboratory. He told me we worked here like a family. The word, family, touched my heart and I realized this was the type research group with which I had always dreamed of working. He has shared his knowledge and wisdom over many topics in physics. In the early morning, I enjoyed very much starting a day talking with him about interesting news in the the world and the physics about which we thought the previous night. I learned from him how to think about new topics and address them with logic and intellectual curiosity. In addition, I became aware of the basic and very important lesson that often the most interesting results come, if we firmly keep working on them, even with no beginning expectation for them to occur.

I was grateful to work with Dr.Mark Tracy who is a genius. He introduced me to experimental equipment and techniques when I was a newbie in our group. The amazing thing was that he always answered my questions and knew almost everything I wanted to know. His teaching formed the cornerstone of my research skill in such areas as data acquisition systems, electronics, and optics. I also appreciate our former post-doctoral researcher, Dr.Goga Veshapidze. He gave me creative and practical solutions to our research. He invited me to dinner with wonderful Georgian foods and shared his many outside interests with me. I appreciate Prof. Charles Fehrenbach for his teaching and his ingenious support. When Brett was out of town, Prof. Charles Fehrenbach was my advisor.

Thank you to my former graduate student colleague, Dr.Mudessar Shah, for his wisdom. Thank you to my friend, Bachana, as well. When I ask a very naive question, it is magically turned into a meaningful question during our discussion. His wise advice was essential to figuring out my problems and leading me to accomplish my work. The good nature and

humor of former and current colleagues made me enjoy my experimental work. I could enjoy doing experiments during the hardest times, because all experiments with them are joyful experiences. I could not have better colleagues and friends.

I appreciate the support of the faculty, graduate students, and staff in the JRM laboratory. Special thanks to Scott Chainey for helping me to design electric circuits and Mr. Bob Krause for his smile every morning and for sharing his 30 years of experience.

I am grateful to my parents and younger brother who have always believed in me and supported me. Although we are separated by a long distance, their advice and love have sustained me through the difficult times. They work so hard all the time that it has encouraged me to keep studying hard. Finally, I offer my deepest gratitude to my fiance, Sookyong Kim. Her encouragement and love are the heart of my inspiration and strength. Watching her smile on the picture at my wallet fills me with happiness and laughter all the time. I am grateful to my Lord as I repeat the words in 2 Corinthians 4:16-18, "Therefore we do not lose heart . . . but what is unseen is eternal."

Dedication

To my family and my fiance.

Chapter 1

Introduction

Controlling interactions between light and matter has been a long standing goal in atomic physics. The work presented in this dissertation investigates the interaction between a train of laser pulses and matter. The aim of this dissertation is to build up a general picture of how a train of pulses interacts with an atomic ladder system in cold atoms. In a ladder system, an excitation is transferred to the higher energy levels like climbing a ladder. A well known special case, experiments using a 2-pulse train, pump and probe, has been done for various applications. This is the simplest case in terms of the number of pulses in a train. The other extreme in terms of the number of pulses in the train is the frequency comb. Between these two limits, various experimental and theoretical research has been done.

We believe that looking at the interaction with a small number of pulses helps us understand the physics of a ladder system's interaction with an arbitrary number of pulses in a train. Experiments in different subfields of atomic, molecular, and optical physics focus on distinct aspects of light-matter interactions. However, it is interesting to note that many of these experiments can be approached by using ultrafast lasers. Significant achievements in ultrafast laser technology have produced a new generation of optical short pulses whose duration (<10 fs) is shorter than the atomic relaxation time and, indeed, the time scale of nuclear motion[1]. Shaping the spectral phase and amplitude of ultrafast laser pulses is already a commercially available technology for many research endeavors[2,3]. Generating a train of femtosecond laser pulses offers a new set of useful properties and has great poten-

tial for further development in many applications. For example, the ultrashort interaction time of ultrafast lasers provides the capability to study the interaction with an atomic ladder system because these short pulses coherently interact with the system before radiative relaxation occurs.

In spectroscopic experiments, ultrafast pulses are used to directly measure time resolved fundamental microscopic motions such as collective vibrations of crystal lattices and molecular vibrations and rotations[4–6]. In addition, in studies using attosecond laser pulses, the short exposure time and ultra-high fields show the possibility of investigating electron dynamics[7] without causing decoherence. The techniques, based on careful control of strong-field laser-atom interactions on this short time scale, provide greater capability to understand the motion of electron distributions inside atoms and molecules[8].

Technology advancements in atom cooling and trapping has made it possible to study atoms without the complication of significant Doppler broadening. It is currently known how to easily obtain clouds of cold atoms near one hundred microkelvin. In particular, one convenient way to cool and trap atoms is with a Magneto Optical Trap (MOT). To build a MOT, it is necessary to have a couple of lasers tuned near resonances in target atoms situated in a weak magnetic field gradient that have closed cycling transitions. Applying the technique of a MOT to other research areas in atomic and molecular physics has resulted in the successful investigation of complicated level structures of atoms and molecules. This is largely due to the fact that there is negligible Doppler broadening.

In this work, we take advantage of small Doppler broadening in order to observe a combination of constructive and destructive interference in an atomic ladder system due to a train of pulses. We use a train of pulses to control these interferences in the multi-level atomic structure of trapped atoms. The focus of my research is on understanding the complicated interaction of the atomic ladder system with a train of pulses and improving techniques for producing a train of pulses by shaping the spectral phase of an ultrafast laser.

1.1 Cooling and trapping atoms

Over the last century, many experimental and theoretical studies on the interaction between light and matter have paved the way for modern atomic physics and its applications. In 1933, Frisch observed a collimated sodium atomic beam was deflected by resonant light from a Na lamp[9]. In 1975[10], Hänsch and Schawlow proposed that the radiation force of light could be used to cool atoms and ions, if the atoms were irradiated with light red-detuned from a resonant transition: When atoms move toward the radiation source, the photons are Doppler shifted closer to resonance and are therefore preferentially absorbed. The atoms that absorb photons spontaneously re-emitt in a random direction. The emitted photons, therefore, impart no net momentum to the atom. Thus, atoms experience a force opposing their motion. Cooling of the atoms by three pairs of counter propagating laser beams is called on optical molasses. That is, atoms are slowed by the interaction with the laser field in the interaction region of the six laser beams, and that slowing force is proportional to the magnitude of the atom's velocity.

Optical molasses was first demonstrated by Chu et al. for Na atoms in 1985[11]. Subsequently, many different mechanisms for laser cooling and trapping have been described. Two years after the first achievement of optical molasses, Raab et al. proved that the addition of an inhomogeneous magnetic field could generate a spatially and velocity dependent dissipative molasses force[12]. This first MOT was used on a pre-slowed beam to trap and cool Na atoms. A simplified MOT setup was developed by Monroe et al. in 1990 by loading atoms from room temperature vapor without pre-slowing the atoms[13]. Since the establishment of laser cooling and magneto-optical trapping[12] of neutral atoms, the interest for exploiting this technology has increased in atomic, nuclear, and particle physics. For instance, trapped radioactive atoms can be employed in a new generation of fundamental symmetry experiments such as nuclear beta decay, atomic parity nonconservation, and the search for parity and time-reversal violating electric dipole moments[14]. In atomic physics, MOTs have played an essential role in producing cold and dilute samples of atoms, and ever

more atomic species have been laser cooled.

1.2 Interaction of a train of pulses with ladder systems

1.2.1 Two pulse sequence

One of the long term goals in physics is to develop a technology to more quickly and more robustly drive a desired interaction in a ladder system. To control light and matter interactions, ultrafast lasers have been used as a powerful tool because of their broad spectral bandwidth and coherent nature. The intrinsic property of ultrafast lasers, having a broad bandwidth, makes it possible to excite a wide range of energy states in atomic or molecular systems. For instance, ultrafast lasers can be used to excite inhomogeneously broadened states in atomic or molecular systems to explore fundamental properties such as excited state lifetimes of atoms. Furthermore, the phenomena of coherent excitation[15] by ultrafast lasers in atoms or molecules has obtained more attention in quantum optics.

To investigate interactions of atoms and molecules with light, a well-known scheme employs a pair of pulses to interact with an atomic or a molecular multi-level system. Pump-probe experiments are widely used for studying the interactions of atoms and molecules with light, such as control of coherent atomic wave packet motion[17,18] and multi-photon ionization. Our interest in this dissertation focuses on a specific subset of a pump and probe experiments in which the pump pulse is identical to the probe pulse. The basic configuration is shown in Fig. 1.1 where one light source produces a pump and a probe beam that are focused onto the sample, in which they undergo splitting and interferometric recombination.

We consider two cases of a two-pulse train interacting with an atom or molecular system. The first case describes the interaction of a two-level system with the pump and probe pulses both resonant with the transition. The second case is the excitation of a three-level system with the pulses resonant with both transitions. We are interested in theoretical and experimental aspects of quantum interference to study control of the interaction.

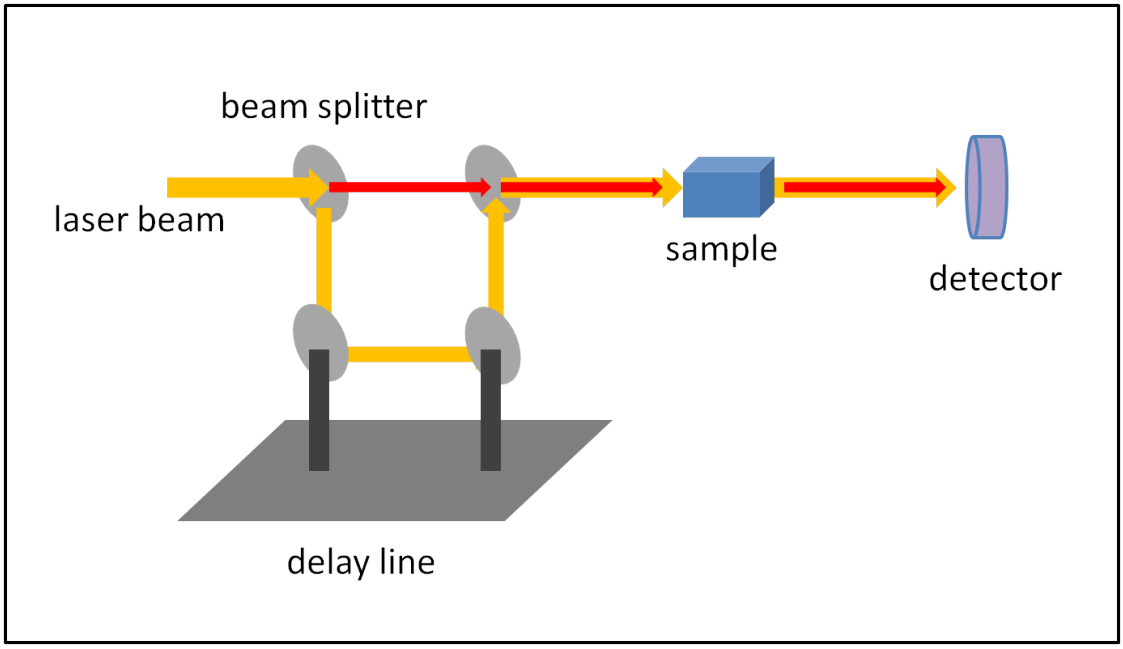

Figure 1.1: *This configuration*[16] *describes a conventional two pulse sequence experimental setup. From an identical source, one beam is split into the pump and the probe pulse. The pump pulse is separated from the probe pulse with variable relative delays between them. Usually, a delay line is built to achieve high time-resolution. Here, we use different colors to distinguish pump and probe pulses although they are identical pulses coming from the same light source.*

The simplified process is shown in Fig. 1.2 which describes an experiment where the sequence of two pulses interacts with a two-level system. The pump pulse excites atoms to an upper energy level and then the probe pulse with time delay (τ) probes the excited state dynamics. That is, the temporal evolution of the excited state population by a pump pulse is monitored by a probe pulse. There are experiments[19,20] varying the relative pulse timing with different delays to have time-dependent data which describe the interaction between pump-probe pulses and a two-level system.

In our experiment, we investigate the interactions in an atomic ladder system. However, many applications of pump and probe scheme have been broadly developed as an effective technique in molecular systems. In other experiments, various molecular dynamics processes related to wave packet oscillations in bound states have been studied by varying the

relative pulse timing in the sequence of pulses[21–23]. Moveover, the detailed control of the internal motions of a molecule was achieved by using two tailored laser pulses[24]. In that experiment[24], various interference effects associated with molecular motion were observed where a timed sequence of laser pulses controlled the population of a specified vibrational state. In addition, one-color coherent control of wave packet motion in a diatomic molecule was accomplished in the experiment[19], where the wave packet interference producing beats is modulated by the vibrational recurrences and allows one to determine the vibrational period.

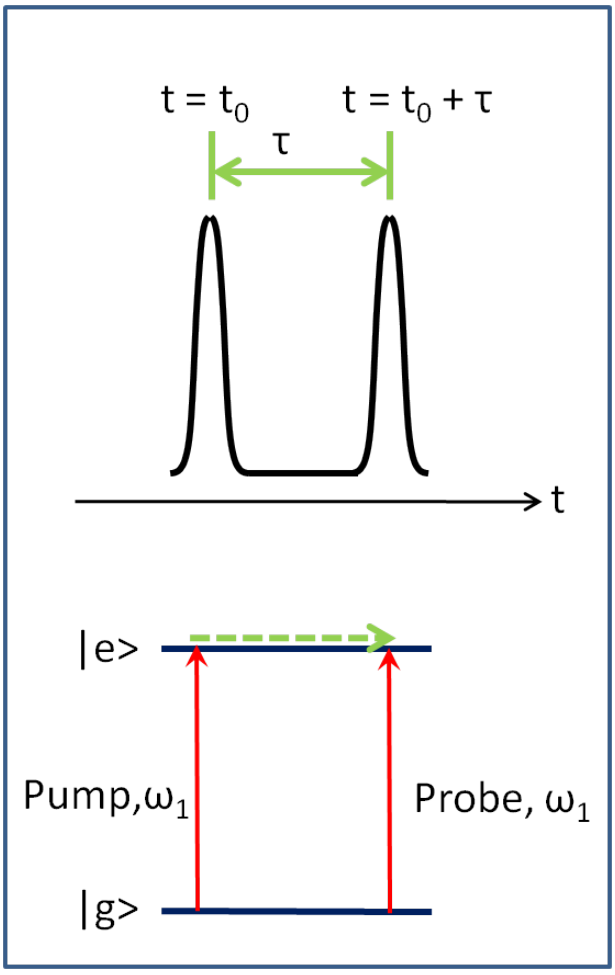

Figure 1.2: *Schematic diagram in a two-level system using pump and probe pulses. This figure illustrates how a pump pulse and a probe pulse interact with a two-level system. A timing diagram of a pump and a probe pulse is also shown in this scheme where τ is time delay between the pump and the probe pulses.*

Controlling quantum interferences in an atomic ladder system is one of many challenging topics in quantum optics[25]. Using an ultrafast laser such as a femtosecond mode-locked laser is a very effective tool for controlling the interaction of two-level ladder system with pump and probe pulses because it is coupled with the capability to manipulate the relative time delay and the relative phase[26] between pulses. A succession of two identical ultrafast laser pulses with a well-defined phase relation enables one to build up quantum interferences[18] so that the excitation to the desired state is optimized. As a novel spectroscopic technique[20], a two-pulse sequence of femtosecond laser pulses is applied to resonantly excite vibronic transitions of a molecule where the interpulse delay is varied with high precision while the phase of pulses is maintained at several different values. This experiment[20] sensitively and directly observed the total phase evolution of the wave packet prepared by the initial pulse.

In a three-level ladder system, several experiments[26–28] investigated coherent control of two-photon transitions with quantum interferences. For example, in the weak field region, a temporal coherent control technique was applied to two-photon transitions[27] where all the spectroscopic information on the system was obtained by probing the excited states wave packet dynamics. One experiment[26] demonstrated that well-defined phase relationships between two pairs of nanosecond laser pulses are useful for two-photon coherent control. It was observed that oscillations in excited state populations caused by quantum interference are strongly modulated by varying the delay between femtosecond pump and probe pulses in the atomic three-level system[28].

1.2.2 Interaction with infinite number of pulses

We expect to observe various interesting effects in the interaction of atomic or molecular ladder systems since using an infinite number of pulses is a unique condition in the time domain. The best known example having an infinite number of pulses is the frequency comb[29–31]. Recently, frequency combs have become a standard tool in several essential branches of atomic and molecular physics because the well-characterized relationship between pulses in

the train make it possible to investigate both fast dynamics in the time domain and atomic energy-level structures with high-resolution in the frequency domain[31].

In the frequency domain, combs provide the high precision that the traditional ultrafast laser spectroscopy cannot reach because the broad bandwidth of pulses in traditional ultrafast lasers excite a wide range of energy states[32]in measurements. It is essential to have well-characterized narrow frequencies in metrology. Usually, continuous wave (cw) lasers were used to do precision spectroscopy before many laboratories began to use frequency combs and established an impressive revolution in metrology[33–35] by providing precise atomic and molecular structural information[36,37]. Frequency combs provide the absolute frequency reference[38] because the narrow linewidth of individual comb teeth enables one to selectively interact with a very fine energy level structure. For instance, it was demonstrated that a broad-bandwidth optical frequency comb can be coherently coupled to a high-finesse optical cavity which provides the reference frequency[39]. In the time domain, a well-defined phase relation among successive ultrashort pulses in a train plays an important role in coherently controlling the interaction with atoms or molecules. This property makes it possible for one to observe coherent pulse accumulation and quantum interference effects.

Particularly, direct frequency comb spectroscopy (DFCS)[32,34,40,41] shows the progress that the phase stabilized femtosecond pulses in a train enable to bridge the area of ultrafast dynamics and high-resolution spectroscopy. In the DFCS, the bandwidth of the femtosecond pulse is broad enough to excite many fine and hyperfine atomic states into resonance by tuning the optical frequency of a particular comb mode, $f_n = nf_r + f_0$, where f_r is the pulse repetition rate, f_0 is the carrier envelope offset frequency, and n is an integer on the order of 10^6. Scanning one of the two comb components, f_r and f_0, changes the optical frequency. Therefore, in measurements of the broad energy-level structures, only one frequency comb laser can replace many absolutely referenced cw lasers which are broadly tunable. For example, all of the allowed single-photon and two-photon transitions within the laser bandwidth are measured in two-photon DFCS[32]. Moreover, real-time transition

dynamics of the atomic system are observed by using the two-photon DFCS technology. For example, coherent population accumulation in the 5D state in cold ^{87}Rb atoms is observed where the 5D population increases as the square of the number of pulses until the accumulation is restricted by the atomic decoherent effects.

1.2.3 Interaction with a finite number of pulses

Applications of how to manipulate a train of pulses strongly depend on what we want to observe from the interaction with a ladder system. So far, we reviewed two extreme cases from pump and probe experiments to frequency comb to investigate the interaction. The region between the two extreme cases still needs more research to get further interpretation of the interaction. Our desired goal is that applying a finite number of short pulses to an atomic system can give us valuable general knowledge to interpret the two extreme cases. As it was already mentioned about properties of ultrafast lasers, an experiment using a finite number of pulses from ultrafast lasers also provides capabilities for coherent control and excitation in broad energy levels.

In the aspect of coherent control, accumulation effects on the excited states populations can be controlled by manipulating short pulses in a train. In many cases, the typical accumulation effects are avoided or neglected in coherent control[42]. However, a recent experiment proves that considering accumulative effects is necessary to provide the entire explanation for the obtained coherent control signal from a rubidium vapor[43]. To manipulate quantum coherence processes, sufficiently short interacting times or short intervals between pulses are necessary[44] because pulses can then interact with the quantum system before the external environment of the quantum system affects it[45]. Generally, ultrafast lasers satisfy this requirement because the atomic relaxation times are longer than the laser pulse repetition period. Mostly, the time scale of the decay lifetime of states in atoms is nanoseconds and the pulse repetition period of ultrafast lasers is femtoseconds. From this condition, one can observe accumulated effects in the population of a two-level system by using ultrafast lasers

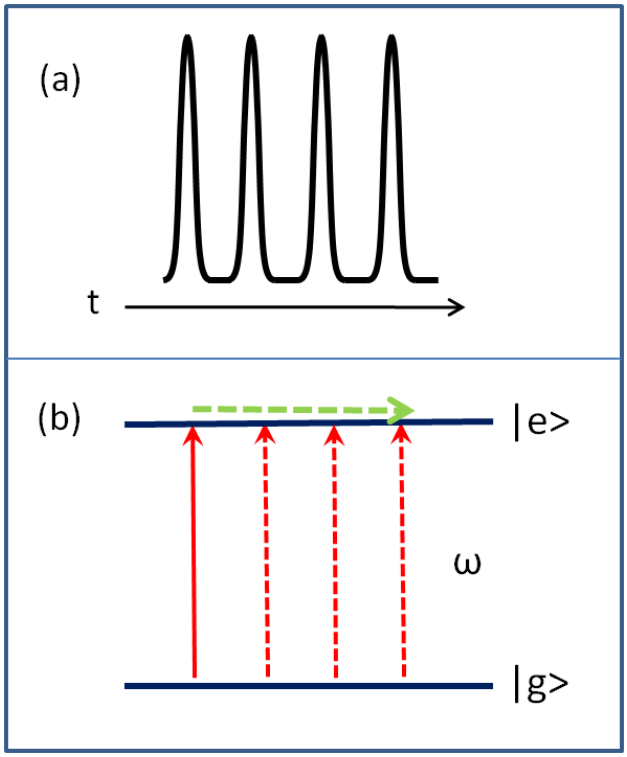

Figure 1.3: *Schematic diagram of the energy levels with the application of a finite number of pulses. The sequence of pulses in a train have the same transition frequency with a fixed relative delay between them. After atoms or molecules are excited from the ground state, their excited state wave function interacts with the next sequence of pulses.*

because the atoms can not completely decay in the time interval between consecutive pulses.

In addition, optical control technique for various molecular motions has been improved with a train of femtosecond pulses produced by pulse-shaping techniques. For example, the train of femtosecond pulses having a high-repetition-rate was used to repetitively drive selected vibrations of a molecular crystal lattice[46]. That is, repetitively pushing molecules along selected paths in the lattice can give rise to optical control of molecular motions. Recently, coherent control of molecular motion has been demonstrated by using a stable ultrahigh-repetition-rate train with hyperbolic secant envelopes in the experiment[47]. Furthermore, in Fig. 1.4, specially shaped femtosecond pulses in a train achieve enhanced amplification for selected vibrational modes and discrimination against other modes[4]. The femtosecond pulses in a train also are used to improve the control for repetitive impulsive

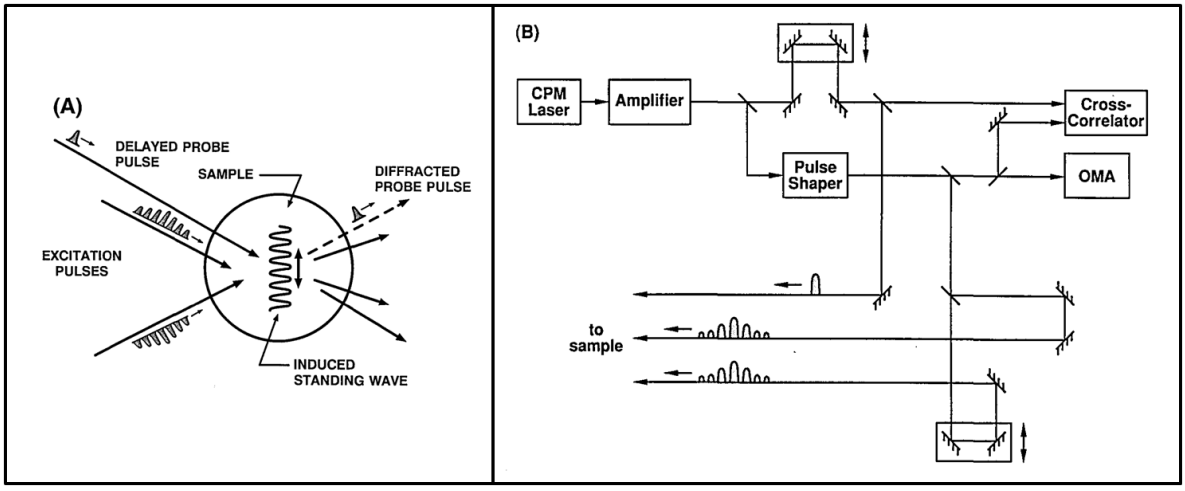

Figure 1.4: *Femtosecond pulse sequences allow the selective amplification of optical phonons matched to the pulse repetition rate*[4].

excitation in impulsive stimulated Raman scattering (ISRS) experiments[4].

Previously we have looked at the benefits of using ultrafast lasers. However, we need to carefully consider that ultrafast lasers typically have broad bandwidths. Typical femtosecond lasers have bandwidths from 5 to 100 nm. If the energy levels probed in the two-level system have a continuum of states or broadened states, the observed excitation is the averaging result caused by many excitations. In addition, excitations to a continuum state or multiple states have many decay channels giving rise to incoherent processes so that the selected excitations with pulses in a train can have disruption from unexpected decays. Therefore, careful analysis is necessary to explicitly extract the underlying information in the excitations[19,27].

1.3 Overview of dissertation

We designed experiments to study the interaction of a finite number of optical pulses in a train with an atomic three-level ladder system. We performed these experiments with the hope that we could bridge the gap between pump-probe experiments and experiments using an infinite number of pulses. This dissertation is organized as following. In chapter 2, a

description of the theoretical models is given to explain the interaction of an atomic ladder system with a finite number of pulses in a train. In addition, various theoretical aspects are described. In chapter 3, the measurement process for the interaction is explained with a brief description of the MOTRIMS apparatus and pulse shaping technique. The experimental results are shown in chapter 4. Finally, chapter 5 contains a summarized conclusion as well as future directions for further experiments.

In chapter 2, a simple model is designed to describe cumulative phase effects of the interaction in a 2-level ladder system. Simple second order perturbation theory is developed to describe the excitation probability amplitude in a three-level ladder system with ultrashort pulses. The experimental data we obtained ware found to be in very good agreement with the simple model.

In chapter 3, the experimental apparatus is described in detail. Two effective experimental techniques support us to achieve the goal for studying the interaction. The shaping technique for the spectral phase in pulses of an ultrafast laser generates a train of pulses where the sinusoidal spectral phase is applied to a transform-limited ultrafast optical pulses. We developed the mathematical analysis to select the effective number of pulses in a train. The details are explained in Appendix C. The brief description for building a MOT and controlling CW lasers is also presented in this chapter.

Much of chapter 4 focuses on measuring the excitation of the atomic Rb ladder system by the train of pulses from an ultrafast laser. The experimental results are compared with a simple intuitive model. We investigate the population of the excited states by plotting 2D landscape maps. The discussion of the obtained interference patterns in the 2D landscape maps are included. In addition, the reason the structures in the landscape plots become dramatically sharper as we increase the number of pulses in the train is explained.

In chapter 5, a brief conclusion of our experimental results is presented. The study of the interaction allows us to have more understanding for the general cases of the interactions between a train of pulses and a ladder system. We expect that the experimental results

will be a beginning point to lead critical breakthroughs in the study of the interactions. A general description for possible future experiments related to our experiments is discussed. We can study the interaction on the femtosecond time scale by using short optical pulses in a train.

We demonstrate the interaction of a three-level Rb atomic ladder system with a train of optical short pulses by observing population transfer to a desired final state. The 5d population in the 2D landscape maps as a function of pulse-to-pulse time delay T and pulse-to-pulse phase shift ϕ_0 shows the interaction. Structures of constructive and destructive interference are observed in the 2D landscape maps as strong functions of T and ϕ_0. The structures depend on the total accumulated phase of the excited state wave function.

Chapter 2

Theoretical aspects

During the past two decades, several theoretical investigations[48,49] provided extensive knowledge toward the goal of controlling the interaction between ultrafast lasers and a ladder system. The theoretical achievements[48] in a two-level system and multi-level systems[49] have explored population transfer due to interaction with a train of pulses. Theoretical models have been developed to predict how manipulating the parameters of ultrafast lasers affects excitation in atomic and molecular systems. For example, the interaction between a train of ultrashort pulses[50] and a three-level atom driven by a CW laser has been studied in the context of electromagnetically induced transparency resonances[51].

The development of control technology in ultrafast lasers requires a theoretical framework to support rigorous experiments. Appropriate ultrafast laser pulse shaping abilities, like multi-dimensional pulse shaping and direct space-to-time pulse shaping, have recently become feasible and practical so that we can investigate new coherent population transfer phenomena. For example, suitably designing the spectral phase of pulses more significantly enhances resonant multiphoton transitions than maximizing the peak intensity of pulses[52].

Theoretically, we developed a simple model for two-level systems and applied simple second order perturbation theory to a three-level system in order to interpret our experimental data. The simple two-level model was applied extensively to the three-level system in our experiments and provided good qualitative understanding of the interaction between a train of pulses and a ladder system.

2.1 Simple intuitive 2-level model

Several theories of the interaction of coherent laser excitation in a two-level atomic system have been broadly researched[53,54]. Previous research showed that, if the pulse energy is in the weak field regime, population transfer in atomic systems with a train of short pulses is generally ineffective. However, we can strongly control the population transfer by using cumulative effects of pulses in a train even though the energy of each individual pulse is weak. That is, the cumulative effects in the total phase of an excited state can be controlled by changing the delay between pulses.

The effect of coherent excitation of an atomic system by a series of short pulses in a train[48] was theoretically investigated by Temkin *et al.* where it was assumed that the atom is an isolated two-level system and the relaxation of the system occurs only by radiative decay from the upper to the lower state. In addition, optical pulses in the train were assumed to be in phase with respect to one another. This theoretical study demonstrates why cumulative effect of pulses in the train should be considered in the atomic system if the spacing between pulses and the duration of each pulse is comparable with or shorter than the atomic decay time of the atomic system.

We developed a simple model for the 2-level system to gain an intuitive understanding for the interaction between an atomic ladder system and a finite train of pulses. Adjacent pulses in the train are separated by a constant time interval T and have a pulse-to-pulse phase change ϕ_0. These two parameters are an essential to controlling the interaction. We assumed that the entire population is in the ground state before the train of pulses interacts with the 2-level atomic system.

Some of atoms are excited by the first pulse in the train at time $t = 0$. The phase of the excited state wave function $\Psi_e(t)$ evolves as $\exp(i\omega t)$, where $\hbar\omega$ is the energy difference between $|g\rangle$ and $|e\rangle$, until the next pulse comes along after time T. At this time, the excited state wave function interacts with the next pulse whose phase is different from the previous one by ϕ_0. The total phase, which is sum of the accumulated phase of the excited state

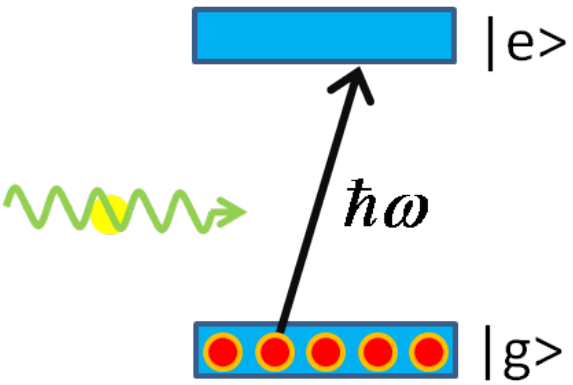

Figure 2.1: *The 2-level system as a simple intuitive picture. $\hbar\omega$: energy difference between $|g\rangle$ and $|e\rangle$, $|g\rangle$: ground state, $|e\rangle$: excited state.*

wave function and the additional relative phase ϕ_0, determines the degree of interference in the excitation probability for the transition. The excitation probability is maximized when the total phase is equal to some integer times 2π. Constructive interference therefore occurs when

$$\omega T + \phi_0 = 2\pi m. \tag{2.1}$$

Destructive interference occurs when

$$\omega T + \phi_0 = \pi(2m + 1), \tag{2.2}$$

where m is an integer. This simple intuitive model was developed in pump-probe experiments[19] where the theory of one-color coherent control with two identical time delayed laser pulses was presented by Blanchet *et al.*. This simple model was also applied to interpret direct frequency comb spectroscopy experiments[42].

In the interaction of laser pulses and atoms, spontaneous and stimulated emission are often considered as important processes. Particulary, spontaneous emission is necessary to provide a full explanation for phase cumulative effects in the interaction of optical pulses with the atomic ladder system because spontaneous emission is a stochastic process that can cause significantly incoherent population distribution in the atomic ladder system[55].

In this simple model, spontaneous emission should be considered if radiative decay lifetime of states is comparable to or shorter than T. In our experiments, spontaneous emission need not be considered because the radiative decay lifetimes of the relevant states[56] are much larger than T, which has a maximum of 400 fs. Furthermore, when this model is applied to an arbitrary two-level system, if pulse intensity is strong, appropriately analyzed results requires that saturation effects from the pulses is considered. In addition, collisional relaxation between atoms is not considered in our experiments. This is reasonable because the MOT density is about 10^{10}atom/cm^3.

We can use Eq. 2.1 or Eq. 2.2, to obtain the transition frequency associated with the energy difference between the ground and excited states. The transition frequency can be obtained by creating a 2D landscape map showing excited population as a function of T and ϕ_0. Then, the ridges and valleys correspond to constant populations since the interference patterns should be created in the 2D landscape map having slopes obtained by the derivative of Eq. 2.1 or Eq. 2.2:

$$d\phi_0/dT = -\omega. \tag{2.3}$$

As a consequence, the slopes of these ridges and valleys in such a 2D landscape provide the transition frequency in the simple two energy level system. This is, admittedly naive, but it is still useful for a qualitative understanding of the experimental results.

The simple model for a two-level system can be extended to a multi-level ladder system. For example, one can independently consider population transfer of two transitions in a three-level ladder system by separately applying the simple model to each transition where the first transition is from the ground state $|g\rangle$ to the intermediate state $|i\rangle$ and the second transition is from intermediate $|i\rangle$ state to the excited state $|e\rangle$. The justification is that population in a ladder system is continuously transferred from a lower state to an upper state. Then, we would expect that the final excited state population is proportional to the intermediate state population because, when we consider the population transfer in the second transition, the intermediate state can be considered the ground state of the second

transition in an independent two-level system.

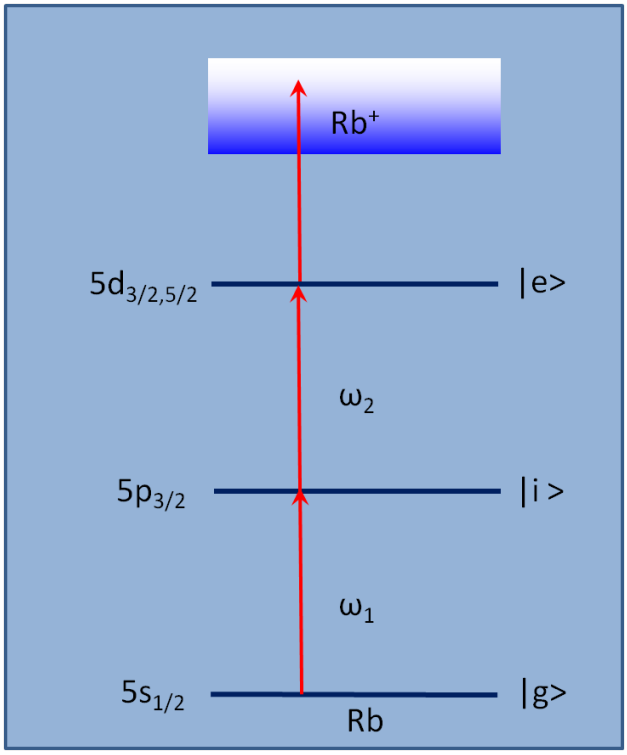

Figure 2.2: *The three-level system in a Rb atom.* $5s_{1/2}$*: ground state* $|g\rangle$*,* $5p_{3/2}$*: intermediate state* $|i\rangle$*,* $5d_{3/2,5/2}$*: excited state* $|e\rangle$

The simple model anticipates that the maximum population in the excited state $|e\rangle$ occurs when both transition frequencies, ω_1 and ω_2, simultaneously satisfy Eq. 2.1. However, the transitions can have different values of the integer m because, for fixed T and ϕ_0, different transition frequencies cannot simultaneously satisfy Eg. 2.1 for a single value of m. In addition, we expect that ridges with large population and valleys with small population should be shown along lines with slopes given by $d\phi_0/dT = -\omega_1$ and $d\phi_0/dT = -\omega_2$.

2.2 Second order perturbation theory

In recent years, theoretical approaches using second order perturbation theory have been used to provide an efficient way to describe processes controlling quantum systems from simple atoms to complex molecules and semiconductors. As a relatively intuitive and simple

method, second order perturbation theory has generally explained the complicated effects of the interactions of a ladder system with ultrafast laser pulses. Here, our experimental results are compared with calculations using second order perturbation theory because the theory should explain experiments performed in the low-field regime.

Second order perturbation theory describes the excitation probability amplitude in a three-level ladder system with ultrafast pulses where two photons are absorbed from the ground state g to final state f via intermediate states i. The excitation probability amplitude is given by

$$a(t) = -\frac{1}{\hbar^2}\mu_{fi}\mu_{ig}\int_{-\infty}^{t1}\int_{-\infty}^{t2} E(t_1)E(t_2)exp(i\omega_{fi}t_1)exp(i\omega_{ig}t_2)dt_2dt_1 \ , \tag{2.4}$$

where E is the electric field; $\mu_{x,y}$ is the dipole matrix element coupling states x and y; and $\omega_{ig,fi}$ is the transition frequency in a three-level ladder system.

We use the simple model[52] based on second order perturbation theory described by Dudovich *et al.*. The model demonstrates the effects of the shaped ultrafast laser pulses with resonant excitation rates in an atomic ladder system. In the frequency domain, and for resonant or near resonant two photon absorption from the ground state g to final state f via intermediate states i in a three-level ladder system, the excitation probability amplitude is given by

$$a \approx \sum_i -\frac{1}{i\hbar^2}\mu_{fi}\mu_{ig}\left[i\pi E(\omega_{ig})E(\omega_{fg}-\omega_{ig}) + \wp\int_{-\infty}^{\infty}\frac{E(\omega)E(\omega_{fg}-\omega)}{\omega_{ig}-\omega}d\omega\right] \ , \tag{2.5}$$

where subscripts indicate the relevant states, $\mu_{x,y}$ are the dipole matrix elements coupling states of x and y and $\wp$ is the Cauchy principal value. The first term in the square brackets corresponds to resonant excitation and the second term in the square brackets includes the contribution from off-resonant excitation.

This model has several advantages. It only requires calculating a single integral. It also requires relatively simple knowledge of the energy level structure of the atomic system, so it

may be useful for various types of shaped pulses. Thus, we readily get the excitation probability from a^*a in Eq. 2.5. The result of using this simple model by applying a sinusoidal spectral phase is shown in Fig. 2.3.

The theoretical calculations in Fig. 2.3, can be compared with our experiment. The diagonal structures are like our experimental results in Fig. 4.2. The contrast in count rate is similar, but the widths of the sloping ridges and valleys are different from the 2D maps of experiment. We can not currently provide a clear explanation of this. However, we know that second order perturbation theory is appropriate for interpreting experiments using small driving fields, or with off-resonant excitation. In our experiments, we can not explicitly claim our experiments were performed in the weak field regime, so if our experiments are performed in strong field regime, the model may disagree with our experimental results. In general, in the strong field regime, the analysis of the data is difficult because one should start to consider ac Stark effects or multiple Raman processes populating numerous states. As an alternative theoretical method, solving the appropriate optical Bloch equations could be more appropriate.

2.3 Theoretical considerations in a three-level ladder system

Applying other theoretical models to our three-level ladder system is also useful in understanding our experimental results. Other available approaches for interpreting excitation processes in our system include solving the optical Bloch equations. In addition, carefully doing numerical integration of the time dependent Schrödinger equation can be another solution. The advantage of using these two is the need to make fewer assumptions about cross terms in the excitation. For example, a model is given by Felinto *et al.* in which the optical Bloch equations are applied to a three-level system interacting with a train of pulses delivered by a frequency comb. This theory reported the results of the sequential two-photon absorption process while discussing the role of parameters like the laser repetition period

and the phase difference between the femtosecond pulses.

However, using optical Bloch equations has its disadvantages. It has a less flexible formulation and loses intuitiveness if we compare it to the second order perturbation theory. In addition, the numerical integration of the optical Bloch equations mostly requires more computation time. In our case, the final excited state population in the three level ladder system is detected by ionizing of atoms in the excited states. However, the final step for ionization has continuum states. Including the continuum states makes use of the optical Bloch equations much more difficult.

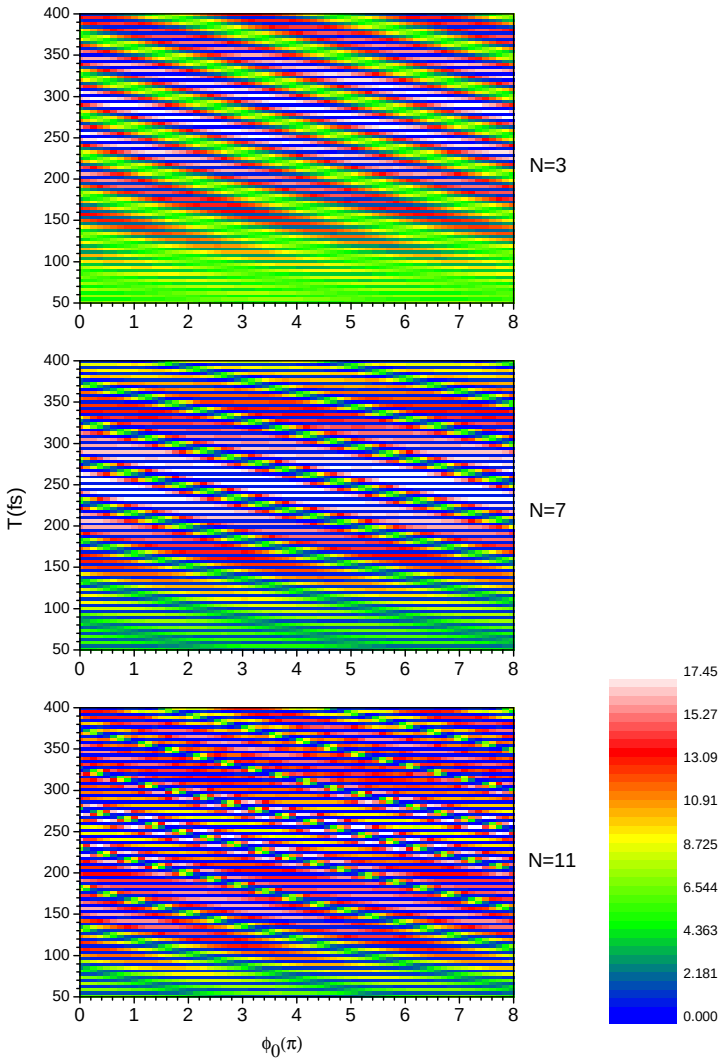

Figure 2.3: *Simple theoretical calculations using Eq. 2.5 show the count rate in the* $5d_{3/2,5/2}$ *state as a function of* T *and* ϕ_0*. The level structure used in these calculations is a three level Rb atom ladder system with* $5s_{1/2}$*,* $5p_{3/2}$ *and* $5d_{3/2,5/2}$*. N is the effective number of pulses in the train.*

Chapter 3

Experimental Setup

The goal in this dissertation was to study the interaction between a train of pulses and an atomic ladder system. Before analyzing and explaining the experimental results and laying a foundation for understanding the interaction, we look at the experimental setup. The basic process of collecting data allows us to outline the experiment and how the experiment obtains results. This chapter describes our experimental apparatus.

The experimental setup has four sections. In the first section, we discuss how the MOTRIMS technique produces the cold target. Detecting ions are also described with this general overview of the development of the MOTRIMS technique. Second, we discuss the laser control as an essential for preparing cold target atoms and generating a train of pulses for coherent control in the atomic ladder system. This section discusses frequency locking, saturated absorption spectroscopy, timing for narrow bandwidth CW lasers, and the ultrafast laser. Third, we explain the technical aspects of preparing a train of short pulses by shaping the spectral phase of an ultrafast laser. Fourth, the data acquisition system is discussed in detail.

3.1 MOTRIMS technique

The basic experimental setup in this dissertation used magneto-optical trap recoil ion spectroscopy (MOTRIMS). In the experiment studying interaction between light and matter, the MOTRIMS[57,58] setup measured ions created from a cold target in a MOT. MOTRIMS

measures the population transfer of the atomic or molecular system with high resolution. The MOTRIMS technique has sensitive time-of-flight discrimination of detected ions with high temporal resolution ($\sim$ 2 nsec). The system resolution is not restricted by target momentum spread as long as atoms are cold enough to be held in the MOT. It is limited by timing and detector resolution. The technique of MOTRIMS, as it was used here, is used within the context of measuring the interaction between light and cold atoms; other details can be found elsewhere[59–61].

3.1.1 Development of MOTRIMS

Many methods of trapping and cooling atoms have been used in atomic and molecular physics. MOTRIMS combines the cold target recoil ion momentum spectroscopy (COLTRIMS) technology for measuring the momentum vectors of the target fragments and technology using lasers to cool and trap target atoms. COLTRIMS uses inverse kinematics by measuring the momentum vectors of target fragments that are charged when a target interacts with the projectile.

Three groups[57,62,63] in different places independently developed the MOTRIMS technology. The technology for the cooling and trapping of target atoms using lasers was merged with the COLTRIMS technology. Using a magneto-optical trap (MOT) for cooling and trapping the target in a localized area provides several advantages. First, recoil momentum resolution can be improved because of the extremely low temperature of the target atoms. It thus became possible to do high-resolution spectroscopy requiring finer precision in the dynamics because one can resolve the initial and final states involved in the collision. In addition, MOTRIMS technology allows investigating cold collision dynamics because the temperature regime of an ion-atom collision experiment is far lower than the temperature regime of COLTRIMS cooling technology. The COLTRIMS method is limited by target temperature even though it cools down the target atoms by using a combination of supersonic expansion, collimated jets, and cold finger pre-cooling[64,65]. Second, MOTRIMS

provides the possibility to study a wider range of atomic species than COLTRIMS[60]. The elements having optically active electrons such as alkali and alkaline-earth atoms can be trapped in a MOT; these elements cannot be efficiently cooled in the COLTRIMS technique, with its supersonic expansion, because the elements tend to compose molecules or clusters. Moreover, this class of atoms can be initially prepared in excited states. Therefore, it extends the sphere of targets in recoil ion momentum spectroscopy (RIMS) measurements where one can adjust the initial excited state of target atoms. Finally, COLTRIMS provides all kinematic information for all ejecta but typically only a few ions per laser pulse can be detected because the time of fight (TOF) is measured by delay-line anodes coupled to multi-hit time-to-amplitude converters with high resolution.

3.1.2 Cold atoms in a Magneto-optical trap (MOT)

Much of the literature already covers how to construct a MOT, so we include only an explanation for a MOT as it applies to the system used in this research. Laser cooling and trapping was used to prepare cold target atoms, an achievement used in several frontiers[12,66,67], using a MOT, which is widely used in many applications of atomic physics because it is a useful tool for trapping atomic gases at high density and very low temperatures.

One fascinating aspect of using a MOT is that it offers cold atoms that ignore the Doppler broadening effect. Therefore, MOTs are often used in atomic physics when having no Doppler broadening effect is necessary. Laser cooled atomic clouds are used to study the interaction between atoms and light and serve as cold atom sources for other experiments like atom interferometry; the construction of better atomic clocks; Bose-Einstein condensation; collision studies; and metrology like precision measurements of time and frequency, tests of fundamental symmetries, and basic laws of nature.

Two basic conditions of a MOT should be satisfied in its construction. One is slowing down atoms using radiation pressure forces from near-resonant laser light. That is, the radiation field produced by a laser provides a velocity-dependent force that interacts with

atoms and cools them. However, the cooled atoms still move slowly without a fixed location if there is no position-dependent force. The other necessary condition to build a MOT is an inhomogeneous magnetic field, making the light forces position dependent by adding a magnetic field gradient to a MOT where a spatially dependent Zeeman shift in the atomic transition frequencies is produced by the magnetic field.

One attractive candidate for precision control of multi level atomic systems is ^{87}Rb, the selected element in this research, an alkali metal atom and having a relatively simple spectrum, making it convenient to cool and trap. It has a smaller nuclear spin (I=3/2), meaning fewer hyperfine states. ^{87}Rb has two D-line components. However, only the D2 line, with a transition from $5s_{1/2}$ to $5p_{3/2}$ is used to produce our MOT. The hyperfine structure of the $5s_{1/2}$ ground state and $5p_{3/2}$ excited state are shown in Fig. 3.1. The transition wavelength of the trapping laser is 780.03 nm. The population is excited by a trapping laser from $5s_{1/2}$ ground state into $5p_{3/2}$ state, which has a lifetime of 26.63 ns.

In a ^{87}Rb MOT, the two critical effects induce atoms to be trapped and cooled to about 120 μK in a vapor cell. The applied magnetic field gradient of the MOT is approximately 1 gauss/cm, which induces maximum Zeeman shifts of approximately 1MHz. The atom cloud was monitored by a CCD detector. In a localized trapping region, the diameter of the MOT is typically a few millimeters.

Two lasers are used to construct the MOT. One laser does all the trapping and cooling, coupling the $F = 2$ hyperfine level of the $5s_{1/2}$ ground state to the $F = 3$ of the $5p_{3/2}$ excited state. The trapping laser is slightly detuned about 15 MHz to the low frequency side of the $5s_{1/2}, (F = 2) \rightarrow 5p_{3/2}, (F = 3)$ transition, as shown in Fig. 3.1. Atoms in a particular velocity group are Doppler shifted into resonance transition and can be trapped by absorbing the momentum kick from photons. This slight detuning from resonance transition is necessary to trap atoms because if the lasers are tuned exactly to the $5s_{1/2}, (F = 2) \rightarrow 5p_{3/2}, (F = 3)$ transition, only the atoms that move very slowly at the zero-point of the magnetic field gradient can be excited from the ground state. That is, the trapping laser

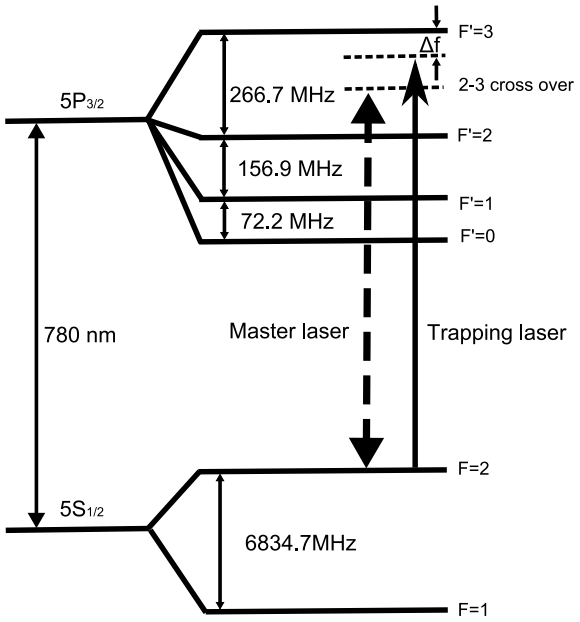

Figure 3.1: *^{87}Rb D2 line hyperfine energy levels and the MOT trapping transition. The master laser is locked to the crossover of the transitions from F=2 to F'=2 and F'=3. The master laser is injected into an acousto-optic modulator (AOM) and locked by the saturation absorption peak where the master laser frequency is shifted by the AOM. The trapping laser is red-detuned with Δf from the cycling transition from the $5s_{1/2}, (F = 2)$ state to the $5p_{3/2}, (F' = 3)$ state.*

must to be detuned from the resonant transition to increase the number of trapped atoms. The optimum detuning of a trapping laser is generally a few linewidths. However, one also needs to consider the details of the atom source and the trapping laser intensity[68].

Another laser is required, because one excitation out of 1000 is to the $F' = 2$ level and the atom can decay to the $F = 1$ state instead of the $F = 2$ state. This atom is then out of cycling transition with the trapping laser. Another laser called a repumping laser excites the atom from the $5s_{1/2}, (F = 1)$ to the $5p_{3/2}, (F = 2)$ state, as shown in Fig. 3.2. Therefore, the atoms decaying to $5s_{1/2}, (F = 1)$ can be recycled by the repumping laser to again be excited by the trapping laser.

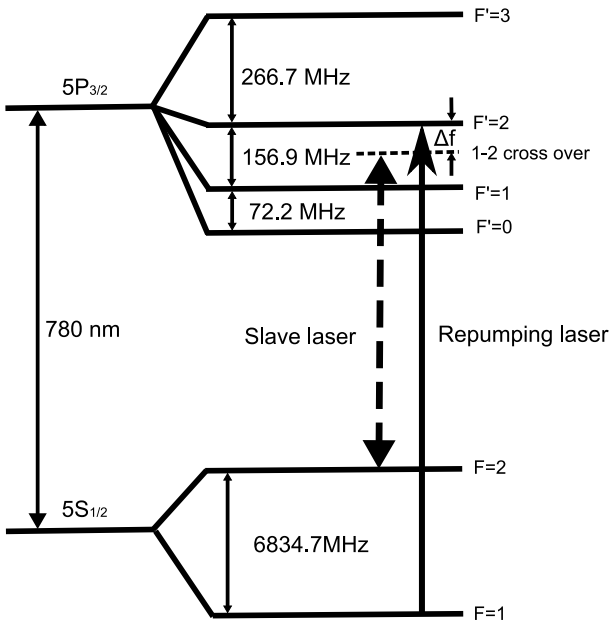

Figure 3.2: ^{87}*Rb D2 line hyperfine energy levels and the MOT repumping transition. The slave laser is locked to the 1-2 crossover of the transitions from F=1 to F'=1 and F'=2. The slave laser is injected to a AOM and locked by the saturation absorption peak where the laser frequency is shifted by the AOM. The repumping laser is matched to the on-resonant transition from the* $5s_{1/2}, (F = 1)$ *state to the* $5p_{3/2}, (F' = 2)$ *state.*

3.1.3 Recoil ion momentum spectroscopy technology

The MOT explained in the previous section is a target of MOTRIMS shown in Fig. 3.3. Another essential part of MOTRIMS is Recoil Ion Momentum Spectroscopy (RIMS), which is important in detecting ions from the target. The MOT is located inside of an electrostatic momentum spectrometer in the stainless steel vacuum chamber. Ions produced in the trapping region are extracted by the electric field generated from the spectrometer and detected by a micro-channel plate and resistive anode 2-dimensional position sensitive detector[59].

The spectrometer is made of a solid plate and rings connected together with 1 MΩ resistors[70]. The rings and the holes allow laser light to pass through the spectrometer.

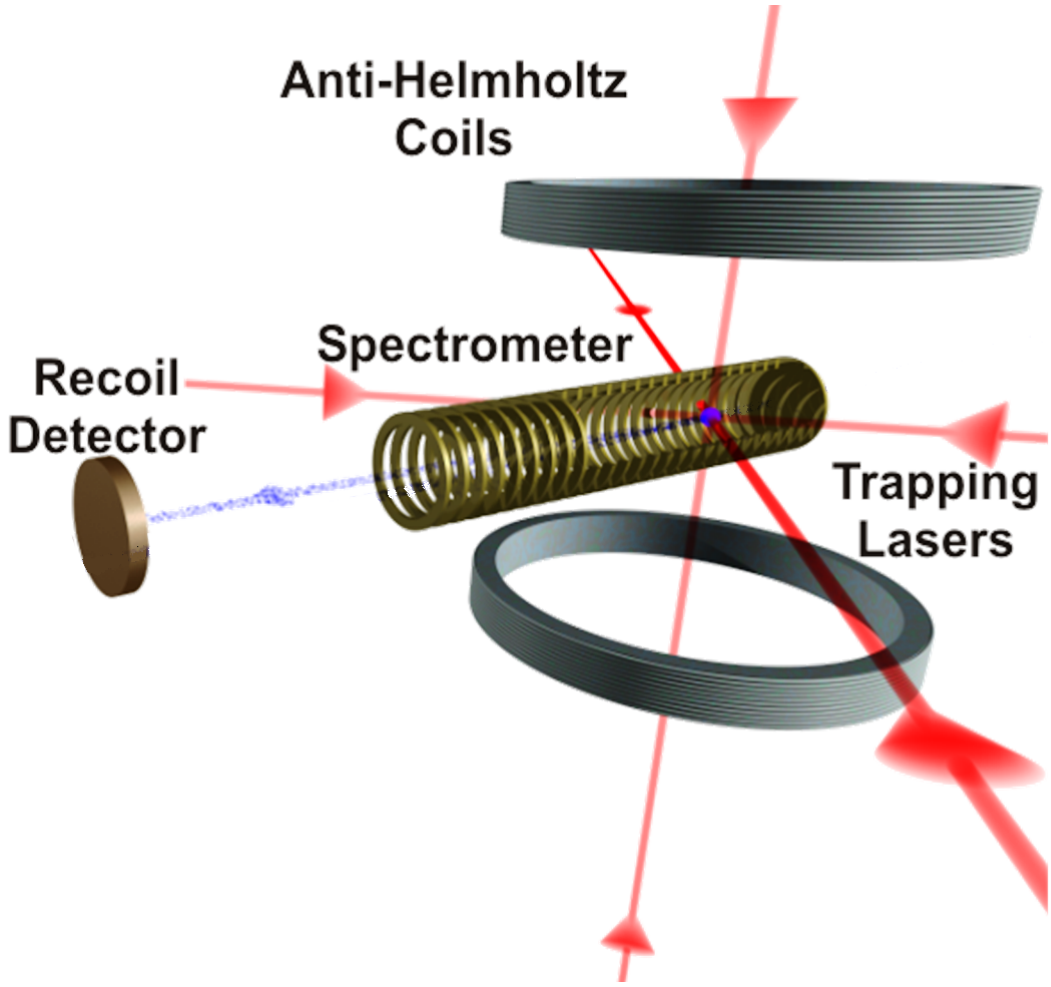

Figure 3.3: *The simplified MOTRIMS experimental apparatus*[69]*. The six red beams represent the trapping lasers. The blue spot at the center of chamber represents the MOT. Ions produced from the MOT are extracted by the spectrometer (brass rings) and hit the 2D position sensitive detector (PSD). Anti-Helmholtz coils produce the magnetic field gradient.*

The spectrometer makes it possible to separately detect atomic Rb ions and molecular Rb ions in TOF. The ions produced from the interaction region are extracted by a weak electric field of approximately 10 V/cm in the spectrometer[71]. In a subsequent drift region, atomic and molecular ions have different TOF so that we can separately measure different species ions. The spectrometer was originally designed to precisely measure both Q-Value and scattering angle[59,70]. The solid plate, also called a pusher plate, extracts ions and so has a voltage applied to it. A focus voltage is applied independently to one of the rings.

The spectrometer spatially focuses ions and improves momentum resolution. The time and spatial focusing configuration of the spectrometer provides high resolution 3 dimensional momentum measurements of ions created in the MOT.

The resolution of the spectrometer as limited by electronics is about 2 nsec. Information about TOF with high resolution is important, but especially for experiments using ultrafast lasers. The measurement of TOF is critical for accurately determining the time from the initial laser pulse input into the system to the time an ionization occurs. The measurement allows us to separately identify particular ions in which we are interested, which is useful for analyzing molecular dynamics by setting a time window for TOF[72].

3.2 Laser control

Controlling the laser is essential to this experiment. The techniques related to laser control are described below. This section explains four separate ways to control lasers: saturated absorption spectroscopy, laser dither lock, magnetic field dither locking and control of laser pulse timing of continuous wave (CW) and ultrafast lasers.

3.2.1 Laser stabilization

Special powerful sources providing narrow output lines and the possibility of wavelength detuning are necessary for atom cooling. Typically, CW single-frequency Ti:sapphire lasers and diode lasers are used to cool Rb. Diode lasers are more commonly used than the Ti:sapphire laser because Ti:sapphire is far more expensive although it provides higher power (1 W). Accordingly, the cooling and trapping process for target atoms are done by CW lasers. Narrow linewidth CW diode lasers at 780 nm are used as repumping and trapping lasers. The lasers require a stable frequency locking system to build a robust and reliable laser trapping experimental apparatus. The peak intensity of the trapping laser after an amplifier is about 100 mW/cm^2. The trapping laser need an accurate and stable frequency lock because it must be red detuned by 18 MHz from the $5s_{1/2}, (F = 2) \rightarrow 5p_{3/2}, (F = 3)$

transition in atomic Rb to optimally cool and trap the target atoms.

Locking a laser frequency can be done with various methods, but a peak locking scheme is suitable for obtaining accurate frequency locking in this experiment. Side-locking techniques cannot conveniently control the frequency lock point even though they provide a wide frequency tuning range. The large tuning range is, however, is unnecessary for repumping and trapping lasers. Considering the requirements of the experiment, Doppler-free saturated absorption method[73–75] is useful for peak-locking, and has been used for locking lasers because the lasers require a known frequency reference to lock laser frequencies.

Other frequency locking schemes[76,77] can be used to lock the lasers. However, Doppler-free saturation absorption is a reasonable compromise because it is low cost and convenient in constructing the whole experimental setup; it requires only a Rb vapor cell, photodiodes and a simple feedback electronic system. The technical details are illustrated elsewhere[61,70].

3.2.2 Repump laser with laser dither lock

Figure 3.4 shows a schematic diagram of the Doppler-free saturated absorption optics. After the frequency of the slave laser is shifted by the repump AOM, it is called a repump laser. The repump laser uses only the saturation absorption spectroscopy method and does not use a magnetic field dither locking scheme. The output power of a commercial tunable external cavity diode laser is about 30 mW and the linewidth is less than 1 MHz. A beam splitter splits the laser beam into two beams. By adjusting a half-wave plate, a tiny portion (0.3 mW) of laser output goes to the Rb cell to prevent laser power broadening. The tiny fraction of laser beam toward a Rb cell produces two probe beams with roughly the same intensity as they are reflected from the front and back sides of a thick glass plate (6 mm). The beam passing through the thick glass is a pump beam with an intensity about ten times higher than the probe beams. However, a large portion of the repump laser output is sent to the repump AOM which controls the pulse timing of a repump laser. The repump AOM also slightly tunes the frequency of the input beam to the blue by about 80MHz.

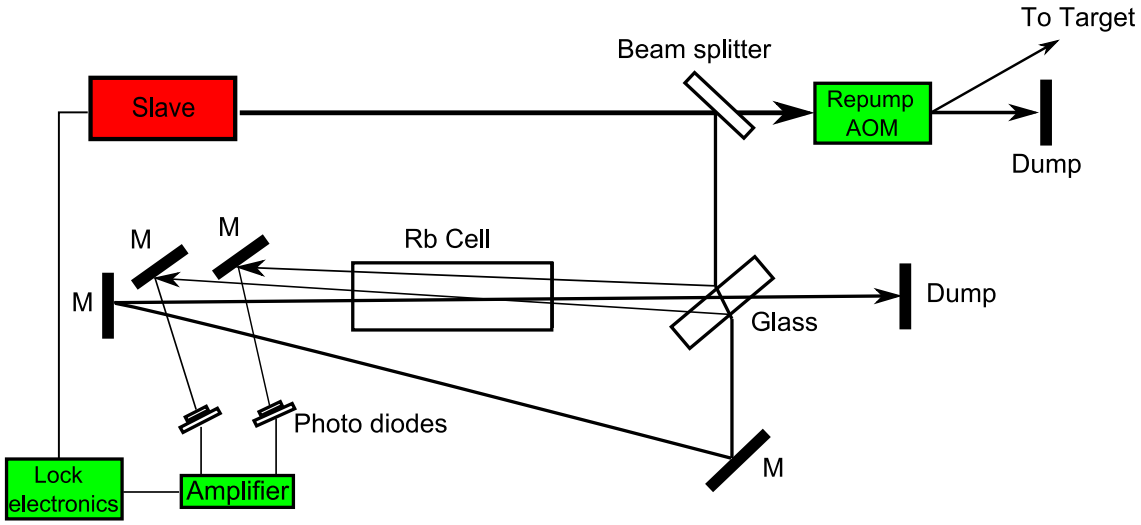

Figure 3.4: *Schematic of the basic locking apparatus for a repump laser. Saturated absorption spectroscopy is used for the laser dither locking technique. The laser is dithered to create an absorption spectra. M represents a mirror.*

Figure 3.2 shows that the repump laser is locked to the 1-2 crossover peak which is in the middle of the $5s_{1/2}, (F = 1) \rightarrow 5p_{3/2}, (F = 1)$ transition and the $5s_{1/2}, (F = 1) \rightarrow 5p_{3/2}, (F = 2)$ transition. The locking point is $\sim$ 79MHz to the red of the $5s_{1/2}, (F = 1) \rightarrow 5p_{3/2}, (F = 2)$ repump transition. The transition of a repump laser matches to the atomic resonance transition by shifting the frequency using the repump AOM.

3.2.3 Trap laser with magnetic field dither lock

Magnetic field dither locking has similarities to the laser dither lock. A magnetic field dither locking technique is added to the locking scheme using the saturated absorption spectrum

of the Rb atom. However, the frequency of the atomic spectral line is dithered by applying a weak magnetic field, instead of dithering the frequency of the laser. The optical setup is basically same as the laser dither lock, except a solenoid around the rubidium cell applies a magnetic field, and quarter wave plates convert linear polarized light into circular polarized light. Figure 3.5 shows the optical setup of the magnetic field dither locking scheme. The basic electronics to lock the laser are also very similar to the electronics used in the laser dither lock, while the frequency of the laser field is not dithered itself. A magnetic field generated from a solenoid around the rubidium cell is dithered. The solenoid has one layer of windings of 180 turns and a length of 20.5 cm. A stable root mean squared AC current (2.6 A) is carried to the solenoid creating a dithering magnetic field amplitude of 0.004 T. This magnetic field dithering causes Zeeman shifts in the atomic frequency, which produces similar absorption peaks as in absorption spectrum of the laser dither lock. The same technique of integrating over an absorption peak is used, and the lock electronics operate identically to the laser dither lock scheme. Dithering the magnetic field instead of laser frequency has the advantage of avoiding laser line width broadening due to frequency modulation. A feedback signal from the locking electronics to provide correction is supplied to the laser only when the lock point of the absorption spectrum is shifted by external noises.

The locking point of the trap laser is $\sim$ 133MHz to the red of the $5s_{1/2}, (F = 2) \rightarrow 5p_{3/2}, (F = 3)$ transition. The trap AOM slightly tunes the frequency of the input beam to the blue by about 118MHz. The frequency shifted beam is sent to the experimental chamber that traps Rb atoms. The master laser is locked to the 2-3 crossover peak, which is in the middle between the $5s_{1/2}, (F = 2) \rightarrow 5p_{3/2}, (F = 2)$ transition and the $5s_{1/2}, (F = 2) \rightarrow 5p_{3/2}, (F = 3)$ transition in Fig. 3.1.

3.2.4 Pulse timing control for CW lasers and KLS

To drive coherent excitation from the MOT target, appropriate control for pulse timing of lasers is critical. The Kansas Light Source (KLS), an ultrafast laser, provides excitation

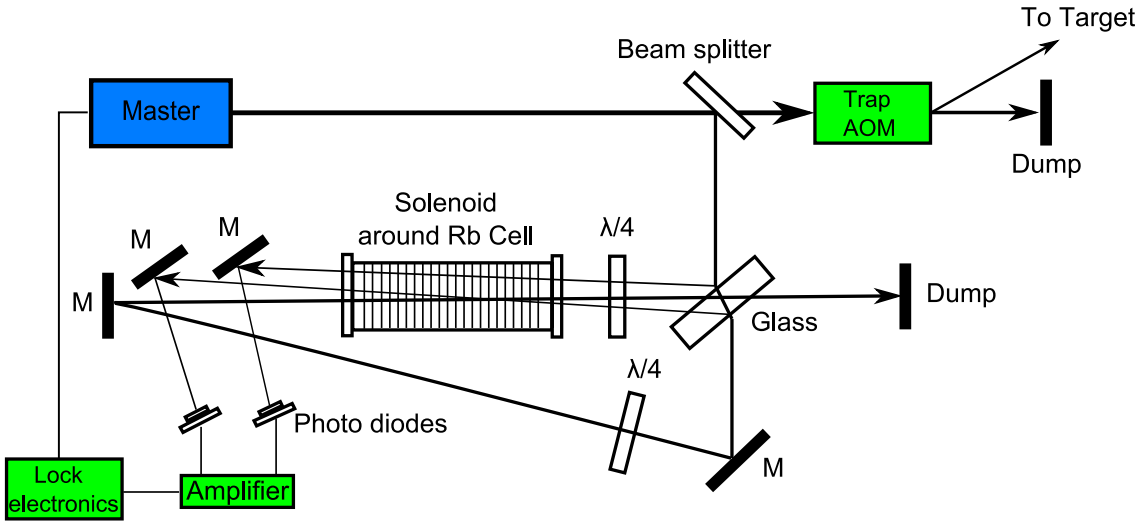

Figure 3.5: *Schematic of the basic locking apparatus for the trapping laser. Saturated absorption spectroscopy is used for the magnetic field dither locking technique. The magnetic field is dithered to produce an absorption spectrum. M represents mirrors.*

in the atomic ladder system. The excitation laser must be synchronized to the trap and the repump signals and has a 2 kHz repetition rate. A delay gate generator, called the main delay gate generator, was constructed for this purpose. It generates the signals (TTL) necessary to control the AOMs and supplies the appropriate electrical pulses (NIM) for timing to the data acquisition system. The circuit design of the main delay gate generator is explained in Appendix B with more detail.

The TTL pulses from the delay gate generator are sent to the AOMs. As we noted in the previous subsection, the AOMs control pulse timing by turning on and off on nanosecond time scales. The AOMs also shift frequencies as needed. Thus, AOMs manipulate pulse

timing of CW lasers like the trap laser and the repump laser. The proper control of pulse timing allows us to build a MOT. It can turn the trap and repump lasers on and off as well as synchronize them with an excitation laser in nanoseconds. In the experiments, we adjust the laser pulse timing to start with all the population in the ground state for the coherent excitation process. The trap and repump lasers were turned off by the AOMs for 300 nanoseconds before the excitation laser was turned on. The time is chosen to be much longer than the lifetime of the Rb(5p) and Rb(5d) states, but shorter than a few milliseconds[78] which is the time required for atoms to escape from the trapping region. In addition, the trap and repump lasers were turned on again approximately 2 microseconds after the excitation laser was turned off. Therefore, we can be sure that the trap and repump lasers don't provide excitation from the ground state while the excitation laser is turned on. The lasers in a MOT shouldn't excite the target while excitation lasers interact with atomic ladder system, thus assuring the observations of the interaction come from the excitation lasers.

3.3 Technical aspects of shaping ultrafast laser

An ultrafast laser and a pulse shaper are used for coherent excitation to study the interaction in multilevel atomic ladder systems. The output of the ultrafast laser has a broad bandwidth covering all atomic resonance transitions required by a given atomic Rb ladder system. A train of pulses is generated by applying a sinusiodal spectral phase with a pulse shaper.

3.3.1 Ultrafast pulse shaping

Over the past three decades, a huge number of devices, materials, and methods have been developed for shaping ultrafast laser pulses. Pulse shaping techniques have been used in a broad range of applications[79–81] such as coherent control over ultrafast physical processes, high field physics, nonlinear optical biomedical imaging, and high-speed communications. One great pursuit of researchers was developing an ultrafast laser to control chemical re-

actions by using the shortest possible length of laser pulses. For instance, the technology for pulse compression[82] has been developed to obtain bandwidth-limited pulses which offer the best possible time resolution in time-resolved measurements. However, to attain desired chemical reactions, more technologies based on coherent control were required in a wide range of applications in spectroscopy, laser pulse compression[82], and optical metrology[83]. The advent of technology for the shaping of ultrafast laser pulses wholly satisfied the requirements.

Recent techniques showed that the relative spectral phase[84,85] between driving laser fields was used as a convenient control parameter in quantum optics. In principle, this technique is very beneficial for manipulating quantum interference between multiple-atomic-transition pathways which gives rise to many interesting applications. Progress in the field of coherent control has been closely linked to the development of femtosecond pulse shaping techniques. In particular, shaping the phase and amplitude of a pulse in the frequency domain provides a mechanism for controlling excitation in an atomic ladder system. A shaped pulse in an ultrafast laser is conveniently described by an electric field in the frequency domain as,

$$E(\omega) = E_0(\omega)\exp(-i\phi(\omega)), \tag{3.1}$$

where $E_0(\omega)$ is the electric field amplitude and $\phi(\omega)$ is the spectral phase. Shaping the pulse in the frequency domain by adjusting $E_0(\omega)$ and $\phi(\omega)$ is equivalent to shaping the pulse in the time domain because they are related through the Fourier transform.

3.3.2 Experimental setup with KLS and AOPDF

The ultrafast laser used in this experiment is generated by the KLS of the J.R. Macdonald Laboratory[86,87]. KLS is an ultrafast high intensity laser facility for studying the fastest dynamics in atoms and molecules. The entire KLS will not be explained here because it is a large facility, and some parts are not related to this experiment. Basic information is provided for the parts associated with this dissertation.

Figure 3.6 shows the entire experimental setup with the KLS: a pulse shaper and

MOTRIMS by following the order of manipulating pulses and detecting of ions. A Ti:Sapphire oscillator and an amplifier together generate a 2 kHz, approximately 40 fs laser pulse with a central wavelength of roughly 790 nm. The laser system can generate extremely short pulses, as short as 8 femtoseconds. An oscillator produces the ultrafast and wide bandwidth pulses with a repetition rate of 80 MHz. The energy of each pulse is on the nanojoule scale. The pulses can be amplified to $\sim 1 - 2$ mJ. The oscillator beam consists of a Ti:Sapphire crystal pumped by a CW laser. In the resonating cavity of the oscillator, the created standing waves generate discrete frequencies where the mode separation is inversely proportional to the cavity length. To be amplified, pulses are picked out of the oscillator pulse train at a 2 kHz repetition rate by a Pockels cell. The selected pulses are passed through a grating stretcher, which creates a positive second order phase term to the pulses to temporally stretch them in the time domain. This process makes it possible to avoid damage to the amplifier crystal because the pulse peak power goes down after passing through a stretcher.

The temporally stretched pulses are used as the input for a pulse shaper. The pulse shaper manipulates the spectral phase of a train of pulses selected by a Pockels cell. The pulse shaper turns each single pulse into an infinite train of pulses. That is, the infinite train of pulses from the pulse shaper is amplified by passing multiple times through the gain medium, the Ti:Sapphire crystal, which is cryogenically cooled. The output pulse train from the amplifier is subsequently compressed by a grating-compressor into a train of 40 fs pulses while the grating compressor takes off the large second order phase term caused by the stretcher. Therefore, before shaping the spectral phase, the output beam after stretcher is a transform-limited pulse having a flat spectral phase.

Shaping a pulse with the acousto-optical programmable dispersive filter (AOPDF) can give rise to a slightly changed pulse energy. We use an integrating optical power meter to measure the pulse energy at the downstream of the target cold atoms. The output from the power meter is fed back to the Pockels cell to maintain a constant pulse energy on target. The pulses are then sent through a 20 meter evacuated transport line to hit the

experimental target. The direction of a laser beam can be misaligned because the transport line is very long, so an Automatic Laser Pointing Stabilizer (ALPS) can help keep the laser beam pointing at the target atoms. Any ions produced in the MOT are extracted by the electric field and detected by the 2-dimensional position sensitive detector.

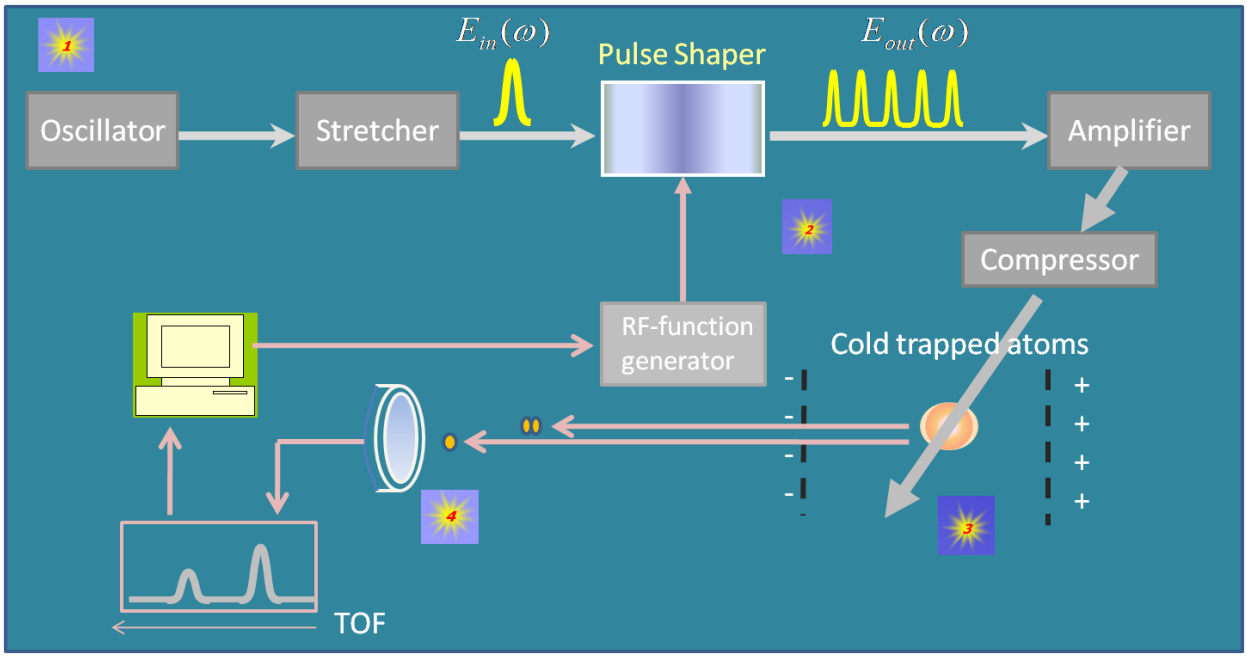

Figure 3.6: *Simplified schematic for generating a train of pulses and detecting signals. The experiment has a sequence of four main parts. First, a source from a laser oscillator is generated. Second, a sinusoidal spectral phase is applied to the pulses by a pulse shaper. Third, shaped pulses hit cold trapped atoms. Fourth, ions are detected by a time-of-flight spectrometer.*

A pulse shaper can arbitrarily manipulate the phase and amplitude of the optical pulse in the frequency domain. We are only interested in changing the spectral phase so that the AOPDF was not used to modify the spectral amplitude of the pulse. In some experiments, indirect pulse shaping is needed because pulse shapers cannot be used directly on the pulse to shape. In these experiments using the KLS, the pulse shaper, AOPDF manipulated only the spectral phase of the light because the amplifier would partially "undo" any spectral amplitude shaping. However, this pulse shaping can still from pulse train. The amplified power in the amplifier is carefully monitored and kept in the low power region where the

amplifier is linear for the spectral phase.

3.3.3 AOPDF

Ultrafast optics have been revolutionized in the past two decades, driven by novel technologies to generate, amplify, and manipulate pulses. For example, a pulse shaper has been used to make more complicated alterations to the spectral phase and the spectral amplitude of ultrafast laser pulses. This technology is relatively new. For example, pulse shaping has been done by using programmable spatial light modulators, acousto-optic modulators, holographic masks, and deformable mirrors[79]. The AOPDF is one such technology, here briefly explained with its effects. In the next chapter, the experimental results using the AOPDF are explained in more detail, specifically focusing on how the AOPDF[3,88–90] allows us to generate a train of pulses.

The AOPDF has an arbitrary radio frequency (RF) generator coupled to a crystal of TeO_2 via a piezoelectric transducer. Called the Dazzler commercially, it supplies RF acoustic waves to a crystal which enables one to shape the spectral phase and amplitudes of an optical pulse through the acousto-optic interaction. The RF generator includes the fast electronics and produces an analog high power RF signal. Two critical effects demonstrate how the AOPDF operates to shape pulses. First, two different polarizations of light create different velocities of propagation in a crystal because of the crystal's birefringence. Second, the coupling of an acoustic wave with an electromagnetic wave operates as a control knob to selectively rotate the light polarization.

In the AOPDF, each optical frequency component is independently controlled. For example, the amplitude of an optical frequency component is adjusted by rotating the polarization of its component. To obtain the maximum output magnitude, the frequency component is rotated by 90 degrees. If it doesn't rotate at all, the output magnitude is zero because it dumped. The only output from a crystal is the frequency component perpendicular to the input polarization because of the birefringence of the crystal. The

phase of a frequency component is controlled by the traveling distance of light in the crystal after its rotation. Each frequency component has a different time delay because the velocity of light in different polarization axes differs.

The finite length of the crystal restricts the AOPDF in shaping pulses because the length of the crystal limits the maximum group delay to be applied to any frequency components. The length of TeO_2 crystal is approximately 2.5 cm where the speed of sound along an optical axis is 1000 m/s, the index difference is Δn=0.04, and to the maximum achievable group delay is about 3 ps[89]. The wavelength calibration of the shaper was independently verified by programming a narrow hole in the spectrum. The wavelength calibration of the shaper was tested by monitoring the shaped output of the device with a spectrometer. In this way, the wavelength calibration of the shaper was better than 1 nm. In addition, the work of Chatel et al[91] showed that the acoustic power should generally be kept between 10 and 20 percent of the maximum value of the optical pulses because the accuracy of shaping is best at lower acoustic power.

3.3.4 Sinusoidal spectral phase

The sinusoidal spectral phase is sometimes used in the coherent control because it gives rise to an interesting temporal profile. Here, single pulses are chosen from an oscillator having an 80 MHz repetition rate by using a Pockels cell whose a repetition rate is 2 kHz. We apply a sinusoidal spectral phase to the pulses by using an AOPDF pulse shaper. Each single pulse becomes a train of pules which is amplified and then hits target atoms. The sinusoidal spectral phase is given by

$$\phi(\omega) = A\sin(\omega T + \phi_0), \tag{3.2}$$

where A, T, and ϕ_0 are free parameters. The electric field envelope after application of sinusoidal spectral phase is as

$$E_{out}(\omega) = E_{in}(\omega)\exp(-i\phi(\omega)), \tag{3.3}$$

where E_{in} is the input electric field envelope in frequency domain before application of the sinusoidal phase and E_{out} is the output electric field envelope after application of the sinusoidal phase. The Jacobi-Anger identity,

$$\exp(iz\cos(\theta)) = \sum_{n=-\infty}^{+\infty} i^n J_n(z)\exp(in\theta), \tag{3.4}$$

is applied to Eq. 3.3. When the spectral phase of Eq. 3.2 is inserted into Eq. 3.3, the output is a series of replicas of the input pulse in the time domain. As a consequence, the temporal profile of a pulse which is shaped by applying the sinusoidal spectral phase is expressed by

$$E_{out}(t) = \sum_{n=-\infty}^{+\infty} J_n(A)E_{in}(t-nT)\exp(-in\phi_0), \tag{3.5}$$

where E_{in} is the electric field envelope in time domain before application of the sinusoidal phase and E_{out} is the electric field envelope after application of the sinusoidal phase. The replicas are thus a train of optical pulses which are regularly separated in time by T. The amplitude of each pulse in Eq. 3.5 is weighted by the Bessel function, $J_n(A)$, and pulse-to-pulse phase difference is ϕ_0. As we can see, there is an infinite series of replicas in Eq. 3.5. However, one can choose the effective number of pulses in them by the selection of A. In Appendix D, more detail discussion describes an approach for suitable choice of A.

To show an example of a generated train of pulses, we take $E_{in}(t)$ as a Gaussian 40 fs in width. Fig. 3.7 shows a plot of $|E_{out}|$ from Eq. 3.5 *versus* time. In addition, Fig. 3.7 shows a plot of the relative phase shift between the pulses in units of π where, as an example, the chosen values are $A = 2.5332$, $T = 250$ fs, and $\phi_0 = \pi/4$. The interesting thing is that the train of pulses in Fig. 3.7 is similar to the output of a frequency comb laser in the time domain except for the Bessel function amplitudes and the phase jump irregularity. The phase shifts shown in Fig. 3.7 are asymmetric about the central $n = 0$ peak because of the well-known relationship $J_{-n}(x) = (-1)^n J_n(x)$ which causes an additional π phase jump between pulses for odd negative values of n. It is not clear how the truncated nature of the pulse train affects observed results in our experiments.

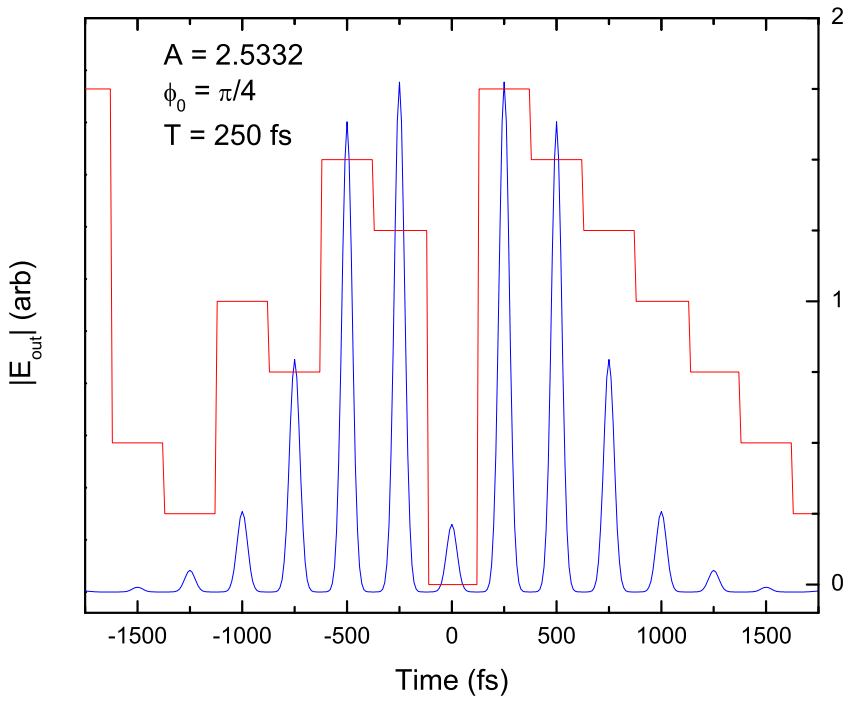

Figure 3.7: *The output pulses in the time domain when a sinusoidal spectral phase like that of Eq. 3.2 is applied to a Gaussian transform-limited input pulse.* $|E_{out}|$ *is shown as a curve of pulse-like structures in blue color, while the boxy curve in red shows the absolute phase of each pulse which is relative to some arbitrary zero.*

The generated train of pulses is sent to the target region where it has an energy of about 2 μJ in a 2 mm^2 area. The peak intensity is about 10^8 W/cm^2. As already mentioned, the target consists of ^{87}Rb atoms which are trapped and cooled so that we can ignore Doppler effects. Fig. 2.2 shows the relevant energy levels in the atomic ladder system.

3.4 Data Acquisition System

The data acquisition process is designed to measure atomic or molecular ions. The data acquisition system, one of main parts in the MOTRIMS technology, measures the TOF and ion position on the detector. In each data run, the data acquisition computer controls the operation of various experimental instruments. The acquisition system records the time difference between the initial laser pulse and ion events with the relevant 2D position information on the detector. When a signal from the detected ion triggers an event, the data acquisition system starts recording data. The operational signal is sent into the TDC on the CAMAC crate and is read into the computer by the acquisition program which is programmed to read information from the CAMAC modules.

The data acquisition system has three main parts. First, the constructed main delay gate generator controls the pulse timing for CW lasers and the ultrafast laser. In this experiment, a delay gate generator allowed control of the pulse repetition rate, pulse width, pulse delay, and pulse amplitude. Second, a Time to Digital Converter (TDC) measures TOF with two input signals to start and to stop. Third, an analog-to-digital converter (ADC) recorded the 2D position information of the ions.

Figure 3.8 shows the basic diagram of the data acquisition system. The repump laser and the trap laser must be synchronized with signals from the pulses from the KLS based on its 2kHz repetition rate. For appropriate control of pulse timing, the main delay gate generator generates the TTL signals to control the AOMs and provides the appropriate NIM pulses to the data acquisition system. More details are described in Appendix C. In the main delay gate generator, a TTL pulse from KLS is converted into a NIM level pulse which provides the start signal for a coming event. If a laser pulse does not produce an ion, there is no event. By appropriately adjusting the delay and gate width, unwanted signals of atomic Rb ions coming from warm background atoms are gated out and the signals from cold atoms are measured.

The signal from KLS triggers the main delay gate generator. The KLS pulse arrival goes

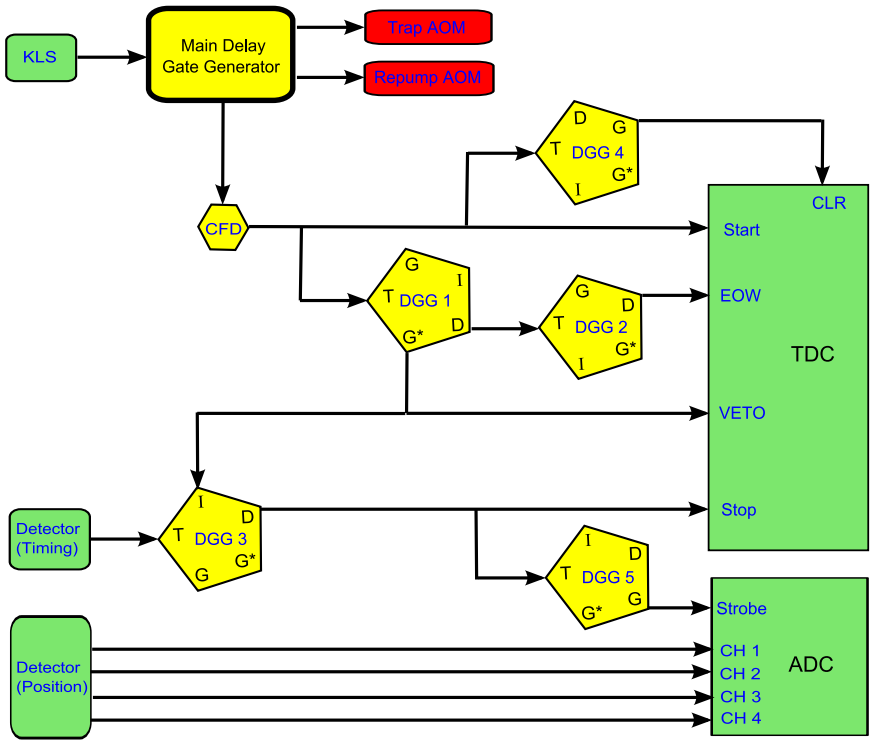

Figure 3.8: *The data acquisition system with basic electronics. TDC:Time to Digital Converter, ADC: Analog-to-Digital Converter, CFD: Constant Fraction Discrimnator, DGG: Delay Gate Generator; T: Trigger, G: Gate, I: Inhibit, D:Delay*

to a TDC as a start signal. The timing signal from the arrival of an ion at the detector triggers the delay gate generator (DGG3) from which the TDC obtains a stop signal. In the delay gate generator (DGG1), a gate is generated where the gate is a NIM false for the short interval of times after a pulse arrives from the KLS; otherwise it is a NIM true. This signal inhibits the delay gate generator (DGG3) that strobes the ADC and is also used as a veto input to the TDC. The veto signal is an event window. That is, only the ion signals in

the window of a veto fail can be selectively recorded. Therefore, the KLS timing signal and ion signals prevent unwanted counts from registering and selectively taking wanted counts in the data acquisition system. The ion that arrived at the detector in the window of a veto fail determines the end of the event. The multi-channel ADC records the position of the ion on the detector. The ADC is also strobed by the signal from ions after the delay gate generator (DGG5) which is triggered by the timing signal from the arrival of an ion at the detector.

From the end of the delay gate generator (DGG1), a pulse is delayed by the gate delay generator (DGG2) and then is sent to the TDC as an End-Of-Window (EOW) signal. The EOW signal controls the operation of the TDC determining the end of the event. Moreover, a signal must clear the TDC in the event that an ion is not detected because to correctly measure a TOF for the next event; the TDC must stop and prepare for the next event. The TDC starts with every KLS shot, and an ion signal stops it. Therefore, a signal is necessary to clear the TDC instead of stopping the TDC from an ion signal. The signal called CLR comes from the delay gate generator(DGG4) and is time delayed nearly one full KLS period from the arrival of the KLS pulse because the data acquisition system needs sufficient time to finish its communication with the CAMAC crate when an event occurs.

In summary, the TOF of each ion is measured starting with the arrival of a laser pulse from KLS and stopping with a hit on the detector. If an event takes place, the status of the excitation laser is recorded so the event correlates with the arrival time of the laser pulse. Recording the laser timing signal corresponding to the event is essential for properly interpreting the data. Eventually, the TDC measures the TOF of ions we want by measuring the time interval between the KLS pulses and the ion events. Figure 3.9 shows the acquisition timing diagram with the essential events in a given detection cycle. The entire acquisition process begins with the timing signal of KLS called common start. The complicated data acquisition software is further explained in Appendix C.

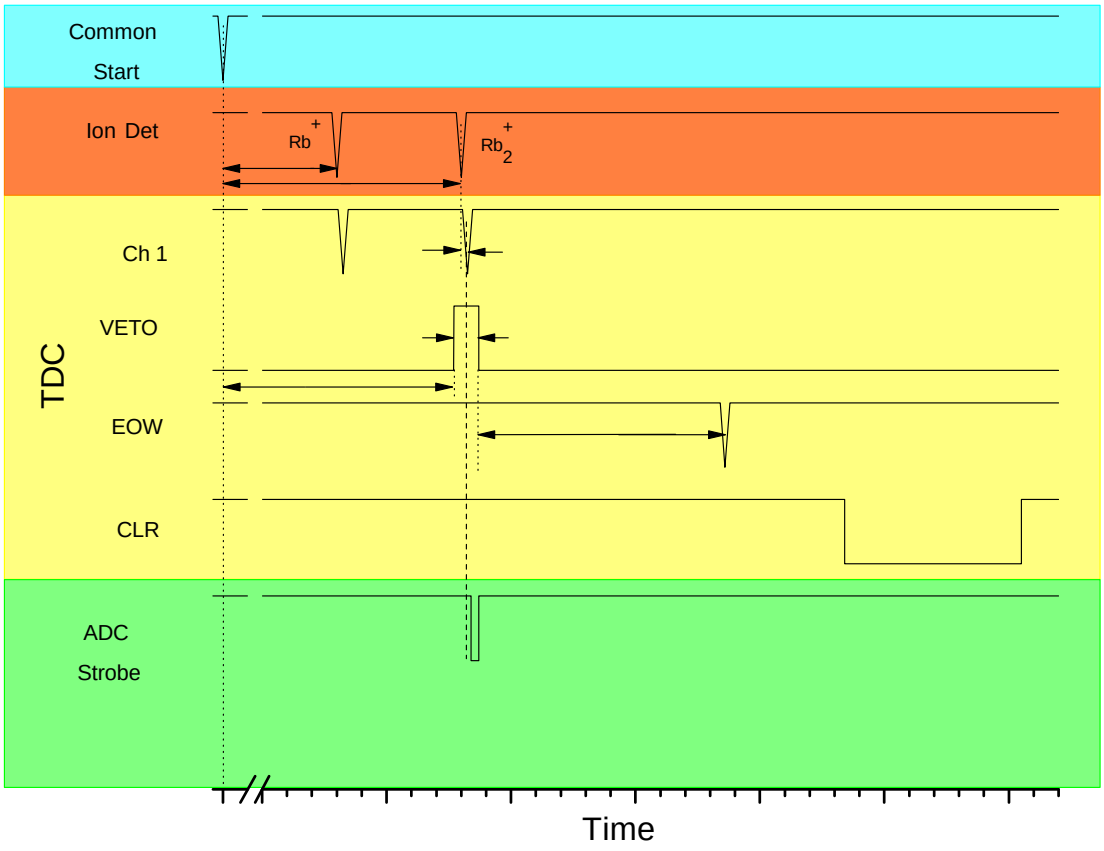

Figure 3.9: *Data acquisition timing diagrams with the corresponding important events in a typical event cycle.*

Chapter 4

Experimental Results

The experimental data in this chapter focus on investigating the interaction between an atomic ladder system and optical fields. More specifically, the purpose of this research is to study the interaction of an atomic ladder system with a train of pulses which is generated by an AOPDF pulse shaper. We use the pulse shaper to modify the phase of each frequency component. The pulses in the train give rise to a substantial control of the populations in the ladder system where the time delay and relative phase between pulses are controllable parameters.

Our experiments are carried out in cold atomic rubidium, where two-photon absorption from the $5s_{1/2}$ ground state to the excited $5d_{3/2,5/2}$ is resonantly enhanced via the $5p_{3/2}$ intermediate state. The two resonant transition frequencies are included within the bandwidth of the KLS pulse. Excitation accumulation should be considered in atomic excitation by a train of pulses if the probed excited state lifetime is longer than the train repetition period[51]. The reason is that the atoms do not have enough time to completely decay down before the next pulse comes along[42,92]. In our experiments, the maximum pulse period is 400 fs and all pulses in the train are in time window of less than 4 ps. On the other hand, the lifetime of the 5p state is about 27 ns and the lifetime of the 5d state is about 90 ns. Therefore, excitations in the atomic Rb three level ladder system are coherent because spontaneous emission is neglected in this situation.

The results obtained from such experiments measure population transfer from the $5s_{1/2}$

to $5d_{3/2,5/2}$ state by controlling various parameters. For example, the intensity of pulses and the number of pulses in a train are changed to study the interaction of atomic ladder system with the train of pulses. Experimental results are shown in a two-dimensional (2D) landscape map as a function of phase and pulse-to-pulse time separation. We measure the population of $5d_{3/2,5/2}$ state to observe the interaction. Our laser does not resolve the fine structures in 5d state so that the two states, the $5d_{3/2}$ and $5d_{5/2}$, are treated as one state because the energy separation between two states is less than the bandwidth of the excitation laser pulse. This state is detected through photoionization by the same laser pulse in which excitation takes place. Therefore we clearly measure the population of 5d state through measuring the Rb^+ signal.

We compare our experiment results to the simple two-level model which is valid within several assumptions. For example, in the simple model, we exclude possible effects caused by spontaneous emission. The interaction between a three-level ladder system and a train of pulses has an analogy to a multi-slit experiment. When we draw lines following the slopes of diagonal structures in a 2D landscape map showing populations of the 5D excited state, the slopes correspond to the transition wavelengths in the three-level ladder system. By looking at the slopes of diagonal structures showing interference, we are able to know the interference structures in the 2D landscape map are related to the interaction between a train of pulses and the three-level atomic ladder system.

Resolution in the given experimental system and errors caused by calibration of the experimental apparatus are also discussed in this chapter. The control of time sequences for typical data runs are shown in Chapter 3. All of data shown in this chapter were carefully taken after we made sure that the optical setup was stable and the data acquisition system was functionally working. In the future, we hope to build a variety of theoretical models to verify our experimental results and to have extensive understanding.

Our experimental setup was designed to study the interaction of a finite train of pulses with a 3-level ladder system in a Rb atom. Goals in our experiments are testing the simple

model how reasonably it explains our results and provides useful data to be compared with other models[92,93]. The research of two-photon excitation of a cold rubidium by a train of ultrashort pulses has also been experimentally and theoretically investigated in other research groups[29,30,93].

4.1 Transition wavelength

The lower transition wavelength from $5s_{1/2}$ to $5p_{3/2}$ is $\lambda_1 = 780.03$ nm and the upper transition wavelength from $5p_{3/2}$ to $5d_{3/2,5/2}$ is $\lambda_2 = 775.79$ nm, as shown in Fig. 2.2. The ultrafast laser has approximately a 30 nm bandwidth and includes both transition wavelengths. If the bandwidth of the laser were broad enough, we should see the interference structure related to the $5p_{1/2} - 5d_{3/2,5/2}$ transition. However, this transition is outside of the bandwidth of our laser. Furthermore, the resolution of the AOPDF pulse shaper is about 1 nm so that the fine structure splitting between Rb($5d_{3/2}$) and Rb($5d_{5/2}$) cannot be distinguished in our experiments.

It is hard to claim that the technique used here is the best tool for spectroscopy with high resolution. The bandwidth of the pulses is very broad if it is compared with a linewidth in a Rb atom. However, we obtain the transition wavelengths which are involved with the interaction between the train of pulses and the atomic Rb ladder system. The transition wavelengths assist us to interpret the interaction because slopes of the diagonal interference structures match well with the associated transition wavelengths. As a result, we can find out which transitions in the atomic ladder system are related with the observed interference patterns. The slope from Eq. 2.3 is put into Eq. 2.1 or Eq. 2.2. The wavelength from those equations is

$$\lambda = \left[\lambda_0^{-1} - \left(2\pi c \frac{dT}{d\phi_0}\right)^{-1}\right]^{-1}. \tag{4.1}$$

For convenience, an offset wavelength of $\lambda_0 = 790$ nm is used to get the transition wavelengths. This does not give rise to a change in the physics. It enables us to more readily determine slopes and makes it simpler to compare a 2D landscape with the predictions of

the simple intuitive model.

4.2 Interference structures in a two dimensional landscape plot

We focused on studying the interaction of a train of pulses with a Rb atomic ladder system by observing excitations in that system. The interaction is observed by measuring photoionization of the final upper $5d_{3/2,5/2}$ state. That is, the same train of optical pulses, which is employed for excitation of the three levels, also gives rise to photoionization from excited atoms in the 5d state. In consequence, the population in the 5d state is detected by looking at the Rb^+ signal where a time-of-flight spectrometer is used to detected Rb ions.

In Fig. 4.1, the Rb^+ signal is shown in a 2D landscape plot as a function of T and ϕ_0. A train of 11 pulses, which is produced by choosing an appropriate value of $A = 2.5332$ in the sinusoidal spectral phase, is prepared to interact with cold Rb atoms. Various features are observed in the 2D landscape plot. The most obvious features are the diagonal structures which are shown as ridges and valleys. We expected to see parallel ridges of large population and valleys of small population following the slopes corresponding the transition wavelengths. As in Eqs. 2.1 and 2.2, the structures in Fig. 4.1 show constructive and destructive interference associated with the $5s_{1/2} \rightarrow 5p_{3/2}$ and $5p_{3/2} \rightarrow 5d_{3/2,5/2}$ transitions.

First, the coarse diagonal structure shows the constructive or destructive interference which occurred in the first $5s_{1/2} \rightarrow 5p_{3/2}$ transition as we vary T and ϕ_0. The red and green color ridges correspond to constructive interference. The blue color valleys correspond to the destructive interference. Second, fine diagonal structures corresponding to the $5p_{3/2} \rightarrow 5d_{3/2,5/2}$ transition are shown as constructive and destructive interference in the 2D landscape plot. If we look at carefully the coarse diagonal structure caused by the $5s_{1/2} \rightarrow 5p_{3/2}$ transition, there is a gash cutting across the ridge in the coarse diagonal structure. In addition, in this signal scale, it is difficult to see the small ridge inside the blue valley of the coarse diagonal structure. However, when the figure scale is expanded, it is possible to

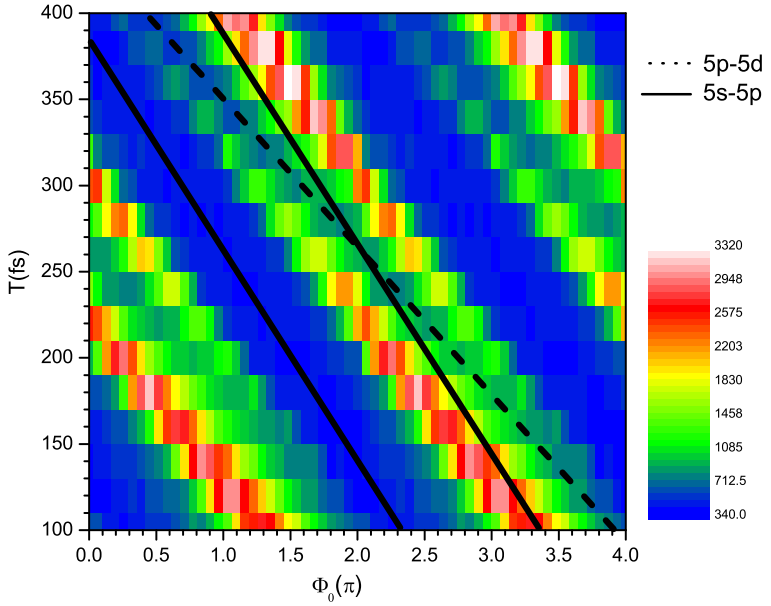

Figure 4.1: *Landscape plot of Rb^+ counts versus T and ϕ_0 for $A = 2.5332$ which creates a train of 11 significant pulses. The structures correspond to constructive and destructive interferences of Eqs. 2.1 and 2.2 from the $5s_{1/2} \rightarrow 5p_{3/2}$ and $5p_{3/2} \rightarrow 5d_{3/2,5/2}$ transitions. We obtained this experimental result while ϕ_0 is scanned from 0 to 2π. The obtained data from 0π to 2π were copied and re-plotted to manually expand the range of the ϕ_0 axis out to 4π, to obviously see the diagonal structures.*

observe the small ridge which is parallel to the gash, cutting across the blue valley.

As we follow the above analysis, we drew the lines on Fig. 4.1 based on slopes from the interference diagonal structures which are related to transition wavelengths in the atomic Rb energy levels. The solid lines match to the ridges and valleys in the coarse diagonal feature. When the slope of the solid lines is inserted into Eq. 4.1, a wavelength of 781.6 nm is obtained from their slope. The wavelength approximately corresponds to the $5s_{1/2} \rightarrow 5p_{3/2}$ transition.

The dashed line fits the gash cutting across the ridge in the coarse diagonal structure. When the dashed line inserted into Eq. 4.1, the slope of the dashed line provides a wavelength of 778.0 nm, which approximately corresponds to the $5p_{3/2} \rightarrow 5d_{3/2,5/2}$ transition. As we look at the features in the 2D landscape plot, the structures and their slopes match the expected results based on the simple model of Chapter 2. That it, the interference structures in the 2D landscape plot are explained with the slopes obtained by the derivative of the interference conditions of Eq. 2.1 and Eq. 2.2.

However, there are unpredicted results and we need to discuss them to get further insight in the physics. First, when both transition frequencies, ω_1 and ω_2, in a Rb three-level ladder system simultaneously satisfy Eq. 2.1, a maximum production of the $5d_{3/2,5/2}$ state is expected. Nevertheless, the experimental result shows destructive interference between the two transition channels. The cause of this discrepancy is unknown but it is worthwhile to search for the reasons.

The first aspect we should reconsider is that both spontaneous and stimulated emission afford only a negligible effect on our results. In our experiment, the time interval between pulses T, is varied from 100 fs to 400 fs and the time scale of the entire pulse train is less than 4 picoseconds which is limited by the pulse shaper. On the other hand, the shortest lifetime time involved in the three-level system is 27 ns from the $5p_{3/2}$ state. In addition, the lifetime of the $5d_{3/2}$ state is about 246.3 ns, and the lifetime of the $5d_{5/2}$ state is about 238.5 ns[94]. The excited atoms cannot relax to the ground state between consecutive laser pulses. As we already described in the simple model, spontaneous emission can be neglected when we investigate the interaction of a train of pulses with the Rb atomic ladder system in our experiments because the scale of T is much smaller than the lifetime of excited states. The experimental technique yields ample resolution to measure such coherent population dynamics in detail. As a result, spontaneous emission can not provide a great effect to alter our results. The fact that we can ignore spontaneous emission simplifies the description of coherent population because spontaneous emission is an incoherent process.

The second aspect to be considered is that stimulated emission still exists even though we believe that our experiments occur in the weak-field regime. We found that there was no difference in our experimental results except for a corresponding decrease in the signal of a count rate when our laser pulse energy was diminished by an order of magnitude. This supports the notion that our experiments are made in the weak field regime. We expect stimulated emission should not change the general form of the 2D landscape plot because the mechanism for redistributing the population in the given atomic ladder system is coherent. Nevertheless, it could change the magnitude of the excitation when the laser pulse energy is changed. We prefer to perform our experiments in the weak-field excitation regime, like most coherent control schemes, because the energy level structure of atoms in the weak-field is effectively unchanged by the external excitation field. Furthermore, in high intensity light, atoms respond in a nonlinear fashion. In addition, strong-field interactions are accomplished by level broadenings and level shifts which circumvent simple analytical treatments. In theory, employing perturbation theory to explain our experimental results is possible because it is suitable to describe dynamics in the weak-field regime.

In recent experiments, interference effects in the excitation of atomic ladder systems have been seen in both the weak and strong field limits by using ultrafast optical pulses[95]. The features of the interference are altered in going from resonant weak fields to broadband strong fields. For instance, in the weak-field limit only interference coming from the two resonant excitation pathways is observed. Accordingly, fine features in interference are depended on whether the system is in the strong or weak field regime.

The third consideration in interpreting the unexpected results is that there is an additional π phase shift in pulses for odd negative values of n in our experiments. This is not included in the simple model. It is not clear to us how the additional π phase would produce the destructive interference between the two excitation channels we described above.

Finally, the slopes of the structures in the 2D landscape plot show transition wavelengths which are qualitatively consistent with the $5s_{1/2} \rightarrow 5p_{3/2}$ and $5p_{3/2} \rightarrow 5d_{3/2,5/2}$ transitions

when we apply Eq. 4.1. The measured transition wavelengths are quantitatively different by more than expected from fitting errors. One possibility is that poor calibration for our pulse shaper causes this difference where the absolute spectral uncertainty of the AOPDF we use is approximately 1 nm.

4.3 A series of landscape plots

The simple model is analogous to the classic multi-slit interference experiment. As the number of slits is increased, the diffraction image becomes sharper. Similarly, as we increase the number of pulses in a train, the resolution of the interference structures should become higher. To see this phenomenon, a series of 2D landscape plots like Fig. 4.1 were created in Fig. 4.2 in which different values of parameter A give different numbers of pulses in the train. Each plot in Fig. 4.2 has the same characteristic diagonal structures. However, the contrast in the interference structures becomes more explicit and sharper by increasing the number of pulses from 3 to 7 to 11, as we expected. That is, the resolution of the interference between pulses and the excited state wave function become sharper, as more interference terms are added.

One can predict that the resolution in the interferences is able to reach that of a typical frequency comb if the number of pulses N in the train is increased to several thousand. In that case, we expect the contrast in the interferences becomes clearer and sharper so that the slopes of the structures should enable us to determine the transition frequencies with very high precision just like direct frequency comb spectroscopy provides extremely high resolution[32]. In principle, a sinusoidal pulse train can yield very high resolution by generating an arbitrarily large number of pules in the train and lessening the pulse-to-pulse interval, T, by selecting an appropriate value for the parameter A. However, the number of pulses in a train is restricted by the temporal width of the pulses. For instance, when T is below 50 fs we observed that the interference structures in 2D landscape maps were washed out because our input pulses from an oscillator, having a temporal width of 40 fs, started

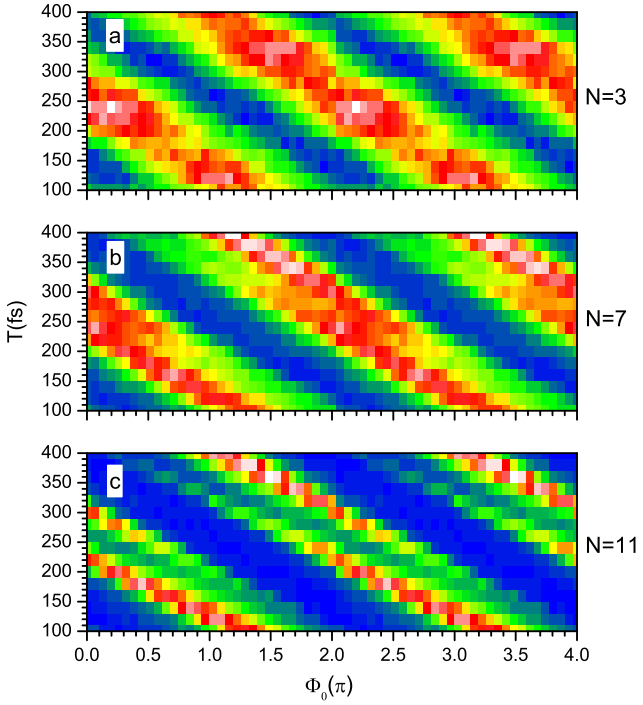

Figure 4.2: *A series of landscape plots of Rb^+ counts versus T and ϕ_0 for different numbers, N, of pulses in the train. Plots labeled a, b, and c have $N = 3$, 7, and 11, corresponding to $A = 0.3672$, 1.3152, and 2.5332.*

to overlap each other. The theoretical calculation in Fig. 2.3 also showed similar effects because of overlapping pulses. It is also possible to generate a large number of pulses by increasing the temporal length of the train itself. However, the maximum temporal length of the train is limited by the pulse shaper because of its finite crystal length. In our pulse shaper, the maximum temporal width by which we are available to extend is about 4 ps.

Therefore, improving the resolution by increasing the number of pulses N is restricted by the temporal width of an input pulse from the oscillator and the length of the pulse shaper.

4.4 Interference in a one-dimensional plot

The dependence of the diagonal structures gained from the multilevel excitation on two parameters, T and ϕ_0, was already seen by mapping the data into 2D landscape plots in Fig. 4.1 and Fig. 4.2. Both of them explicitly show the Rb^+ signal in the 2D landscape plots as a function of T and ϕ_0 where T is stepped through 16 values and ϕ_0 is stepped through 32 values. It is possible that there are additional interference structures that we can not observe due to the coarse step size. To get further insight, experiments only scanning one of the parameters are performed with a fine step size. For instance, experiments were done by stepping ϕ_0 through 512 values at a fixed value of T and by stepping T through 512 values at a constant ϕ_0. These experiments were designed to independently observe the influence of an individual shaping parameter in the atomic ladder system.

In these 1D scanning experiments, we hope to see details of an interference pattern we might miss in a coarse 2D landscape plot. Figure 4.3 shows the Rb^+ signal for a range of T at $\phi_0 = 0$. The gross interference features we get by scanning T is not different from the interference structure in the 2D landscape plots. There are no interesting distinguishing difference between the 1D scanning plot and the 2D landscape plots even though 1D plot has a much smaller step size in T. On the other hand, when we scan ϕ_0 and hold T fixed, we see regular small spikes over the broad structure shown in Fig. 4.4. We suppose the regular small spikes are due to the limited temporal width of our pulse shaper. It is possible that one might consider the temporal width of our pulse shaper causes the regular spiky feature in the interference structure. It is still not obvious to interpret the spiky feature we obtain in Fig. 4.4 although we suppose ignoring pulses outside of the limited time window in our pulse shaper gives rise to the spiky feature. More investigations are needed to understand the interesting interference feature.

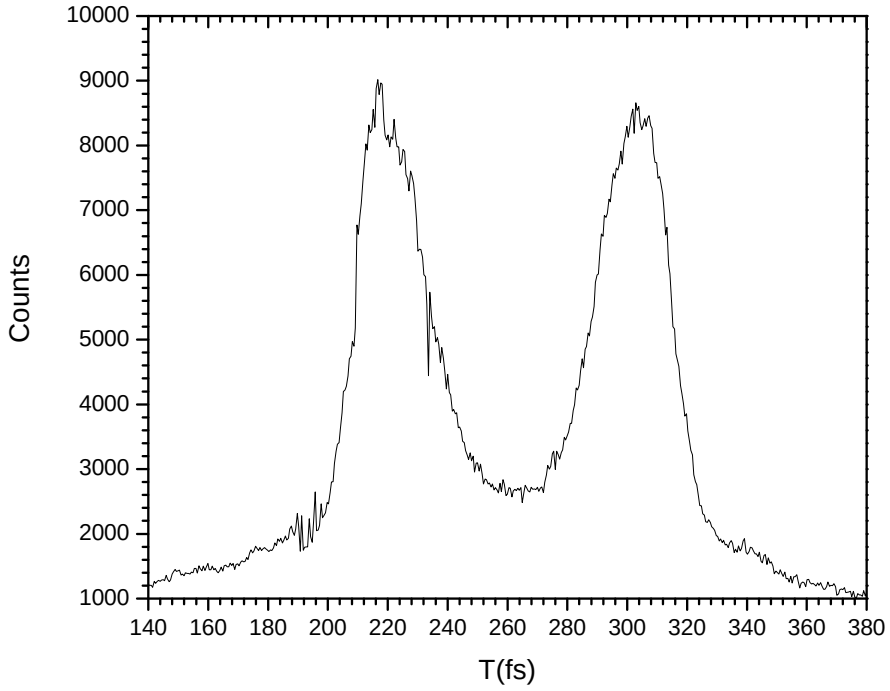

Figure 4.3: *Plot of Rb^+ counts as a function of T at $\phi_0 = 0$ and $N = 11$*

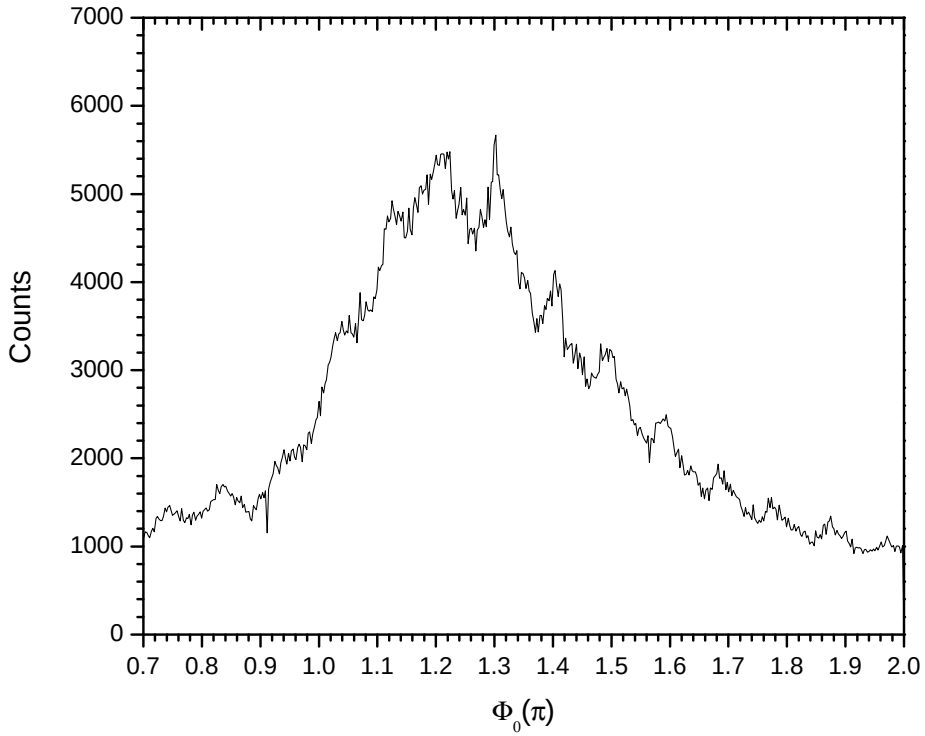

Figure 4.4: *Plot of* Rb^+ *as a function of* ϕ_0 *at* $T = 100$ *fs and* $N = 11$

Chapter 5

Conclusion and future directions

This chapter provides a brief summary of our experimental results presented in this dissertation. This is followed by a discussion of possible directions of future research in this field.

5.1 Summary

The goal of this dissertation was to provide general knowledge allowing one to understand the interaction of pulses in a train with a ladder system. The interaction of a three-level Rb atomic ladder system with a train of optical short pulses has been experimentally demonstrated by observing population transfer to a desired final state. We use the technique of MOTRIMS to prepare a cold target of Rb atoms and to measure the population of the desired final state 5d. A train of optical short pulses is generated by using sinusoidal spectral phase modulation of transform-limited ultrafast optical pulses with a pulse shaper.

The goal was to understand how an atomic ladder system interacts with the sequence of ultrashort optical pulses. The interaction is shown by plotting the 5d population in the 2D landscape maps as a function of pulse-to-pulse time delay T and pulse-to-pulse phase shift ϕ_0 which are controlled by the pulse shaper. We observe structures of constructive and destructive interference in the 2D landscape maps that are strong functions of T and ϕ_0. The cause of these structures is that the total accumulated phase of the excited state wave function depends on T and ϕ_0.

Another important parameter that affects the interaction is the number of pulses in a train. When we increase the number of pulses in a train, the structures in 2D landscape plots became dramatically sharper. This phenomenon is analogous to optical spectra progressively sharpening as the number of slits are increased in a multiple slit interference experiment. Increasing the number of pulses means that more interference terms are added so that the interference patterns become sharper in our experiment. This is equivalent to saying that more pulses in the time domain gives rise to narrower comb teeth in the frequency domain. This trend toward narrower teeth is ultimately limited by the finite time window of our pulse shaper. Since our experiments use a small number of pulses in the train, one can see resolution and contrast significantly improve by adding just a few more pulses.

Several models were used to explain the excitation of a two-level atom with a train of short optical laser pulses. Such models enable us to have insight into the characteristics of the interaction we study here. We also developed a simple intuitive model to explain cumulative phase effects in a 3-level ladder system. In this dissertation, the interference structures in the 2D landscape maps are well described by the simple intuitive model except for an interference discrepancy: we observe destructive interference instead of the expected constructive interference when both transition frequencies simultaneously satisfy Eq. 2.1. In addition, we obtained a slight quantitative discrepancy in the measured transition wavelengths compared with the transition wavelengths in the 3-level ladder system.

Furthermore, we did a simple second order perturbation theory calculation to compare to the experimental results. There is only partial agreement between the calculation and the experimental results. Solving the appropriate optical Bloch equations would be a more robust approach to see if the interference discrepancy in our experiments can be resolved because the optical Bloch equations should be more suitable if our experiments are, in fact, in a non-perturbative regime.

5.2 Future directions

Atomic physicists have studied how light interacts with matter since long before Max Planck introduced the concept of quantum physics. Recently, understanding the interaction between atomic ladder systems and trains of short pulses is rapidly developing and greatly impacts atomic physics. Much of this advance is due to new technology using ultrafast lasers and an enhanced ability to control light. It is worthwhile to look at the future direction of using the trains of pulses along with current theoretical and experimental interpretations of the interaction in our work.

One significant difficulty in using ultrafast lasers is the loss of spectral selectivity because within the broad bandwidth of an ultrafast laser many excitation channels in atomic and molecular ladder systems can complete. It is possible to overcome this limitation by using quantum coherent-control methods that control the interference between different quantum paths arriving at the same final state. In recent years, extensive efforts in various schemes have been proposed to accomplish selective population transfer. The advantage of our approach is that we have several control parameters such as T and ϕ_0 in a train of pulses. By scanning T and ϕ_0, we can find optimized values that effectively drive the system into a desired state with constructive interference while destructive interference reduces the excitation to undesired states.

Recent experiments[95,96] which investigate interference effects in the excitation of ladder systems by ultrafast optical pulses show that the details of interference effects depend on whether the system is in the weak or strong field regime. Mostly coherent-control schemes are applied to weak-field interactions because of the simple relation between the optical pulses and the resulting excitation. We also performed our experiments in the weak field regime. However, in the future, it might be valuable if we can develop control schemes in the strong-field regime as well.

We focused on a particular example of interaction, but the nature of the interaction using a train of pulses could be quite general. In this point of view, one example having similar

underlying physics is the soft x-ray attosecond pulse train (APT)[97,98]. Experiments using APT to study electron dynamic in atoms and molecules generally employ a pump-probe scheme where a train of pump pulses excites a sample and the probe pulse measures the time evolution. We can scan through ionization of the pulse-to-pulse temporal spacing of the pump pulses by changing the carrier frequency of the fundamental pulse with a pulse shaper before high-order harmonic generation. This is possible because the time between pulses in an APT is simply twice the optical period of the carrier electric field; this can be manipulated by using a pulse shaper. Therefore, scanning pulse-to-pulse temporal interval in APT might be helpful for testing the general nature of the interaction between APT and an appropriate system.

The structure in our 2D landscape maps is reminiscent of a quantum carpet[99]. We can see that constructive and destructive interferences cause the structure in a quantum carpet just like in our 2D landscape maps. I think closer relations between these two phenomena could be found if a more thoughtful analysis were made on both carpets and our landscapes.

In summary, we mentioned a few examples of the possible experimental research applications which are related to the techniques presented in this dissertation. Our experimental technology can be expanded to more schemes when our experimental techniques for the interaction of an atomic ladder system with a train of optical pulses become more robust in the future. There are still plenty of remaining tasks which should be undertaken in order to have better understanding of the interaction. We hope the research performed here opens a door to a rich environment of future experimental work studying the interaction.

Bibliography

[1] M. R. Armstrong, J. P. Ogilvie, M. L. Cowan, A. M. Nagy, and R. J. D. Miller, PNAS **100**, 4990 (2003).

[2] A. Barman, N. T. Form, and B. J. Whitaker, Chem. Phys. Lett. **427**, 317321 (2006).

[3] FASTLITE, 45-47 rue Croulebarbe, 75013 Paris, France.

[4] A. M. Weiner, D. E. Leaird, G. P. Wiederrecht, and K. A. Nelson, J. Opt. Soc. Am. B **8**, 1264 (1991).

[5] N. F. Scherer, C. Sipes, R. B. Bernstein, and A. H. Zewail, J. Chem. Phys. **92**, 5239 (1990).

[6] M. Dantus, M. J. Rosker, and A. H. Zewail, J. Chem. Phys. **89**, 6128 (1988).

[7] P. Corkum, Nature. **403**, 845 (2000).

[8] P. H. Bucksbaum, Science. **317**, 766 (2007).

[9] R. Frisch, Z. Phys. **86**, 42 (1933).

[10] T. W. Hänsch and A. L. Schawlow, Opt.Commun. **13**, 68 (1975).

[11] S. Chu, L. Hollberg, J. E. Bjorkholm, A. Cable, and A. Ashkin, Phys. Rev. Lett. **55**, 48 (1985).

[12] E. L. Raab, M. Prentiss, A. Cable, S. Chu, and D. E. Pritchard, Phys. Rev. Lett. **59**, 2631 (1987).

[13] C. Monroe, W. Swann, H. Robinson, and C. Wieman, Phys. Rev. Lett. **65**, 1571 (1990).

[14] S. G. Crane et al., Phys. Rev. Lett. **86**, 2967 (2001).

[15] D. Felinto, L. H. Acioli, and S. S. Vianna, Opt. Lett. **25**, 917 (2000).

[16] P. R. Poulin and K. A. Nelson, Science. **313**, 1756 (2006).

[17] X. Chen and J. Yeazell, Opt. Express. **5**, 93 (1999).

[18] T. C. Weinacht, J. Ahn, and P. H. Bucksbaum, Nature. **397**, 233 (1999).

[19] V. Blanchet, M. A. Bouchene, O. Cabrol, and B. Girard, Chem. Phys. Lett. **233**, 491 (1995).

[20] N. F. Scherer et al., J. Chem. Phys. **95**, 1487 (1991).

[21] T. Baumert, M. Grosser, R. Thalweiser, and G. Gerber, Phys. Rev. Lett. **67**, 37533756 (1991).

[22] T. Baumert, V. Engel, C. Meier, and G. Gerber, Chem. Phys. Lett. **200**, 488 (1992).

[23] R. M. Bowman, M. Dantus, and A. H. Zewail, Chem. Phys. Lett. **161**, 297 (1989).

[24] S. A. Rice and M. Zhao, Nature. **403**, 496 (2000).

[25] L. D. Carr, D. DeMille, R. V. Krems, and J. Ye, New J. Phys. **11**, 055049 (2009).

[26] Q. Zhang, M. Keil, and M. Shapiro, J. Opt. Soc. Am. B **20**, 2255 (2003).

[27] V. Blanchet, C. Nicole, M. Bouchene, and B. Girard, Phys. Rev. Lett. **78**, 27162719 (1997).

[28] M. Mudrich, F. Stienkemeier, G. Droppelmann, P. Claas, and C. P. Schulz, Phys. Rev. Lett. **100**, 023401 (2008).

[29] M. C. Stowe, F. C. Cruz, A. Marian, and J. Ye, Phys. Rev. Lett. **96**, 153001 (2006).

[30] M. C. Stowe, A. Peer, and J. Ye, Phys. Rev. Lett. **100**, 203001 (2008).

[31] M. C. Stowe et al., Advances in Atomic, Molecular, and Optical Physics **55**, 1 (2008).

[32] A. Marian, M. C. Stowe, J. R. Lawall, D. Felinto, and J. Ye, Science. **306**, 2063 (2004).

[33] R. H. adn T. Udem, T. W. Hänsch, J. C. Knight, W. J. Wadsworth, and P. S. J.Russell, Phys. Rev. Lett. **85**, 2264 (2000).

[34] A. Apolonski et al., Phys. Rev. Lett. **85**, 740743 (2000).

[35] J. L. Hall, Rev. Mod. Phys. **78**, 1279 (2006).

[36] S. A. Diddams et al., Science. **293**, 825 (2001).

[37] G. Wilpers et al., Phys. Rev. Lett. **89**, 230801 (2002).

[38] L. Chen and J. Ye, Chem. Phys. Lett. **381**, 777783 (2003).

[39] M. J. Thorpe, K. D. Moll, R. J. Jones, B. Safdi, and J. Ye, Science. **311**, 1595 (2006).

[40] T. H. Yoon, A. Marian, J. L. Hall, and J. Ye, Phys. Rev. A **63**, 011402 (2000).

[41] D. J. Jones et al., Science. **288**, 635 (2000).

[42] D. Felinto, C. A. C. Bosco, L. H. Acioli, and S. S. Vianna, Opt.Commun. **215**, 69 (2003).

[43] D. Felinto, C. A. C. Bosco, L. H. Acioli, and S. S. Vianna, Phys. Rev. A **64**, 063413 (2001).

[44] W. Yang, S. Gong, R. Li, and Z. Xu, Phys. Rev. A **74**, 013407 (2006).

[45] G. Slavcheva and O. Hess, Phys. Rev. A **72**, 053804 (2005).

[46] A. M. Weiner, D. E. Leaird, G. P. Wiederrecht, and K. A. Nelson, Science. **247**, 1317 (1990).

[47] M. Katsuragawa, K. Yokoyama, T. Onose, and K. Misawa, Opt. Express. **13**, 5628 (2005).

[48] R. J. Temkin, J. Opt. Soc. Am. B **10**, 830 (1993).

[49] M. Seidl, C. Uiberacker, and W. Jakubetz, Chem. Phys. **349**, 296307 (2008).

[50] T. Ban et al., Phys. Rev. A **76**, 043410 (2007).

[51] A. A. Soares and L. E. E. Araujo, J. Phys. B. **43**, 18 (2010).

[52] N. Dudovich, B. Dayan, S. M. G. Faeder, and Y. Silberberg, Phys. Rev. A **86**, 47 (2001).

[53] L. Allen and J. H. Eberly, *Optical Resonance and Two-Level Atoms*, New York: Wiley, 1975.

[54] B. W. Shore, *The Theory of Coherent Atomic Excitation*, New York: Wiley, 1990.

[55] J. Evers and C. H. Keitel, J. Phys. B. **37**, 27712796 (2004).

[56] Lifetime of Rb($5p_{3/2}$) is ~ 27 ns and lifetime of Rb($5d_{5/2}$) is ~ 240 ns).

[57] X. Fléchard, H. Nguyen, E. Wells, I. Ben-Itzhak, and B. D. DePaola, Phys. Rev. Lett. **87**, 123203 (2001).

[58] X. Fléchard et al., Phys. Rev. Lett. **91**, 243005 (2003).

[59] H. Nguyen, X. Fléchard, R. Brédy, H. A. Camp, and B. D. DePaola, Rev. Sci. Instrum. **75**, 2638 (2004).

[60] B. D. DePaola, R. Morgenstern, and N. Anderson, Advances in Atomic, Molecular, and Optical Physics **55**, 139 (2008).

[61] H. Nguyen, *Magneto optical trap recoil ion momentum spectroscopy*, PhD thesis, Kansas State University, 2003.

[62] M. van der Poel, C. V. Nielsen, M. A. Gearba, and N. Andersen, Phys. Rev. Lett. **87**, 123201 (2001).

[63] J. W. Turkstra et al., Phys. Rev. Lett. **87**, 123202 (2001).

[64] R. Dörner et al., Phys.Rep. **330**, 95 (2000).

[65] J. Ullrich et al., Rep.Prog.Phys. **66**, 1463 (2003).

[66] S. Chu and C. Wieman, J. Opt. Soc. Am. B **6**, 2020 (1989).

[67] C. Wieman, G. Flowers, and S. Gilbert, Am. J. Phys. **63**, 317 (1995).

[68] E. A. Donley, T. P. Heavner, F. Levi, M. O. Tataw, and S. R. Jefferts, Rev. Sci. Instrum. **76**, 063112 (2005).

[69] The figure is modifed from the figure in the dissertation of Dr.Camp at Kansas State University in 2005.

[70] H. A. Camp, *Measurements of the time evolution of coherent excitation*, PhD thesis, Kansas State University, 2005.

[71] M. L. Trachy, G. Veshapidze, M. H. Shah, H. U. Jang, and B. D. DePaola, Phys. Rev. Lett. **99**, 43003 (2007).

[72] G. Veshapidze, M. L. Trachy, H. U. Jang, C. W. Fehrenbach, and B. D. DePaola, Phys. Rev. A **76**, 051401 (2007).

[73] W. Demtröder, *Laser Spectroscopy: Basic Concepts and Instrumentation*, volume 2nd Ed., Springer, 1996.

[74] K. B. MacAdam, A. Steinbach, and C. Wieman, Am. J. Phys. **60**, 1098 (1992).

[75] W. Lu et al., Rev. Sci. Instrum. **67**, 3003 (1996).

[76] S. E. Park, H. S. Lee, T. Y. . Kwon, and H. Cho, Opt.Commun. **75**, 118 (2001).

[77] Y. Xiong, S. Murphy, J. L. Carlsten, and K. S. Repasky, Opt. Eng. **46**, 054203 (2007).

[78] R. Brédy, H. Nguyena, H. Campa, X. Fléchardb, and B. D. DePaola, Nucl. Instrum. Methods Phys. Res. B **205**, 191 (2003).

[79] A. M. Weiner, Appl. Opt. **47**, A88 (2008).

[80] A. M. Weiner, Rev. Sci. Instrum. **71**, 19291960 (2000).

[81] A. M. Weiner, Prog. Quantum Electron. **19**, 161238 (1995).

[82] N. Karasawa et al., J. Opt. Soc. Am. B **18**, 1742 (2001).

[83] F. Huang, W. Yang, and W. S. Warren, Opt. Lett. **26**, 382 (2001).

[84] M. A. G. Martinez, P. R. Herczfeld, C. Samuels, L. M. Narducci, and C. H. Keitel, Phys. Rev. A **55**, 44834491 (1997).

[85] J. Wu and J. Gao, Phys. Rev. A **65**, 063807 (2002).

[86] E. Moon, *Carrier-Envelope Phase Stabilization of Grating-Based Chirped-Pulse Amplifiers*, PhD thesis, Kansas State University, 2009.

[87] H. Wang et al., Opt. Express. **17**, 12082 (2009).

[88] T. Oksenhendler, *Mesures et controles temporels dans le domaine des lasers ultrabrefs*, PhD thesis, Ecole Polytechnique, Europe, 2004.

[89] F. Verluise, V. Laude, Z. Cheng, C. Spielmann, and P. Tournois, Opt. Lett. **25**, 575 (2000).

[90] M. A. Dugan, J. X. Tull, and W. S. Warren, J. Opt. Soc. Am. B **14**, 2348 (1997).

[91] N. T. Form, B. J. Whitaker, and C. Meier, J. Phys. B. **41**, 074011 (2008).

[92] D. Felinto and C. E. E. López, Phys. Rev. A **80**, 013419 (2009).

[93] D. Felinto, L. H. Acioli, and S. S. Vianna, Phys. Rev. A **70**, 043403 (2004).

[94] D. Sheng, A. P. Galván, and L. A. Orozco, Phys. Rev. A **78**, 062506 (2008).

[95] S. Clow and T. Weinacht, Phys. Rev. A **82**, 023411 (2010).

[96] C. Trallero-Herrero and T. C. Weinacht, Phys. Rev. A **75**, 063401 (2007).

[97] P. Ranitovic et al., New J. Phys. **12**, 013008 (2010).

[98] R. López-Martens et al., Phys. Rev. Lett. **94**, 033001 (2005).

[99] A. E. Kaplan, I. Marzoli, W. E. Lamb, and W. P. Schleich, Phys. Rev. A **61**, 032101 (2000).

[100] W. Demtröder, *Laser Spectroscopy: Basic Concepts and Instrumentation*, Springer, 2 edition, 1996.

[101] R. W. P. Drever et al., Appl. Phys. B. **31**, 97 (1983).

[102] E. D. Black, Am. J. Phys. **69**, 79 (2001).

[103] S. E. Park, H. S. Lee, T. Y. . Kwon, and H. Cho, Opt.Commun. **75**, 118 (1990).

[104] T. P. Dinneen, C. D. Wallace, and P. L.Gould, Opt.Commun. **92**, 277 (1992).

[105] H. S. Lee, S. E. Park, J. D. Park, and H. Cho, J. Opt. Soc. Am. B **11**, 558 (1994).

[106] K. L. Corwin, Z. Lu, C. F. Hand, R. J. Epstein, and C. E. Wieman, Appl. Opt. **37**, 3295 (1998).

[107] T. Ikegami, S. Ohshima, and M. Ohtsu, Jap. J. Appl. Phys. **28**, 1839 (1989).

[108] S. Lecomte, E. Fretel, G. Mileti, and P. Thomann, Appl. Opt. **39**, 1426 (2000).

[109] M. A. Gearba et al., Phys. Rev. A **76**, 1 (2007).

[110] U. Schünemann, H. Engler, R. Grimm, M. Weidemüller, and M. Zielonkowski, Rev. Sci. Instrum. **70**, 242 (1999).

[111] M. Ko and Y. Liu, Opt. Lett. **29**, 1799 (2004).

[112] K. Nakagawa, M. de Labachelerie, Y. Awaji, and M. Kourogi, J. Opt. Soc. Am. B **13**, 2708 (1996).

[113] M. de Labachelerie, K. Nakagawa, and M. Ohtsu, Opt. Lett. **19**, 840 (1994).

[114] H. U. Jang, J. Blieck, G. Veshapidze, M. L. Trachy, and B. D. DePaola, Rev. Sci. Instrum. **78**, 094702 (2007).

[115] Viewpoint DIO64; National Instruments Corporation; 11500 N. Mopac Expwy; Austin, TX 78759-3504.

[116] C. Combaret, CAMAC TTL/NIM Translator, 2004.

[117] http://jrm.phys.ksu.edu/Resource/Pubs/SpecTcl/SpecTcl.html.

Appendix A

Locking CW lasers

A stable lock for laser frequency is one of the most essential techniques for various applications such as laser cooling and trapping of atoms, high-resolution spectroscopy, and precision measurements. For instance, precision measurements in atomic physics require lasers to have frequencies which are fixed at the frequencies of atomic resonance transitions. However, the central frequency of a diode laser used in precision measurements is shifted over time by fluctuations of temperature, injected current and mechanical noise. To be locked at a fixed frequency, the laser needs feedback signal to correct undesired change from the outside environment.

Various methods supply laser frequency stability in several types of laser systems and provide the stability required in experimental applications[100]. In our experiments, several locking schemes were developed for stabilizing and tuning diode lasers the near atomic resonance transitions in atomic Rb.

First, we have developed a magnetic field dither locking technique for trapping atoms. It combines the simplicity of the Doppler-free saturation absorption method with a magnetic field induced dichroism where a saturated absorption peak is modulated by dithering a magnetic field. The locking technique is also explained in chapter 3. The locking technique provides the stable frequency lock for one of the two external cavity diode lasers used for laser cooling. In addition, a frequency offset locking technique was built to obtain wide continuous tuning capability for laser frequency because more than a few hundred

megahertz is necessary to probe molecular Rb level structure by scanning a laser around resonance transitions. In addition, frequency offset locking of one laser to another provides large tunability and is a very useful technique for laser spectroscopy[100]. The last scheme is called two-photon transition locking which is used to lock a 1529 nm laser because finding a suitable optical reference at this frequency is difficult.

The underling ideas of these techniques are known and used in several research groups. However, they are unpublished and difficult to design without detail descriptions. Therefore, these laser locking techniques are described in detail here to help others to develop their own laser system. In addition, we provide detail descriptions of our locking electronics[70].

Our experimental setup, shown in Fig. A.1, consists of several diode lasers. One laser locked with a magnetic field dither technique is used as the reference for the other laser locks. After reviewing the characteristics of widely used frequency stabilization methods, our implementations for locking lasers are presented with the expected performance and limitations.

A.1 Introduction of various laser locking schemes

One common method of stabilizing a diode laser frequency is locking the laser to an external reference which reduces the central frequency drift and increases its stability. The methods of laser frequency stabilization can be classified into two types based on whether the laser frequency is locked on a peak or to a zero-crossing of an external reference signal (The method is often referred to as a side lock). For instance, in Doppler-free saturated absorption locking, some fraction of the laser beam goes to a saturated absorption spectrometer. The laser frequency is locked to the center of a narrow peak in the Doppler-free saturation absorption spectrum[100]. A peak-locking scheme generally needs laser frequency modulation which requires a phase-sensitive electronic feedback system. The peak-locking scheme is often less sensitive to external perturbation such as mechanical vibrations and temperature changes than side-locking. However, using laser frequency modulation in the peak-locking

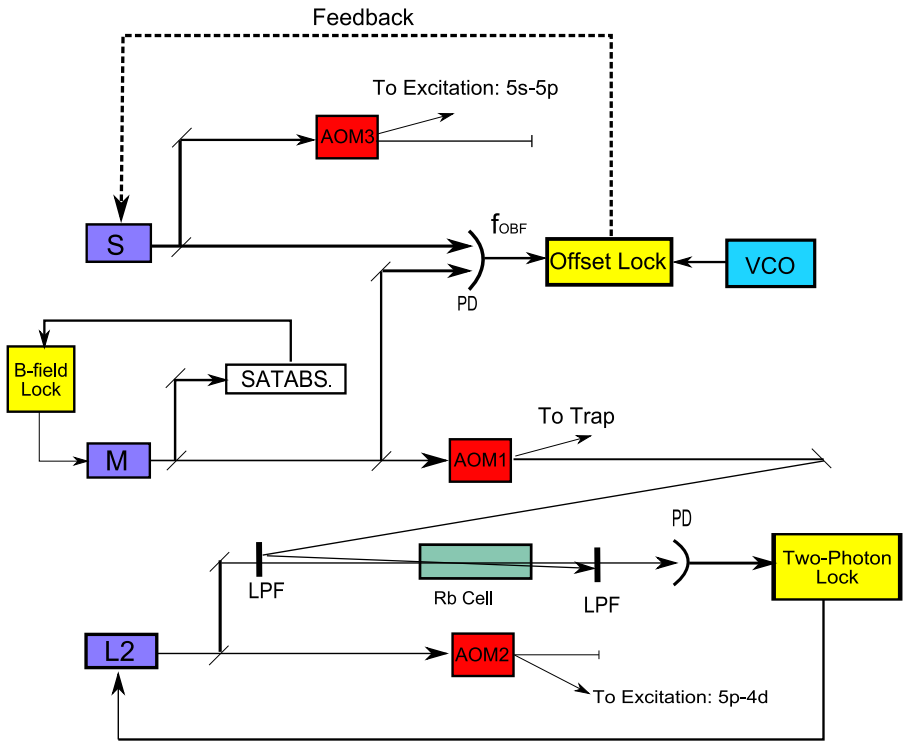

Figure A.1: *Schematic of the laser locking apparatus. AOM: Acoustico-Optical Modulator; LPF: low pass filter; M: Master Laser; S: Slave Laser; PD: Photodiode; SATABS: Optics Setup for Saturated Absorption Spectrum; B-field Lock: Magnetic field dithering lock electronics; Two-photon Lock: Two photon resonance transition lock electronics; Offset lock:Frequency-offset lock electronics.*

scheme effectively broadens the laser bandwidth and is therefore unsuitable in applications which need a very narrow bandwidth laser.

One particularly powerful peak-locking technique is known as the Pound-Drever-Hall (PDH) method[101,102]. It has the advantage of keeping the laser's linewidth narrow. In the PDH method, the laser current is modulated at rf frequency. This puts sidebands on the laser output. A sideband is then locked to an optical absorption line or optical cavity. A

disadvantage of using the PDH lock is that the series of sidebands, which are symmetrically spaced about the frequency of the carrier, can cause unexpected transitions in the atomic or molecular spectroscopy.

Various effective side-lock techniques have been constructed. Using a frequency stabilization signal from an atomic spectral line in saturated absorption spectroscopy is one of the most widely used techniques in side-locking. That is, the laser frequency is locked to the side of a narrow peak in the Doppler-free saturation absorption spectrum[100]. The advantage of a side-locking scheme is that using the side of the peak as its feedback signal does not require any laser frequency modulation. A drawback of side-locking scheme is that any change of beam alignment gives rise to a shifted lock point and induces a frequency drift. Typically isolating mechanical vibrations is necessary for side-lock techniques because their frequency stabilities are very sensitive to the alignment of the laser beams. However, one research group[103] showed that the laser frequency was stabilized by using a dispersion-like signal from an atomic vapor cell as a frequency discriminator without any frequency modulation. This side locking method is simpler and inexpensive.

The Zeeman effect can be used to stabilize a laser[104–108]. A well-known method of side-locking is known as the dichroic atomic vapor laser lock (DAVLL)[106] which utilizes circular dichroism; absorption of a photon in a magnetic field depends on the laser's polarization. The DAVLL method provides a strong signal and has a wide capture range near the atomic transition. However, the lock point is not precisely known in the DAVLL scheme. Furthermore, temperature change gives rise to adding an offset to the lock point and shifting the zero crossing point in the dispersive signal because the retardance of glass windows in a vapor cell is temperature sensitive.

A.2 Frequency offset locking

Another technique we use in locking a laser frequency is the offset locking of two lasers. Relatively large tunability of about 1 GHz is the advantage of this technique. A reference

laser is locked to an atomic resonance transition and the frequency of a second laser locked to a desired offset from the reference frequency. A circuit, which consists of a delay line, a power splitter, and an RF mixer, is used to keep the frequency offset between the optical beat between the two lasers equal to a reference signal from an oscillator. The error signal, which is proportional to the frequency difference between the optical beat note and the reference frequency, is used as the feedback to the laser locking controlled.

As we expect, a CW laser at 1529 nm is used to excite the atomic $5p_{3/2} \rightarrow 4d_{5/2}$ transition of the Rb in our experiments[71,109]. To lock the 1529 nm laser with high accuracy and small line width broadening, we need a reference signal having a well-defined frequency. However, it is hard to construct a reference signal corresponding to 1529 nm. We designed an inexpensive and simple lock by employing some fraction of another laser beam.

We constructed a circuit for stabilizing the difference frequency of two separate lasers referred to as master (L1) and slave (L3). The main parts of the circuit are described in Fig. A.2. There are two independent input sources. One is the optical beat note of the two diode lasers measured by a photodiode. The optical beat note signal is split by a coupler, with part going into a laser frequency monitor (Laser. Mon.) and the rest going to a frequency mixer. The other input signal, which is generated from a VCO, is sent to a reference frequency monitor (Ref. Mon.) and the frequency mixer. In the frequency mixer, the optical beat frequency ($\Delta\nu$) of the two lasers is mixed with the reference frequency from the VCO. This results in a sum and difference frequency. The sum frequency is filtered out by a low-pass filter. The difference frequency is equally divided into two parts by a power splitter. One part is delayed by an external cable is then recombined with the other signal. The phase detector consists of a delay line, a frequency mixer and a splitter.

The output of this beat mixer is a cosine function[110]. Near the zero-crossing of the cosine function, the signal is roughly proportional to the beat frequency between the optical beat frequency ($\Delta\nu$) and the reference frequency from the VCO (ν_{vco}). That is, the voltage output of the beat mixer can be used to lock the frequency difference between the master

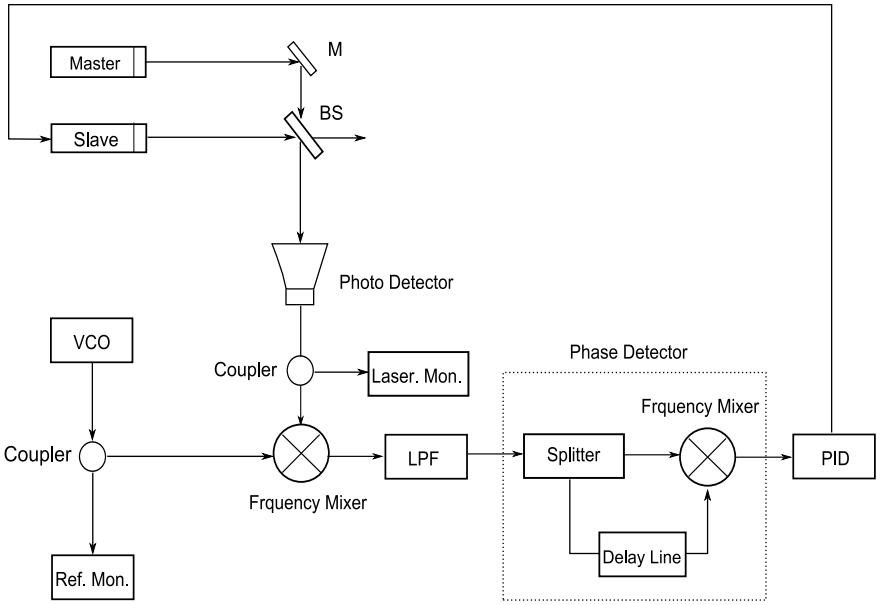

Figure A.2: *Schematic of frequency offset locking. The circuit is explained in the text.*

and the slave laser to the VCO reference. A PID controller is then used to keep slave laser locked to the master, but with a user-controlled frequency offset.

Precision control of laser frequencies is critical for both fixed frequency and tunable lasers. In our case, the trapping laser used as the master (L1), and is locked to one of the hyperfine structures of an atomic transition; this provides the fixed frequency. The lock tightness of the slave laser is about 1 MHz, while the master, to which the slave is locked, is held to a few hundred kHz, as determined by heterodyning measurements. The scheme using frequency offset locking has wide tunability from 50 MHz to 1 GHz. The output frequency of a VCO is swept by a ramp voltage generator. The tunable range of frequency

in our technique is mostly limited by the photodiode detector's bandwidth of 1 GHz.

A.3 Two-photon transition lock

Our experiments require locking the 1529 nm laser ($L2$) to a specific hyperfine structure of atomic Rb with a narrow bandwidth and long term frequency stabilization. For example, $L2$ is used as a probe laser in photoassociation experiments[71] and an excitation laser in stimulated Raman adiabatic passage[109]. To lock the L2 laser at the transition wavelength of 1529nm corresponding to the $5p_{3/2} \rightarrow 4d_{5/2}$ transition of ^{87}Rb, we need an absolute frequency reference which could require extra equipment and cost. For example, the rotational-vibration transitions of acetylene (C_2H_2) having a rich spectrum from 1520 nm to 1560 nm are utilized to lock wavelength-division-multiplexing communication systems in the C-band (1520-1560 nm)[111]. However, more than 100 mW of laser power, when locking the laser frequency using Doppler-free saturation spectroscopy, is needed due to acetylene's weak oscillator strength[112,113].

We developed an alternative technique in which the 1529 nm laser is locked to the $5p_{3/2} \rightarrow 4d_{5/2}$ absorption peak when two lasers are sent to a room-temperature Rb cell and then interact with the same velocity group of atoms. That is, light from a 780 nm laser excites a particular velocity group of atoms in the cell to $5p_{3/2}$; then L2 is locked to the transition that brings the same group of atoms to $4d_{5/2}$. The 780 nm laser is locked to the 2-3 crossover transition in ^{87}Rb, which is 133.4 MHz below the $5s_{1/2}, F = 2$ – $5p_{3/2}, F = 3$ transition in a saturated absorption spectrum. The particular velocity group of atoms excited by this laser were blue-shifted into resonance.

An absorption peak is seen by dithering L2 while the 780 nm laser frequency is locked. Absorption of L2 is maximum when L2 is detuned to the red of atomic resonance by 133 MHz $\times$ 780 nm / 1529 nm due to the wavelength dependent frequency shift from the Doppler effect. This method has the advantage that the frequency of L2 can be tuned by shifting the optical reference frequency of the 780 nm laser. The locking technique makes it relatively

simple and inexpensive to lock the laser frequency near 1529nm; this could be useful for high-speed optical communication systems. In conclusion, we hope our techniques can be used in many applications of atomic physics experiments requiring stability and tunability for diode lasers.

Appendix B

Auto-incrementing nanosecond delay

We designed a circuit that acts as an auto-incrementing delay. The circuit delays an input TTL pulse through successively long times. The circuit is conveniently interfaced to data acquisition systems. It gives us the capacity to adjust the total number of delays in a cycle, the incremental delay value, and the amount of time spent at each delay step. The delay step can be adjusted in the range from 250 ps to 640 ns depending on which delay chip is used. This stand-alone hardware device was simply and conveniently integrated into many applications. In our experiment, the circuit was used in various applications to control the timing of laser pulses. For example, the circuit was used to vary the temporal separation between pulses from separate cw lasers. In particular, it was used to study population dynamics in an optically excited three-level atomic ladder system[109] and to probe the step-wise excitation of a molecular system by shaping the spectral phase of an ultrafast laser. We could have used commercial hardware and software for the requirements of these experiments. However, the auto-incrementing delay circuit satisfies our requirements which need high timing precision and high speed logic decisions in experiments with flexible control.

Figure B.1 simply describes the logic flow in the auto-incrementing delay circuit. The DS1023 8-bit programmable timing chip labeled Delay in Fig. B.1 plays an essential role in this circuit. A TTL-level timing signal is sent to the chip as an input signal and then is delayed by the number of fixed time periods given by a parallel 8-bit TTL level signal, X. This 8-bit signal comes from a circuit that is incremented by a TTL clock. The output of

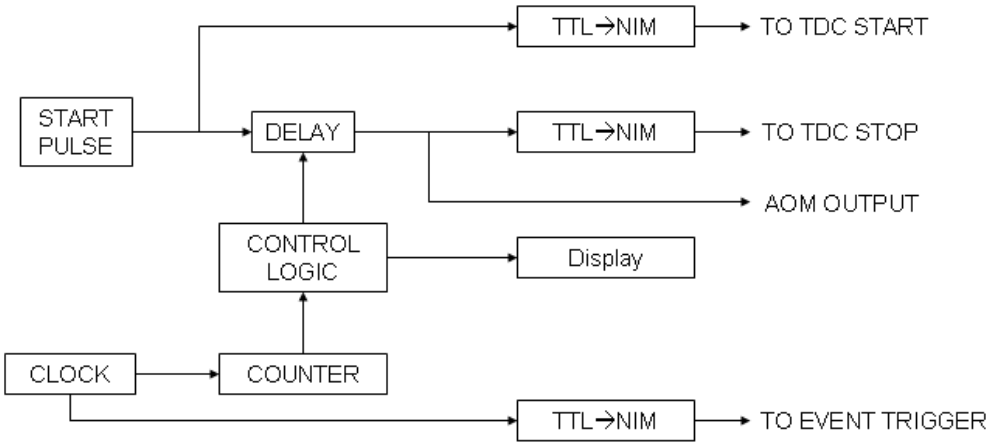

Figure B.1: *Block diagram of the auto-stepping delay circuit.*

DS1023 chip are the delayed TTL signal and a reference TTL pulse. The 8-bit TTL signal X ranged from 0 to 255. This number determines the total delay of the chip which is given by

$$\tau_{total} = \tau_0 + \tau X, \tag{B.1}$$

where τ_0 is the fixed propagation time of a signal through the chip, typically 16.5 ns, and τ is the unit delay time of the chip. One can choose the value of τ with 4 varieties, at 0.25, 0.5, 1.0, and 5.0 ns in the DS1023. The 5.0 ns version is the most suitable choice for our application[109].

The counter output is sent to a control logic module which is a hardware AND mask made up of a bank of 8 DIP switches. This AND mask is used to control the increment in

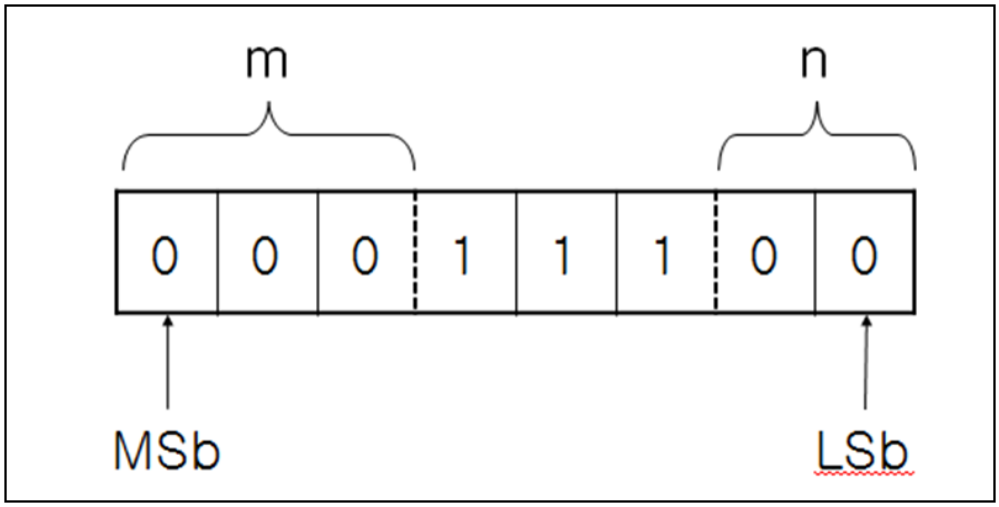

Figure B.2: *Delay duration, increment, and number of steps are controlled by the 8-bit hardware AND mask.*

delay for each step, the delay step time, and the number of steps in a cycle. In Fig. B.2, the switches are arranged so that any of the bits from the counter is passed through to the DS1023 at the mask position occupied by a 1 or replaced by a logical 0. The number of least significant bits (LSb) in the mask set to 0 as the cleared bits provide the delay increment which is expressed by $2^n\tau$ where n is the number of bits cleared. In addition, the cleared LSb controls the dwell time at each delay, $t_{step} = 2^nT$, where T is the clock period. The number of most significant bits (MSb) cleared using the mask provide the total number of delays per cycle[114]. That is,

$$N = 2^{8-(m+n)}, \tag{B.2}$$

where m is the number of cleared MSb, and $n + m \leq 8$. Therefore, the total cycle time is Nt_{step}. For instant, in the experiment[109], if we want to have 32 values of delay, to increment the delay by 10 ns at each step, and to dwell for 10 seconds at each delay, then $m + n = 3$ because N should take the desired value of $2^5 = 32$. We set the version of the DS1023 to τ=5 ns. Therefore, $n = 1$, which means m should be 2.

In order for the dwell time at each delay to be 10 seconds, we set the clock period, $T = 5.0$ seconds. Thus, the least significant bit and the 2 most significant bits were zeroed,

and the rest of the bits from the counter were sent through to the DS1023. Therefore, the bit pattern on the mask is shown as 00111110, where the right-most bit is the least significant. The five 1's means we had 2^5 sequential delays. On the other hand, the single zeroed bit on the right indicates that every other pulse from the clock will matter, giving a $2 \times \tau$ delay increment and a 10 second period for each delay. As a result, the total cycle time is 32×10 seconds $= 320$ seconds.

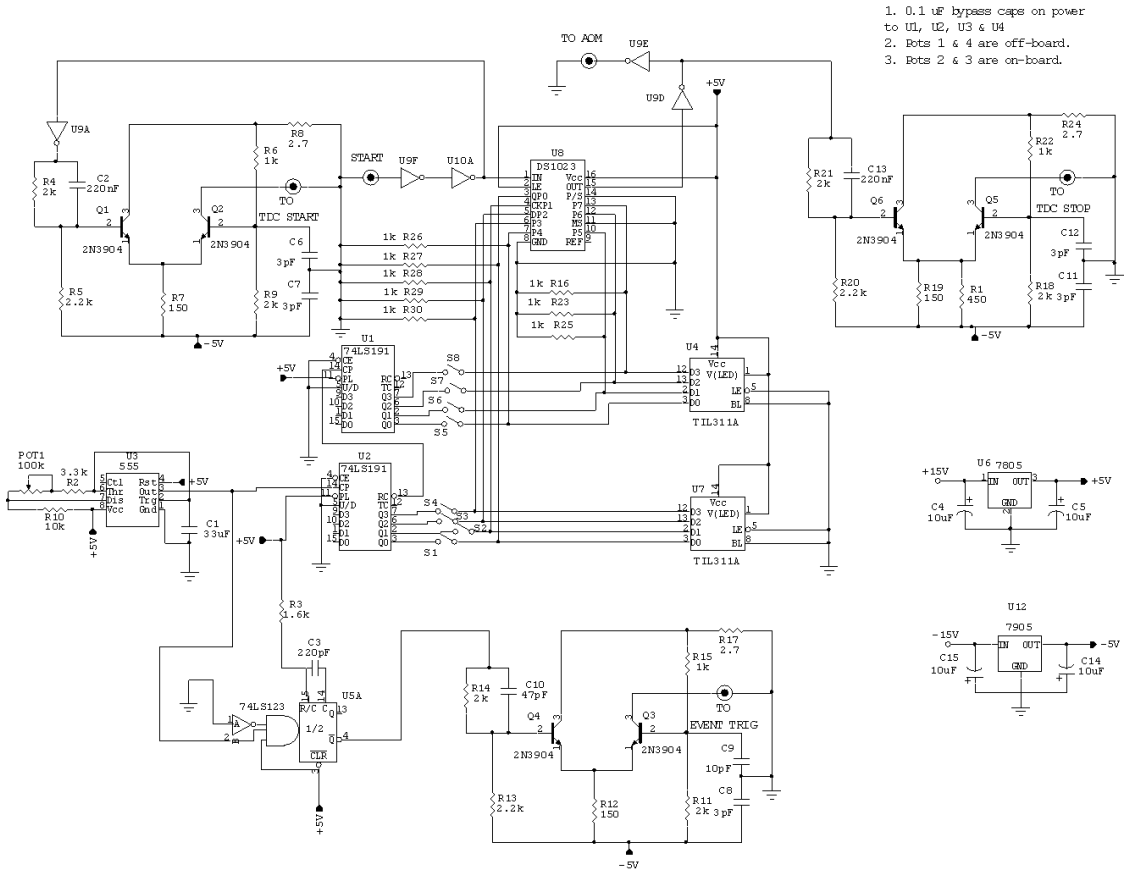

Figure B.3: *Schematic diagram of the auto-stepping delay circuit.*

A schematic diagram of the auto-stepping delay circuit is shown in Fig. B.3. In our application, a PC-controlled data acquisition system[70] generates a TTL pulse, labeled *START*. We note that the flexible pulse generating card[115] used in our data acquisition computer can not have pulse delays less than 50 ns. After passing through a pair of inverters to clean up the TTL signal, the pulse is sent both to the DS1023 (U8) and to one of the TTL-to-NIM

converters[116], where the output labeled TO TDC START is used as the start signal for a time-to-digital converter (TDC). We use a clock circuit designed with the 555 timer chip, $U3$. In addition, counters count the pulses from $U3$. It is advantageous to flexibly select T, therefore we can change the potentiometer POT1 to provide clock periods ranging from 0.5 seconds $\leq T \leq$ 7.0 seconds.

One part of the clock output is sent to the clock input of a pair of 4-bit counters, $U1$ and $U2$, producing X for the DS1023 after passing through the switches from S1 to S8 that form the AND mask. Furthermore, two LED displays, $U4$ and $U7$, show delay steps after they get X. The other part of the clock output is sent to a one-shot and then goes to a second TTL-to-NIM converter. The output of a converter labeled TO EVENT TRIGGER is used to synchronize the clock with the data acquisition system. The delayed TTL pulse from the DS1023 is output as a TTL signal labeled TO AOM. We use the output to send the RF to an acousto-optic modulator (AOM) in our application. In addition, the delayed output is converted to NIM and goes to the TDC's STOP.

Appendix C

Data acquisition software and system

In our experiments, the data acquisition software is the SpecTcl package[117] written by Ron Fox of Michigan State University. SpecTcl was initially developed by Sun Micro Systems and written in C++ as completely open source under the General Public License (GNU). SpecTcl has been widely used for passive event mode data analysis. Therefore, this software was designed to respond to signals when an event is measured by the hardware and collected as data.

The Tcl scripting language is embedded as the command language of this software which provides a powerful and extensible command set to the user. SpecTcl can be also readily modified by the user. For example, it has the ability to build custom graphical user interfaces. The readout part of the system is designed to use CAMAC hardware. In the file, *skeleton.cpp*, various useful functions were written to control the data acquisition system. For example, the function, *initevt*, controls the initialization of the CAMAC system. The function, *readevt*, handles the readout of the event data. The function, *clearevt*, clears the CAMAC modules.

In our experiment, we need to control the Dazzler and transfer the Dazzler control data to the data acquisition computer. The Dazzler is controlled by a LabVIEW program on a laptop computer. The Dazzler is remotely controlled by a program written by the user. The interface of the Dazzler is based on text files generated by the user. The LabVIEW program runs a text file, *request.txt*, to control the Dazzler. The file can change configuration

files, which control Dazzler. The Dazzler software periodically reads *request.txt* and then programs the Dazzler with the contents of the text file pointed to by request.txt. Once this programming is done, the Dazzler software removes *request.txt.* and uses the new configuration. The readout program in SpecTcl on the data acquisition computer changes the Dazzler configuration by writing *request.txt* on the Dazzler laptop.

Appendix D

Generating pulses in the train by best choice of A

In principle, an infinite train of pulses in the time domain can be generated by applying the sinusoidal phase of Eq. 3.2 to pulses in a train as it is shown in Eq. 3.5. However, we have to note that in reality the sum in Eq. 3.5 is effectively truncated when its pulse amplitude is small enough to have no effect on excitation. We therefore consider the total number of pulses to run from $-N'$ to $+N'$, and the total number of significant pulses N is $2N'+1$.

To obtain the desired number of significant pulses in the train, we choose an appreciate value of A in Eq. 3.2. For example, we determine N' when the $(N'+1)th$ pulse is not significant. That is, the amplitude of the $(N'+1)th$ pulse is less than or equal to some fraction of the average amplitude of all the pulses having $|n| \leq (N'+1)$. We define f by

$$f \equiv J_{N'+1}(A)/\bar{J} = NJ_{N'+1}, \tag{D.1}$$

where $\bar{J}$ is the value of $J_x(\mathrm{A})$ averaged over all significant pulses of x. It is required that the last significant pulse has an amplitude greater than f times the amplitude of the average which is obtained from acceptable pulses in the train. With the condition satisfying Eq. D.1, we ran a simple iteration program which determined A for desired values of N and f. When we plot values of A *versus* N in Fig. D.1, it is found that the values of A as a function of N fits quite well to a power law

$$A' = aN^b, \tag{D.2}$$

f	**a**	**b**
0.03	0.0565(9)	1.554(6)
0.04	0.0661(15)	1.500(8)
0.05	0.0797(26)	1.438(11)
0.06	0.0936(3)	1.385(10)
0.08	0.1054(38)	1.352(13)
0.10	0.0981(39)	1.384(14)

Table D.1: *Table of fitted parameters to Eq. D.2 with various values of f.*

N	A	A'
3	0.3672	0.387(13)
5	0.7933	0.807(28)
7	1.3152	1.308(50)
9	1.9012	1.878(70)
11	2.5332	2.506(95)

Table D.2: *Table of the arguments of the Bessel function of Eq. 3.2. N indicates the total number of significant pulses in the train; The column labeled A indicates the value of A used in Eq. 3.2. The column labeled A' indicates the value of A calculated by using the coefficients of Table D.1 for $f = 0.05$. The error in A' comes from the fitting error n a and b.*

where a and b are functions of f. A$'$ is the fitted value of A.

Table D.1 with various values of f shows our fitted values of a and b along with the fit errors. Here we chose $f = 0.05$ to obtain the values of A' from Eq. D.2. These values are shown in Table D.2. We also show the directly computed value of A to compare with A'.

Here we assume that no pulses having $|n| < N'$ falls below this critical amplitude. For a given value of A, it is possible for pulse amplitudes to increase or decrease until n arrives at some specific value after which they monotonically and rapidly decrease. The aim of this appendix is to serve as a convenient guide for choosing A. However, we should note that some unfortunate choice of A and n that are accidentally near a zero in the Bessel function could cause a missing or negligible pulse in the train. Therefore, once A is chosen, the pulse train obtained from Eq. 3.5 should be reexamined for its suitability. We expect this numerical inverse function treatment of Eq. 3.5 is valuable and useful for choosing A.

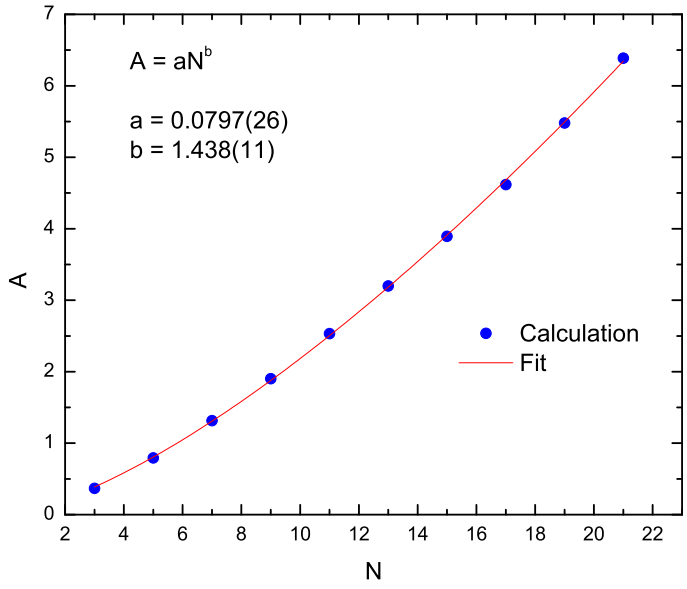

Figure D.1: *We plot values of the Bessel function argument A as a function of the desired number of pulses in the train for $f = 0.05$. The solid curve is a power law which fits to the points obtained from direct computation.*

Appendix E

Staircase generator

E.1 General description for staircase generator

We constructed a staircase generator which is used to supply discrete voltage to a VCO in an application using an offset locking scheme. A schematic diagram of the staircase generator circuit is shown in Fig. E.2. There are two staircase outputs generated in this device; The primary ramp output steps with a constant time delay and the secondary output takes one step each time the primary staircase changes direction. By using internal pots, one can independently determine the span of the staircase and its offset value. The pots labeled $O1$ and $O2$ on the circuit board adjust the offsets of ramp1 and ramp2, respectively. Two pots marked R1 and R2 determine the range or span of the two ramps.

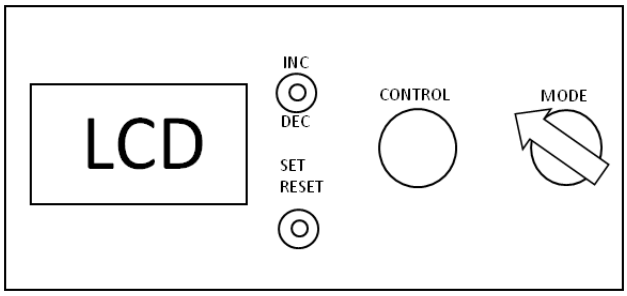

Figure E.1: *Simple diagram of the staircase generator front panel.*

In Fig. E.1, the center control knob changes the ramp outputs with the mode knob in the MANUAL position. Turning the knob clockwise increases the ramp value while turning it counterclockwise decreases the ramp value. This manual control is applied to only ramp1

or simultaneously to ramp1 and ramp2 where the setting in the OFFSET mode determines which function is active. The step size change of the ramp outputs for each control knob is also adjustable by using INC and DEC. Pushing the rocker switch to the INC position causes the step size to double and pushing DEC divides the step size in half. In MANUAL mode, the step size is indicated in the first 4 digits of the LCD display.

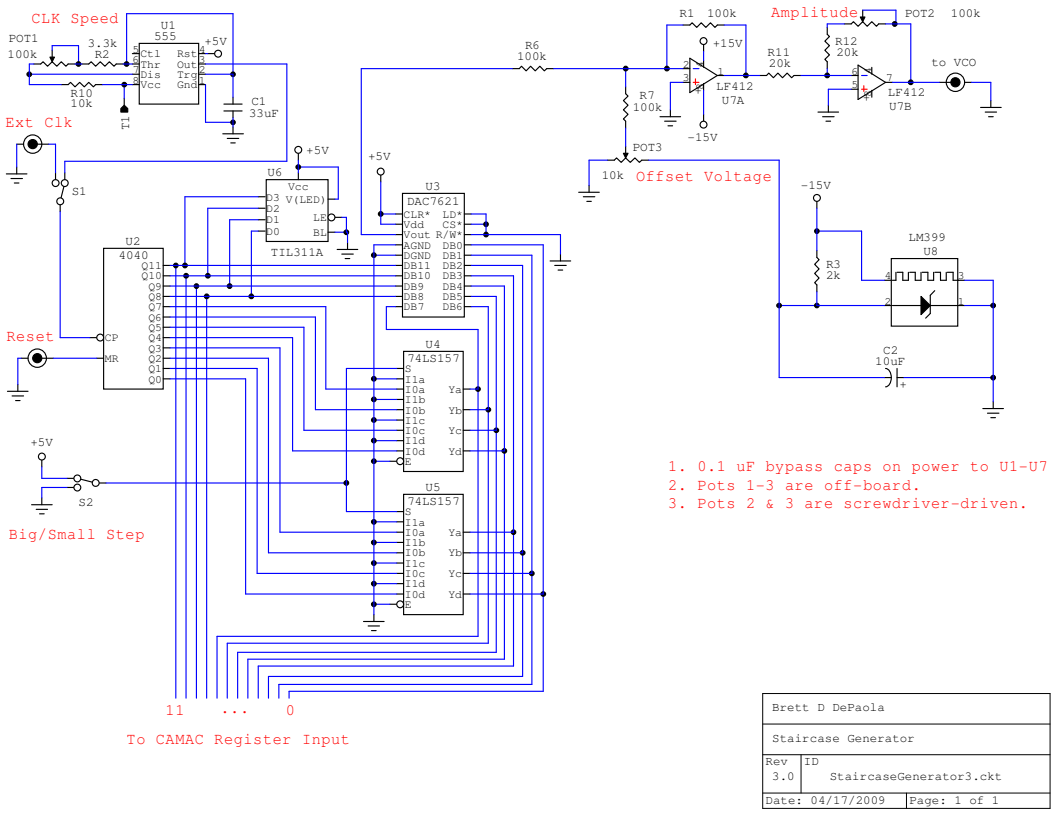

Figure E.2: *Schematic diagram of the staircase generator.*

The staircase will start at MIN and stop at MAX where the user can set the minimum and maximum step values for the staircase. One can independently set MIN and MAX for two ramp outputs. For example, one can turn the mode control to MIN and set the LCD value to the desired step number by using the control knob at MANUAL mode. In addition, the maximum step value for a staircase is similarly determined by setting the mode switch in the MAX position. Finally, the MIN and MAX values are established by pushing the SET rocker switch.

After we set the desired MIN and MAX step numbers, the MODE control has to be turned to the OFFSET position. A channel number of 0 or 1 is shown on the LCD display. Channel 0 applies the current MIN and MAX values to ramp1 while Channel 1 applies the MIN and MAX to ramp2. In OFFSET mode, the MIN and MAX values are fixed while the channel changes. The channel number set in the OFFSET mode also determines which one is changed by the MANUAL control. The manual control only changes ramp1, if the channel is set to 0. Both ramp1 and ramp2 are changed together, if the channel is set to 1. To set various parameters, the MULTI setting of the MODE switch is used. In MULTI mode, the parameters are stepped by using the control knob.

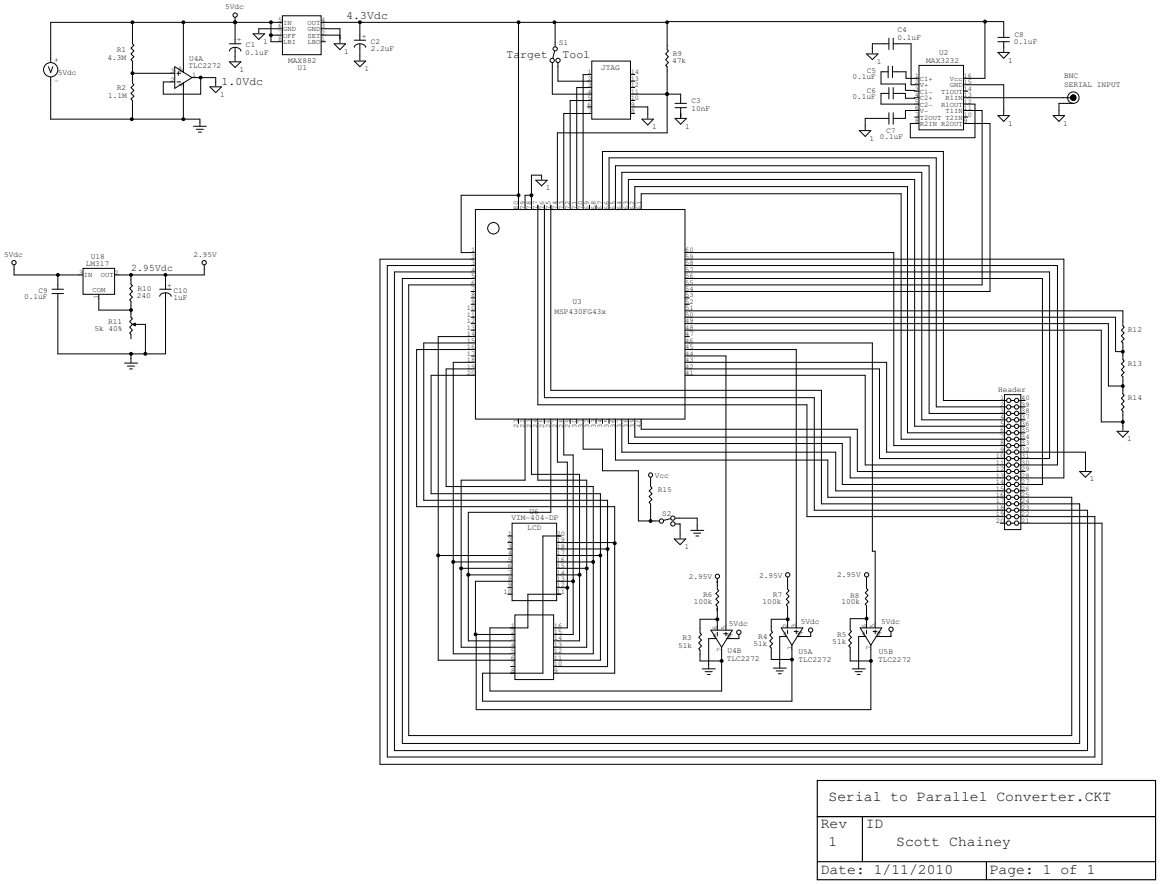

Figure E.3: *Schematic diagram of the receiver circuit.*

A receiver is constructed to read the serial transmission from the stair case generator and to provide the step number as a parallel output. A schematic diagram of the receiver circuit is shown in Fig. E.3. The MPS430FG43x chip is used to interface to a Quad 24-bit input resister.

E.2 Program for staircase generator

The program to run the staircase generator is shown here. The staircase generator communicates with our data acquisition system.

```
//*******************************************************************************
//  Staircase generator for BEAT BOX experiments.
//  dual version 2: output two staircases.  Ramp1 increments(up/down) each time
//  Ramp0 changes direction.
//  3/4/2010
//  Built with IAR Embedded Workbench Version: 3.40A
//*******************************************************************************

#include <msp430x26x.h>
#include <string.h>

#define LCD_EN 0X01
#define LCD_RW 0X02
#define LCD_RS 0X04


const int sh_inc[4][4] = {          // decode whether shaft encoder
  {0, 1, -1, 0},                    // turns positive or negative
  {-1, 0, 0, 1},
```

```
  {1, 0, 0, -1},
  {0, -1, 1, 0}};


int g_sec, g_min, g_hr, g_dy;   //clock memory for seconds, minutes, hours, days
int ramp, mode, offset;         //
int ramp1, r_min1, r_max1, r_min0, r_max0;
int r_max, r_min;                       //stop and start for ramp
int t_i, t_t, t_1;
int com_rx;                             //integer to send to serial line
char com_lsb, com_msb;                  //lsb and msb for serial com
int i2lcd();
int char2lcd();
void shiftlcd();
int *disp, *disp2;          // pointers to integer values to display on LCD
int shaft, sh_enc, sh_eno;              //shaft encoder variables
int updn;               // front panel switches
int r_i;                // increment value for setting variables
int dispw;              // LCD display position

void wait_lcd();

void main(void)
{
  int i;
  WDTCTL = WDTPW + WDTHOLD;                 // Stop Watchdog Timer
  BCSCTL1 = CALBC1_8MHZ + XT2OFF;           // Set DCO to 8MHz
```

```
DCOCTL = CALDCO_8MHZ;
if (BCSCTL1 == 0xFF)                        // Check flash erasure
  while(1);                                 // If DCO constants invalid,trap CPU

WDTCTL = WDT_ADLY_250;                     // WDT 250ms, ACLK, interval timer
IE1 |= WDTIE;                              // Enable WDT interrupt
BCSCTL3 |= XCAP_1;                         // Configure load caps
for (i = 0xFFFF; i > 0; i--);              // Delay for FLL to set

TBCCTL0 = CCIE;                             // TBCCR0 interrupt enabled
TBCCR0 = 1023;                 // 1/32 sec default ramp step time -> period ~ 4 min
TBCTL = TBSSEL_1 + MC_1;                    // ACLK, up mode

TACCTL0 = CCIE;                             // TACCR0 interrupt enabled
TACCR0 = 1023;                 // default poling interval 1/16 sec
TACTL = TASSEL_1 + MC_1;                    // ACLK, upmode


ADC12CTL0 = REF2_5V + REFON;                // Internal 2.5V ref on
DAC12_0CTL = DAC12IR + DAC12AMP_5 + DAC12ENC; // Internal ref gain 1
DAC12_1CTL = DAC12IR + DAC12AMP_5 + DAC12ENC + DAC12OPS;
// Internal ref gain 1, OUTPUT p6.5(4)

P8SEL = 0;
P7SEL = 0;
P8DIR = 0xC7;   // Set 8.0-8.2 (LCD add), 8.6,8.7(step0, dir) to output direction
P7DIR = 0x00;   // Set P7.x for INput (LCD data)
```

```
  P1DIR = 0x00;   // set P1.x for input
  P8OUT = 0xB8;   // P8.7 indicates direction of ramp 1 = up, 0 = down
  P8REN = 0X38;   // set P8.3-P8.5 pull up resistors
  P1OUT = 0X60;   // pull up p1.2, P1.3 for rotary encoder
  P1REN = 0X7E;   // SET P1.1-P1.4 PULL DOWN RESISTORS
  P2SEL = 0;
  P2DIR = 1;



  P3SEL = 0xf0;     // P3.4,5 = USARTA0 TXD/RXD; P3.6,7 = USARTA1 TX/RX
  P3DIR = 0X08;     // P3.3 = T/X ENABLE ON USART0
  UCA0CTL1 |= UCSWRST;      // Disable USART for initialization
  UCA0CTL0 =  UCPEN + UCPAR + UCMODE0;
                       // 8 bit char, EVEN PARITY, ADDRESS MODE, LSB FIRST
                       // even parity, one stop, idle frame enabled

  UCA0CTL1 |= UCSSEL_2;                 // SMCLK
  UCA0BR0 = 69;                         // 8MHz 115200
  UCA0BR1 = 0;                          // 8MHz 115200
  UCA0MCTL = UCBRS2;                    // Modulation UCBRSx = 4
  UCA0CTL1 &= ~UCSWRST;                 // **Initialize USCI state machine**

IE2 |= UCA0RXIE;                        // Enable USCI_A0 RX interrupt


  g_sec = 0;                // initialize variables
  g_min = 0;
```

```
g_hr = 0;
g_dy = 0;
t_i = 1;              // staircase incerement: 1=up, -1=down
t_t = 0;
t_1 = 1;              // increment for second staircase
ramp = 0;             // output value of staircase
mode = 0;
updn = 0;
offset = 0;
r_i = 1;
disp = &ramp;
disp2 = &mode;
r_max = 4095;   // maximum for 12-bit staircase: can be set lower by user
r_min = 0;      // minimum of staircase: can be increased by user
r_min0 = 0;
r_min1 = 0;
r_max0 = 4095;
r_max1 = 4095;
DAC12_0DAT = ramp;            // set initial values of DAC's
DAC12_1DAT = 0;                       // 0V

wait_lcd();               // next we initialize the LCD after power up

P8OUT &= 0XF8;              //CLEAR E, RS, R/W
P7DIR = 0xFF;               // Set P7.x for OUTput (LCD data)
P8OUT |= LCD_EN;          //PULSE ENABLE
P7OUT = 0X30;             //LCD 8 bit
```

```
P8OUT &= ~LCD_EN;
wait_lcd();

P8OUT &= 0XF8;              //CLEAR E, RS, R/W
P7DIR = 0xFF;               // Set P7.x for OUTput (LCD data)
P8OUT |= LCD_EN;          //PULSE ENABLE
P7OUT = 0X01;             //LCD clear display
P8OUT &= ~LCD_EN;
wait_lcd();

P8OUT &= 0XF8;              //CLEAR E, RS, R/W
P7DIR = 0xFF;               // Set P7.x for OUTput (LCD data)
P8OUT |= LCD_EN;          //PULSE ENABLE
P7OUT = 0X02;             //LCD RETURN HOME
P8OUT &= ~LCD_EN;
dispw = 0;                // we set LCD window to start at address 0
wait_lcd();

P8OUT &= 0XF8;              //CLEAR E, RS, R/W
P7DIR = 0xFF;               // Set P7.x for OUTput (LCD data)
P8OUT |= LCD_EN;          //PULSE ENABLE
P7OUT = 0X06;             //LCD increment right
P8OUT &= ~LCD_EN;
wait_lcd();

P8OUT &= 0XF8;              //CLEAR E, RS, R/W
P7DIR = 0xFF;               // Set P7.x for OUTput (LCD data)
```

```
  P8OUT |= LCD_EN;          //PULSE ENABLE
  P7OUT = 0X0C;             //LCD display on
  P8OUT &= ~LCD_EN;



_BIS_SR(LPM0_bits + GIE);
              // Enter LPM3 w/interrupt: the processor stays in an idle state
            // waiting for a clock interrupt
}

void resetlcd(void)
// This sets the LCD data address to zero and moves the display window to zero
{
  wait_lcd();

  P8OUT &= 0XF8;              //CLEAR E, RS, R/W
  P7DIR = 0xFF;               // Set P7.x for OUTput (LCD data)
  P8OUT |= LCD_EN;          //PULSE ENABLE
  P7OUT = 0X02;             //LCD RETURN HOME
  P8OUT &= ~LCD_EN;
  dispw = 0;
}



// Watchdog Timer interrupt service routine
/* The watchdog timer is used as the real time clock.
// It runs every 1/4 sec.  It is also used to update
```

```
// the LCD display and also as a debounce for the panel switches.
// The current ramp value is only put
// out to the LCD every quarter second.
*/

#pragma vector=WDT_VECTOR
__interrupt void watchdog_timer(void)
{
  g_sec += 1;

    if (g_sec >= 240){
    g_min += 1;
    g_sec = 0;
    //i2lcd(g_min,2,4);
    }

    if (g_min >= 60){
    g_hr += 1;
    g_min = 0;
    //i2lcd(g_hr,2,1);
    }

    if (g_hr >= 24){
    g_dy += 1;
    g_hr = 0;
    //i2lcd(g_hr,2,1);
    }
```

```
    if(mode != 5){          // mode 5 writes to LCD on its own
          i2lcd(*disp2,4,0);        //write ramp value to lcd
          i2lcd(*disp, 4,4);
        }
        if(!(P1IN&0x1E)) updn = 0;
//check if up/dn switches are released. This is a debounce for the front
// panel switches. If a switch is detcted as pushed, the status will
// be held until the switch is released at least 1/4 second later.
}

// Timer B0 interrupt service routine
// Timer B is used to time the staircase increments:
// This module has the highest interrupt priority of all
// the timer functions.  The timer counts from zero to the
// set value in TBCCR0 then fires an interrupt.
// The clock comes from the 32kHz watch crystal.
// This interrupt routine changes the ramp value

#pragma vector=TIMERB0_VECTOR
__interrupt void Timer_B (void)
{
    P3OUT |= 8;                          // ENABLE BUFFER OUTPUT

    if (ramp >= r_max0 && !mode) {
    if(t_i == 0) {
        t_i = -1;        // count down next time
```

```
    P8OUT &= 0x3F;
// clear P8.7, P8.6. This is a toggle of the up/dn and step0 outputs
        P2OUT &= 0XFE;
    ramp1 += t_1;
        if (! t_1){
        if (ramp1 >= r_max1) t_1 = -1;
        else t_1 = 1;
        }
        else if ((ramp1 >= r_max1 || ramp1 <= r_min1)) t_1 = 0;
    }
    else if(t_i > 0) {t_i = 0;
    }
}
if (ramp <= r_min0 && !mode) {
if(t_i == 0){
  t_i = 1;          // count up next time
  P8OUT ^= 0xC0;        // set P8.7 (STEP0), reset P8.6(direction)
      P2OUT |= 1;
  ramp1 += t_1;
      if (! t_1){
    if (ramp1 >= r_max1) t_1 = -1;
    else t_1 = 1;
      }
      else if ((ramp1 >= r_max1 || ramp1 <= r_min1)) t_1 = 0;
}
    else if(t_i < 0){
      t_i = 0;
```

```
      P8OUT |= 0x40;}   // set P8.6 output
    }

    if( !mode) ramp += t_i; // increment ramp value when "mode" is zero.
    // ramp is turned off when setting
                // parameters from front panel

//  next write both ramp values to serial line.
//  The protocol is that generator will first
//  send an idle period followed by the address character 'R'.
//  Then it will transmit the
//  two ramp values packed into three characters.
//  The first data byte is the lsB of ramp0.
//  The second character contains the upper 4 bits of
//  both ramps with ramp0 the high nibble
//  and ramp1 as the low nibble.
//  The final character is the lsB of ramp1.

    while (!(IFG2&UCA0TXIFG));  // wait for USART0 TX buffer ready?
    UCA0CTL1 |= UCTXADDR;       // SEND BREAK SIGNAL
    UCA0TXBUF = 0X52;           // "ADDRESS" FOR RECEIVER

    while (!(IFG2&UCA0TXIFG));  // wait for USART0 TX buffer ready?
    UCA0TXBUF = ramp;
    // write ramp lsby to serial line first byte

    while (!(IFG2&UCA0TXIFG));  // wait for USART0 TX buffer ready?
```

```
    UCA0TXBUF = ((ramp>>4)&0xf0) + ((ramp1>>8)&0x0F);
        // transmit msB of ramp as msn + msb of ramp1 as lsn

    while (!(IFG2&UCA0TXIFG));  // wait for USART0 TX buffer ready?
    UCA0TXBUF = ramp1;          // transmit lsB of ramp1

// write values to DAC's after serial transmission
// so that data stream is synchronized.

    while (UCA0STAT&1);      // wait for USART0 TX to finish?
    DAC12_0DAT = ramp;
// ramp sent to DAC0 at end of t/x for constant timing
    DAC12_1DAT = ramp1;

    P3OUT &= 0XF7;     // BUFFER IN HIGH IMPEDANCE STATE
}

int setup;          // state of multi function user input

void blinkcursor();

// Timer A0 interrupt service routine
// Timer A is used to pole the front panel controls.
// The timer function is similar to Timer B.  Priority is
// below the watchdog timer and Timer B.
// The interrupt period is set at 1/32 sec to catch encoder changes
```

```
#pragma vector=TIMERA0_VECTOR
__interrupt void Timer_A (void)
{
    if(!updn) updn = (P1IN >> 1) & 0x0f;
    // status of set/reset & inc/dec switches
    mode = ((~P8IN >> 3) & 0x07);
    // status of function switch, 0 true

    sh_enc = (P1IN & 0x60) >> 5;
    // P1.5, P1.6 from shaft encoder
    shaft += sh_inc[sh_enc][sh_eno];
    // perform 2-phase detection on shaft encoder
    sh_eno = sh_enc;
    // save encoder value to compare with next reading
    if(updn == 4 && r_i < 2048) {
    // inc switch has been activated: change increment value x2
      r_i = r_i << 1;
      updn=260;
    // must change value of status so do not repeat
    // when interrupt reenters
    }
    if(updn == 8 && r_i > 1) {  // "dec" switch has been pushed
      r_i = r_i >> 1;           // decrease increment value 2x
      updn=264;
    }
    if(mode == 0) {         // normal ramp output
      disp = &ramp;
```

```
  disp2 = &ramp1;
  shaft = 0;
  r_i = 1;              // shaft encoder has no function in this mode
  setup=0;              //reset state for "mode 5"
}
else if (mode == 1){        // manual scan
  if(shaft == 1) ramp += r_i;
  // increment ramp output by r_i when shaft turned cw
  else if(shaft == -1) ramp -= r_i;
  // decrement ramp output by r_i when shaft turned ccw
  if(ramp < 0) ramp = 0;
  // the scan limits do not apply in manual mode. can go
  else if(ramp > 4095) ramp = 4095; // from 0 to 4095
  if(offset == 1) ramp1 = ramp;
  // allows a manual scan of ramp1 in parpalle with ramp.
  // set offset at mode 4.
  shaft = 0;            // must reset shaft so don't double add
  disp = &ramp;         // display output at digits 5-8
  disp2 = &r_i;         // display increment value in digits 1-4
}
else if (mode==2){          // set minimum value for staircase scan
  if(shaft == 1) r_min += r_i;  // increment when shaft cw
  else if(shaft == -1) r_min -= r_i;// decrement for shaft ccw
  shaft = 0;
  if (r_min > r_max) r_min = r_max;
  else if (r_min < 0) r_min = 0;
  disp = &r_min;
```

```
  disp2 = &r_i;
}
else if (mode == 3){        // set maximum value for staircase (ramp) scan
  if(shaft == 1) r_max += r_i;
  else if(shaft == -1) r_max -= r_i;
  shaft = 0;
  if (r_max > 4095) r_max = 4095;
  else if (r_max < r_min) r_max = r_min;
  disp = &r_max;
  disp2 = &r_i;
}
else if(mode == 4){
    // determine if ramp0 or ramp1 is to be set with max/min values.
                // the shaft selects "1" or "0".
                // "set" saves values to scan variables
  if(shaft) offset = (offset +1) & 0x01;
  //offset = 0 -> ramp0; 1-> ramp1
  shaft = 0;
  disp = &offset;
  disp2 = &r_i;
  if(updn==1 || updn==2) {
    // push set/reset to move max/min into proper channel
      if (!offset){
    r_max0 = r_max;
    r_min0 = r_min;
  }
  else if( offset == 1){
```

```
    r_max1 = r_max;
    r_min1 = r_min;
  }
      r_i = 1;
      updn=3;
  }

  if(dispw){
    // this is here to reset the display at the end of mode 5.
    if(dispw > 0) shiftlcd(1,dispw);
    // mode 5 shifts the display to a different memory area so that
    resetlcd();
    // the clock timers can keep running while we are in parameter
    dispw = 0;
    // setup.  When the function switch is turned back to mode 4,
    // this routine resets the LCD to its normal display mode
  }
}
else if (mode == 5){      // multiple setup area
  if (setup <= 1){
    char2lcd("setup   ",8,8);
    if(!setup) {shiftlcd(0,8);
    dispw = 8;
    setup = 1;
    }
    if(updn) {setup = 2;
    updn = 7;}
```

```
}
else if(setup == 2){
//change the time between staircase steps.  The display unit is the
  char2lcd("stp_tm:",7,8);
  // crystal oscillator period: 1/32,767 sec.
  if(updn==1 || updn==2){
  //push either "set" or "reset" to enter this function
    setup = 10;
  //next time interrupt runs, we will go to the functional routine
    updn=3;
    r_i = 1;
  //encoder is used to step through functions, so don't let increment accumulate
  }
}
else if(setup == 3){      //zoom the scan range
  char2lcd("range   ",8,8);
  if(updn==2 || updn==1) {    //push "set"/"reset" to enter function
    updn = (DAC12_0CTL & (DAC12IR + DAC12SREF1));
    //read current range from status registers
    if (updn == DAC12IR)      //default full scale output
      setup = 11;
    else if (updn == DAC12SREF1)  // 1/9 scale ramp
      setup = 12;
    else setup = 13;      // 1/3 scale output
    r_i = 1;          // don't accumulate increment changes
    updn = 3;
  }
```

```
}
else if(setup == 4){      // set the real time clock
  char2lcd("clock:  ",8,8);
  if(updn==1 || updn==2) {
    setup = 14;
    r_i = 1;
    updn=3;
  }
}
else if(setup == 5){
// this is a test function. Scroll the LCD display past the display
  char2lcd("scroll: ",8,8);   //window using the encoder
  if(updn==1 || updn==2){
    setup = 17;
    r_i = 1;
    updn = 3;
  }
}
else if(setup == 10){
// change the step time.
// change the delay using the encoder and inc/dec switches
  i2lcd(TBCCR0,4,12);
  i2lcd(r_i,3,8);
  if(shaft==1) TBCCR0 += r_i; //change period using r_i value
  else if(shaft == -1) TBCCR0 -= r_i;
  shaft = 0;
  if(updn == 1 || updn == 2){ //use set/reset to exit function
```

```
    setup = 3;
    r_i = 1;
    updn = 3;
  }
}
else if(setup==11){       //zoom is full scale, change with encoder
  char2lcd("  1", 3, 13);
  if(updn==1 || updn==2){     //exit with set/reset switch
    setup = 4;
    updn = 9;
    r_i = 1;
  }
  if(shaft == 1){         //if shaft turned cw, change zoom to 1/3
    setup = 12;
    DAC12_0CTL &= ~DAC12ENC;
    DAC12_0CTL = (DAC12_0CTL & 0XFF) | DAC12SREF1; // EX REF X3
    DAC12_0CTL |= DAC12ENC;
    shaft = 0;
  }
  if (shaft == -1){       //if shaft turned ccw, change zoom to 1/9
    setup = 13;
    DAC12_0CTL &= ~DAC12ENC;
    DAC12_0CTL = (DAC12_0CTL & 0XFF) | DAC12SREF1 | DAC12IR;// EX REF X1
    DAC12_0CTL |= DAC12ENC;
    shaft = 0;
  }
 }
```

```
else if(setup == 12){     //zoom is 1/3, change with encoder
  char2lcd("1/3", 3, 13);
  if(updn==1 || updn==2){         // use set/reset to exit
    setup = 4;
    r_i = 1;
    updn=3;
  }
  if(shaft == 1){         //set zoom to 1/9
    setup = 13;
    DAC12_0CTL &= ~DAC12ENC;
    DAC12_0CTL = (DAC12_0CTL & 0XFF) | DAC12SREF1 | DAC12IR;
    // EX REF X1
    DAC12_0CTL |= DAC12ENC;
    shaft = 0;
  }
  if (shaft == -1){       //set zoom to 1
    setup = 11;
    DAC12_0CTL &= ~DAC12ENC;
    DAC12_0CTL = (DAC12_0CTL & 0XFF) | DAC12IR; // int REF X1
    DAC12_0CTL |= DAC12ENC;
    shaft = 0;
  }
}
else if(setup == 13){     //zoom is 1/9, change with shaft
  char2lcd("1/9", 3, 13);
  if(updn==1 || updn==2){ //use set/reset to exit
    setup = 4;
```

```
    r_i = 1;
    updn=5;
  }
  if(shaft == 1){         //set zoom to 1
    setup = 11;
    DAC12_0CTL &= ~DAC12ENC;
    DAC12_0CTL = (DAC12_0CTL & 0XFF) | DAC12IR; // internal reference x1
    DAC12_0CTL |= DAC12ENC;
    shaft = 0;
  }
  if (shaft == -1){       //set zoom to 1/3
    setup = 12;
    DAC12_0CTL &= ~DAC12ENC;
    DAC12_0CTL = (DAC12_0CTL & 0XFF) | DAC12SREF1;
     // internal reference x1
    DAC12_0CTL |= DAC12ENC;
    shaft = 0;
  }
}
else if(setup == 14){             //set clock seconds
  char2lcd("  :  :  ", 8, 8);
  blinkcursor(1);       //turn on blinking cursor
  i2lcd(g_hr,2,8);
  i2lcd(g_min,2,11);
  i2lcd(g_sec>>2,2,14);
  if(updn == 260) {     //if "inc" pushed, change minutes
    setup = 15;
```

```
    updn = 261;
  }
  if(updn==1 || updn==2){  //exit with set/reset
    setup = 1;
    r_i = 1;
    updn = 3;
    blinkcursor(0);         //turn off blinking cursor
  }
  g_sec += shaft<<2;
  shaft = 0;
}
else if(setup == 15){            // set clock minutes
  i2lcd(g_hr,2,8);
  i2lcd(g_sec>>2,2,14);
  i2lcd(g_min,2,11);
  if(updn == 260) {   //if "inc" pushed, change hours
    setup = 16;
    updn = 261;
  }
  else if(updn == 264){   //if "dec" pushed, change seconds
    setup = 14;
    updn = 265;
  }
  g_min += shaft;
  shaft = 0;
  r_i = 1;
  if(updn==1 || updn==2){ //exit on set/reset
```

```
    setup = 1;
    r_i = 1;
    updn = 3;
    blinkcursor(0);         //turn off cursor
  }
}
else if(setup == 16){ //set clock hours using shaft
  i2lcd(g_sec>>2,2,14);
  i2lcd(g_min,2,11);
  i2lcd(g_hr,2,8);
  if(updn == 260) {   //if inc puhsed, change seconds
    setup = 14;
    updn = 261;
  }
  else if(updn == 264) {  //if "dec" pushed, change minutes
    setup = 15;
    updn = 265;
  }
  g_hr += shaft;
  shaft = 0;
  r_i = 1;
  if(updn==1 || updn == 2){//exit with set/reset
    setup = 1;
    r_i = 1;
    updn = 3;
    blinkcursor(0);         //turn off cursor
  }
```

```
}
else if(setup == 17){  //scroll display
  if(shaft == 1 && dispw > 0) {
    shiftlcd(1,1);
    dispw -= 1;
  }
  else if(shaft == -1 && dispw < 80){
    shiftlcd(0,1);
    dispw += 1;
  }
  shaft = 0;
  if(updn==2 || updn == 1){//exit with set/reset
    setup=1;
    r_i=1;
    updn = 5;
  }
}

else setup = 1;

setup += shaft;
 //this scrolls through setup functions using shaft
if (setup <=0) setup = 5;
else if(setup ==6) setup = 1;
shaft = 0;
}  // end mode==5
```

```
    else {
      disp = &ramp;
      disp2 = &mode;
    }
}                          //end timer A

#pragma vector=USCIAB0RX_VECTOR
__interrupt void usart0_rx (void)
    //used to read characters recieved on serial port
{
  if(UCA0STAT & UCADDR){           // ADDRESS bit set > msb
    com_msb = UCA0RXBUF;
  }
  else{
    com_lsb = UCA0RXBUF;                          // RXBUF0 to com_rx
    com_rx = com_lsb + (com_msb * 256) ;
  }
}

int i2lcd(j,id,ia)
// write interger value to lcd: j=value to write, id # of digits, ia lcd address*/
  int j, id, ia;
{
int d[4], i;
if(id>4) id=4;
if(id<1) id=1;
// convert argument to decimal
```

```
    d[2] = j/10;
    d[3] = j - d[2]*10;
    d[1] = d[2]/10;
    d[2] -= d[1]*10;
    d[0] = d[1]/10;
    d[1] -= d[0]*10;

// write bcd values in d[] to LCD starting at address ia
  P7DIR = 0xFF;              // Set P7.x for OUTput (LCD data)
  P8OUT &= ~(LCD_RW+LCD_RS);        //CLEAR R/W AND RS BITS
  P8OUT |= LCD_EN;           //PULSE ENABLE
  P7OUT = 0X80 + (ia& 0x7f);        //LCD cursor address ia
  P8OUT &= ~LCD_EN;

  for(i=4-id; i<4; ){
    wait_lcd();
    P7DIR = 0xFF;               // Set P7.x for OUTput (LCD data)
    P8OUT |= LCD_RS;
    P8OUT |= LCD_EN;
    P7OUT = d[i++]+0x30;        //write digit to cursor position
    P8OUT &= ~LCD_EN;
  }

return i;
}

void wait_lcd(void)     //wait for LCD to process command
```

```
{
  _BIS_SR(GIE);                  // enable interrupt while waiting
  P7DIR = 0x00;                // Set P7.x for INput (LCD data)
  P8OUT &= ~(LCD_RS+LCD_EN);
  P8OUT |= LCD_RW;             //READ LCD STATUS
                      // delay
  P8OUT |= LCD_EN;             //SET ENABLE

  while(P7IN & 0X80);              //WAIT FOR LCD BUSY FLAG TO CLEAR
  P8OUT &= 0XFE;               //CLEAR E

  P8OUT &= 0XF8;               //CLEAR E, RS, R/W
  return;
}

int char2lcd(char *j, int id, int ia)
// write characters  to lcd: i=ptr to strng, id # of digits, ia lcd address
{
int i;

// write ascii values in d[] to LCD starting at address 4
  P7DIR = 0xFF;              // Set P7.x for OUTput (LCD data)
  P8OUT &= ~(LCD_RW+LCD_RS+LCD_EN);     //CLEAR R/W AND RS BITS
  P8OUT |= LCD_EN;           //PULSE ENABLE
  P7OUT = 0X80 + (ia & 0x0f);       //LCD cursor address ia
  P8OUT &= ~LCD_EN;
```

```
  for(i=0; i<id; ){
    wait_lcd();
    P7DIR = 0xFF;           // Set P7.x for OUTput (LCD data)
    P8OUT |= LCD_RS;
    P8OUT |= LCD_EN;
    P7OUT = j[i++];         //write digit to cursor position
    P8OUT &= ~LCD_EN;
  }

return i;
}

void shiftlcd(int lr, int id)
// shift LCD display left or right by id positions
{
int i;

  if(!lr) lr = 0x18;                    // shift left
  else lr = 0x1C;                       // shift right

  for(i=0; i<id; i+=1){
    wait_lcd();
    P7DIR = 0xFF;           // Set P7.x for OUTput (LCD data)
    P8OUT &= ~(LCD_RW+LCD_RS+LCD_EN);   //CLEAR R/W AND RS BITS
    P8OUT |= LCD_EN;
    P7OUT = lr;             //write display shift command
    P8OUT &= ~LCD_EN;
```

```
  }

return ;
}

void blinkcursor(int j)   //turn on/off blinking cursor
{
          wait_lcd();
          P8OUT &= 0XF8;          //turn off blinking cursor
          P7DIR = 0xFF;           // Set P7.x for OUTput (LCD data)
          P8OUT |= LCD_EN;        //PULSE ENABLE
          if(!j) P7OUT = 0X0C;        //cursor off
          else P7OUT = 0x0F;              //cursor on
          P8OUT &= ~LCD_EN;
          return ;
}
```